INVESTIGATING THE INTERACTION OF HP1α WITH H1.4 IN HETEROCHROMATIN

A thesis presented in partial fulfilment of the requirements for the degree of
Master of Science
in
Genetics
at Massey University, Palmerston North,
New Zealand.

Maia Ellen Maxine Smart

2022

Abstract

Chromatin is a nucleoprotein complex which organises DNA within the cell and is essential for genome fidelity. However, the underlying mechanisms which regulate its formation are not fully understood. Chromatin forms through complex hierarchical folding. DNA wraps around octamers of the four core histones, H2A, H2B, H3 and H4, forming nucleosomes in an array called the 10 nm fibre, which is then condensed by linker histone H1 into the 30 nm fibre. RNA and architectural proteins such as Heterochromatin Protein 1α (HP1α) then fold the chromatin fibre into higher order domains, that ultimately partition the genome into domains of euchromatin and heterochromatin. The histone code model for HP1α induced heterochromatinization is through the chromodomain of HP1α binding to di- and tri-methylated lysine 9 of Histone 3 (H3K9me2/3). The H3K9me2/3 mark however, is present throughout the genome and so lacks the specificity for HP1α targeting.

An interaction between HP1α and linker histone H1.4 has been identified previously, and through the establishment of an *in vitro* pulldown, it has been shown to be mediated by total RNA. To aid in building a model for HP1α targeting to telomeric heterochromatin, it was proposed that the RNA transcribed from this region, which associates with HP1α at the telomeres, could mediate this interaction. Therefore, Telomeric-repeat containing RNA (TERRA), for which HP1α has a high *in vitro* binding affinity, was tested to determine if it could mediate the interaction. TERRA was shown to mediate the interaction of HP1α with H1.4, indicating that this interaction could potentially be aiding in the targeting of HP1α to telomeric heterochromatin. Work to establish mononucleosomes to explore this interaction in a nucleosomal context has begun, however issues with unbound DNA and heterogeneous mononucleosome populations need to be

overcome before these can be utilised.

A model for HP1α targeting is proposed for reestablishment of telomeric heterochromatin after the S-phase of the cell cycle, through an interaction between H1.4 and HP1α, mediated by TERRA. These factors are essential in heterochromatin organisation, and their loss results in dysregulation which could lead to cancer and ageing.

COVID-19 Statement

Due to the disruption caused by COVID-19, deeming the laboratory inaccessible for several months, the progress of this research was impeded. The completion of Aim 2, outlined in Section 1.5, was not reached due to issues in forming mononucleosomes (Aim 2 objective a), which then could not be resolved due to time constraints (see Chapter 4). Due to lack of time, nucleosomal array studies could not be performed (Aim 2 objective b). Completion of this work has been outlined in the future directions (see Section 5.2).

Acknowledgements

This work is dedicated to my Mum and Dad.

Abbreviations

APS	Ammonium persulfate
BSA	Bovine serum albumin
C	Carboxy
CD	Chromodomain
CDK	Cyclin-dependent kinase
cDNA	Complementary deoxyribonucleic Acid
CSD	Chromoshadow domain
CTCF	CCCTC-binding factor
CTD	Carboxy-terminal domain
DNA	Deoxyribonucleic acid
E. coli	*Escherichia coli*
EDTA	Ethylenediaminetetraacetic acid
EMSA	Electrophoretic mobility shift assay
EtBr	Ethidium bromide
G4	G-quadruplex
HP1	Heterochromatin Protein 1
HP1α	Heterochromatin Protein 1α
His	Hexahistidine
IPTG	Isopropyl β-D-1-thiogalactopyranoside
LB	Luria-Bertani
MSR RNA	Major satellite repeat RNA
N	Amino
Ni-NTA	Nickel-nitrilotriacetic acid
NTD	Amino-terminal domain
PAGE	Polyacrylamide gel electrophoresis
PCA	Perchloric acid

PCR	Polymerase chain reaction
RNA	Ribonucleic acid
rpm	Revolutions per minute
SDS	Sodium dodecyl sulfate
SEC	Size exclusion chromatography
SOC	Super Optimal Catabolite
SUMO	Small ubiquitin-like modifier
Suv39h1/2	Suppressor of variegation 3-9 homolog 1/2
TBS	Tris-buffered saline
TE	Tris-EDTA
TEMED	Tetramethylethylenediamine
TERRA	Telomeric repeat-containing RNA

Contents

List of Tables

List of Figures

Chapter 1

Introduction

1.1 Functional genome organisation

To allow essential genomic function, the genome must be organised within the nucleus. This is achieved through chromatin, a stable yet dynamic nucleoprotein complex. It controls gene expression and maintains genomic stability through several layers of hierarchical folding (Figure 1.1) (Yadav et al., 2018). Nucleosomes are the basic unit which are then folded in stages into higher order structures, that then partition the genome.

Figure 1.1: Hierarchical folding of chromatin. The folding of chromatin is illustrated, beginning with double-stranded DNA wrapping around octamers of core histones, forming nucleosomes, with the beads-on-a-string appearance. Linker histone H1 binds, forming chromatosomes, followed by inter-nucleosomal interactions eventually forming tertiary structures. Figure from Fyodorov et al. (2018).

1.2 Hierarchical folding of DNA

1.2.1 Nucleosome

The most elementary level of folding is the nucleosome (Figure 1.2), where Watson-Crick base-paired double-stranded DNA is wrapped 1.67 times around an octamer

of core histones, forming this basic unit (Luger et al., 1997a). The core histones each consist of a carboxy (C)-terminal head and amino (N)-terminal tail. The N-terminal tails are post translationally modified and engage in protein-protein interactions (Hansen et al., 1998), while the head consists of a histone fold domain which enables heterodimerisation in a head to head manner, through the handshake motif (Arents et al., 1991; Arents and Moudrianakis, 1995). Octamers consist of pairs of heterodimers of the core histones, histone H2A with histone H2B; and histone H3 with histone H4. H3-H4 dimers then dimerise, forming a tetramer which then binds two H2A-H2B dimers, forming an octamer (Eickbush and Moudrianakis, 1978; Germond et al., 1976). Multiple nucleosomes are linked together by linker DNA, generating an array, and is known as the 10 nm fibre which has the appearance of beads on a string (Luger et al., 1997a).

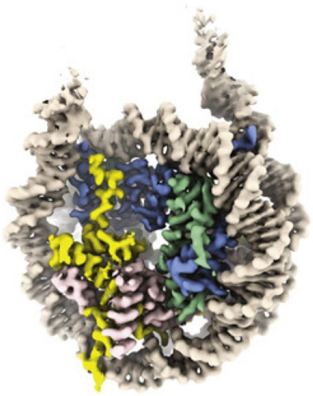

Figure 1.2: Cryo-electron microscopy nucleosome structure. Structure of a nucleosome resolved by high resolution cryo-electron microscopy. Adapted from Zhou et al. (2021).

1.2.2 Chromatosome

Linker histone H1 (H1) is essential to the folding and higher organisation of chromatin. H1 binds nucleosomes through the nucleosomal dyad, forming chromatosomes (Figure 1.3), condensing the chromatin from the 10 nm fibre to the 30 nm fibre (Figure 1.1) (Bednar et al., 1998).

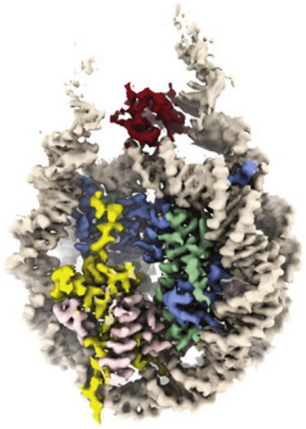

Figure 1.3: Cryo-electron microscopy chromatosome structure. Chromatosome structure resolved by high resolution cryo-electron microscopy, with the nucleosome bound by human H1 (red). Adapted from Zhou et al. (2021).

In mammalian cells, there are five somatic variants of H1, H1.1 through H1.5 (Harshman et al., 2013). All H1 variants consist of a tripartite structure comprised of a central globular domain with two flanking basic lysine-rich intrinsically disordered tails, a long C-terminal domain (CTD) and a short N-terminal tail (NTD) (Figure 1.4). The globular domain of H1 interacts with the core DNA of the nucleosomal dyad, anchoring H1 to the nucleosome, while the CTD interacts with the linker DNA, compacting the 10 nm fibre (Bednar et al., 2017; Horn and Peterson, 2002), however it is unclear the role of the NTD.

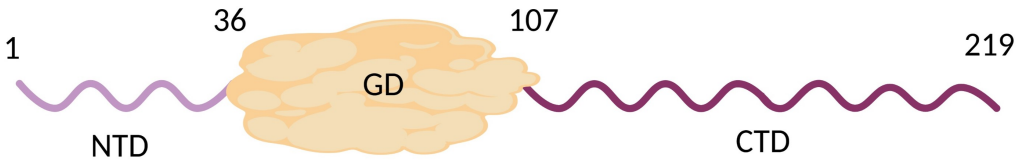

Figure 1.4: Schematic diagram of H1.4. Linker histone variant H1.4 is comprised of a globular domain (GD, orange) flanked by amino- (NTD) and carboxy-terminal tails (CTD). Created with BioRender.

The CTD is divergent between variants and allows differential interactions with nucleic acids (Th'ng et al., 2005). Each variant displays unique chromatin compaction and binding properties, with H1.1 and H1.2 weaker compactors and binders, while H1.3, H1.4 and H1.5 are stronger (Parseghian, 2015). The variants also differ in post-translational modification patterns and enrichment in genomic locations (Parseghian et al., 2001), with H1.2 enriched in active, and H1.4 and H1.5 enriched in inactive regions (Th'ng et al., 2005).

Binding of H1 to nucleosomes condenses the nucleosomal array, although the binding of H1 does not play a role in the positioning of nucleosomes (Shen and Allan, 2021). H1 binds to the nucleosome relative to the dyad (Figure 1.5), either on-dyad, off-dyad or at the newly discovered position dyad escaped, in which post translational modifications on the H1 tails inhibits their interaction with the linker DNA, forcing an interaction with the core acidic patch of the nucleosome (Wu et al., 2019). The location of H1 relative to the dyad is not determined by H1 tails but by the globular domain (Hutchinson et al., 2015; Zhou et al., 2013, 2016), which preferentially binds to superhelical DNA over relaxed DNA (Singer and Singer, 1976). H1 tails are involved in compaction of the chromatin fibre (Hutchinson et al., 2015). It has been implied that the CTD of H1 is responsive to its environment and adjusts conformation accordingly, regulating chromatosome structure. Förster resonance energy transfer studies where H1 was bound to different substrates showed different condensed conformations were formed by the H1 CTD when interacting with free DNA, mononuclesomes (Fang et al., 2012), and oligonucleosomes (Fang et al., 2016). The number of positive amino acid residues in each H1 variant CTD influences the closeness of the linker DNAs to each other in a chromatosome (Zhou et al., 2021), however, it is not the sole determinant (Bednar et al., 2017). It has been hypothesised that the number of T/SPKK motifs, phosphorylated by Cyclin-dependent kinase (CDK), in the CTD could also regulate the closeness of linker DNAs in chromatosomes (Zhou et al., 2021).

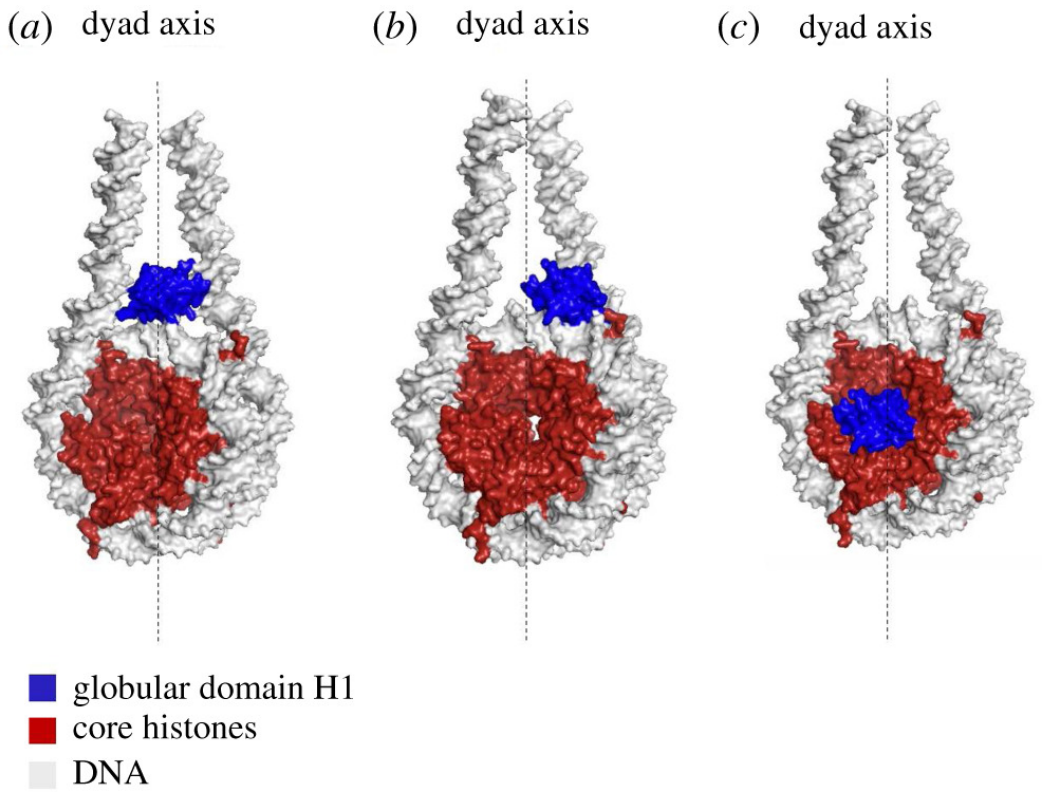

Figure 1.5: Schematic diagram of binding modes of linker histone H1. a) On-dyad binding mode of H1 globular domain to a nucleosome. b) Off-dyad binding mode of H1 globular domain to a nucleosome. c) Dyad escaped binding mode of H1 globular domain to a nucleosome. Figure from Saha and Dalal (2021).

1.2.2.1 Linker histone H1.4

H1.4 binds off-dyad (Song et al., 2014; Zhou et al., 2013) and forms a more closed and compact chromatosome. This behaviour is dependent on the CTD interacting simultaneously with both the entry and exit linker DNAs, while the NTD does not appear to interact with either (Zhou et al., 2021). The binding of H1.4 to a nucleosome influences the behaviour of the N-terminal tail of H3 (Stützer et al., 2016; Zhou et al., 2021), inhibiting post-translational modifications and chromatin remodeling (Horn et al., 2002; Stützer et al., 2016; Zhou et al., 2021). Binding of H1.4 also influences the C-terminal tails of H2A, breaking their symmetrical conformation in the nucleosome by inhibiting their interaction with the linker DNAs, forcing them into the core of the chromatosome, impacting transcription and post-translational modifications (Zhou et al., 2021).

H1.4 is differentially phosphorylated on the CTD by CDK2 at T/SPKK motifs (Hale et al., 2006). This phosphorylation of H1.4 results in decondensing of the chromatin fibre (Contreras et al., 2003). Aberration of the H1.4 CTD through truncation of the CTD is proposed to have a causal role in intellectual disorders such as autism and intellectual disability (Duffney et al., 2018; Tatton-Brown et al., 2017) and has also been implicated in premature aging and accelerated cellular senescence (Flex et al., 2019). These truncations disrupt chromatin compaction through the loss of the CDK phosphorylation sites and positive residues along the tail, giving rise to an overall more relaxed chromatin state (Flex et al., 2019). The truncated H1.4 CTD results in dysfunctional telomeres and disrupted nuclear lamina structure (Flex et al., 2019).

1.2.3 Beyond the 30 nm fibre

Bridging the gap between the 30 nm fibre and higher order structures is the process of loop formation in the chromatin fibre, however this is not a fully understood process (Bascom and Schlick, 2017; Wutz et al., 2017). The formation of loops brings linearly distant regions of the genome into close proximity (Rao et al., 2014; Schleif, 1992), with the loop size and gene level within the loop differentiating active and inactive chromatin (Tiwari et al., 2008). A model for loop formation is through CCCTC-binding factor (CTCF), an insulator binding protein, binding to chromatin, while cohesin binds elsewhere and extrudes a chromatin loop and is then stalled upon reaching the pre-bound CTCF (Sanborn et al., 2015; Wutz et al., 2017) (Figure 1.6). Cohesin and CTCF facilitate the formation of chromatin loops, forming both intra- and inter-domain long-range interactions, aiding in chromatin compaction (Splinter et al., 2006; Zuin et al., 2014). These interactions allow long range gene regulation which direct cellular development and fate commitment (Apostolou et al., 2013; De Laat and Duboule, 2013; Gorkin et al., 2014).

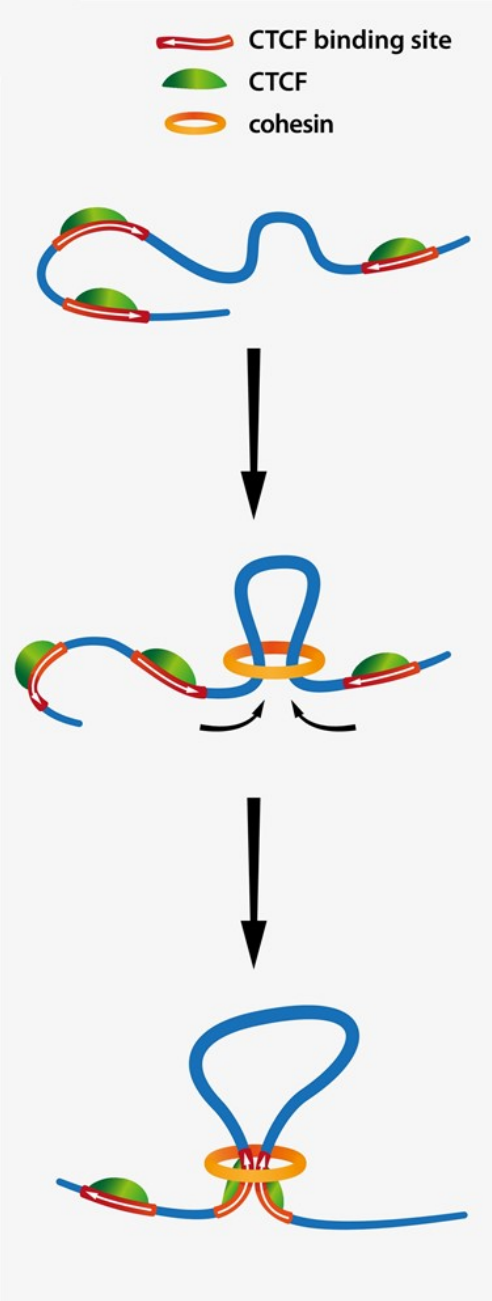

Figure 1.6: CTCF and cohesin loop formation. Proposed loop formation by CTCF and cohesin, where CTCF binds to chromatin and cohesin extrudes a loop and stops upon reaching CTCF. Adapted from Wutz et al. (2017).

1.3 Compartmentation of chromatin

1.3.1 Partitioning at the microscopic level

Beyond the 30 nm fibre and looping, architectural proteins such as Heterochromatin Protein 1 (HP1) further fold the chromatin fibre into higher order formations. This partitions the chromatin into functionally distinct domains within the three-dimensional nucleus (Janssen et al., 2018). The partitioning of the genome can be seen through a microscope, with dark staining highly condensed DNA termed heterochromatin and lighter staining less condensed DNA termed euchromatin (Heitz, 1928). Euchromatin is transcriptionally active and is gene-rich (Grewal and Jia, 2007). The less condensed more open structure allows for DNA transcription and replication machinery to access the chromatin. It is enriched in acetylated core histones, which neutralises the positive charge of histone tails. This impedes the binding of the histone tails, providing accessibility to DNA and reducing nucleosome-nucleosome interactions (Sterner and Berger, 2000). Euchromatin is also enriched in trimethylation of histone H3 on lysine 4 (H3K4me3) which is recognised by chromatin remodelling complexes and other complexes that promote preinitiation complex formation enabling transcription (Hyun et al., 2017).

Heterochromatin is highly condensed and gene-poor (Janssen et al., 2018). The condensed structure makes the heterochromatin less accessible to transcription machinery leading to these regions being transcriptionally inactive. Heterochromatin is enriched in the HP1 paralogue Heterochromatin Protein 1α (HP1α), noncoding RNA and core histone tails with post translational modifications including di- and tri-methylated histone H3 on lysine 9 (H3K9me2/3) (Bannister et al., 2001; Daujat et al., 2005; Kumar and Kono, 2020; Maison et al., 2002; Minc et al., 1999; Muchardt et al., 2002). Heterochromatin is present in two forms: facultative and constitutive. Facultative heterochromatin is associated with development, where developmental genes are switched on or off as required and is regulated by Polycomb group complexes (Saurin et al., 1998).

Constitutive heterochromatin is found at repetitive regions of the genome including telomeres and centromeres, and at regions which contain transposons (Dorer

and Henikoff, 1994; Padeken et al., 2015). This maintains genomic stability during the cell cycle by inhibiting movement and aberrant expression of transposable elements, and maintains the structural regions of the chromosomes. Within the nucleus, constitutive heterochromatin is localised to the perinucleolar space and nuclear periphery (Minc et al., 1999).

Constitutive heterochromatin contains a noncoding RNA component (Maison et al., 2002; Muchardt et al., 2002). Repetitive RNA transcripts are transcribed from respective heterochromatic regions by RNA polymerase II (Schoeftner and Blasco, 2008), such as Telomeric repeat-containing RNA (TERRA) from telomeres (Azzalin et al., 2007; Schoeftner and Blasco, 2008) and Major satellite repeat RNA (MSR RNA) from the centromere (Ferri et al., 2009), and is required for the function and assembly of these regions (Chan et al., 2012; Saffery et al., 2003; Wong et al., 2007).

HP1 was first identified in *drosophila melanogaster* as a "non-histone chromosome protein" which was associated with heterochromatin (Eissenberg et al., 1990; James and Elgin, 1986). It was determined that HP1 was responsible for propagation and maintenance of higher order chromatin folding and enhances position effect variegation in centromeric and pericentromeric regions and decreases position effect variegation in non-centromeric regions (Aagaard et al., 1999; Eissenberg et al., 1990; Festenstein et al., 1999).

HP1 is a tripartite protein consisting of a conserved N-terminal chromodomain (CD) linked by a less conserved flexible hinge region to a conserved C-terminal chromoshadow domain (CSD) (Eissenberg and Elgin, 2000), with N- and C-terminal flanking extensions (Lomberk et al., 2006) (Figure 1.7). The CSD is responsible for dimerisation of HP1 proteins and mediating interactions with other proteins, many of which contain the PXVXL motif (Nishibuchi and Nakayama, 2014) or a unique zinc-finger like motif binder such as Pogo transposable element derived with zinc-finger domain (POGZ) (Nozawa et al., 2010). The CD binds H3K9me2/3 (Bannister et al., 2001), while the hinge region contains a nucleic acid-binding domain which displays paralogue specific affinities for DNA and RNA, which is required for binding chromatin (Bryan et al., 2017; Meehan et al., 2003; Muchardt et al., 2002; Nishibuchi et al., 2014).

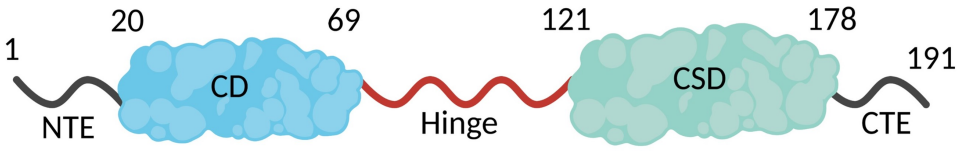

Figure 1.7: Schematic diagram of HP1α. Heterochromatin Protein 1α (HP1α) consists of two globular domains, the chromodomain (CD, blue) and chromoshadow domain (CSD, green), that are linked by the flexible hinge region (red) and flanked at each end by amino- (NTE) and carboxy- (CTE) terminal extensions. Created with BioRender.

There are three mammalian HP1 paralogues, HP1α, Heterochromatin Protein 1β (HP1β) and Heterochromatin Protein 1γ (HP1γ) (Muchardt et al., 2002). While the three HP1 paralogues are structurally similar, they differ in nuclear localisation (Minc et al., 1999), with HP1γ localised to euchromatin, HP1β present in both euchromatin and heterochromatin, and HP1α enriched solely in heterochromatin (Kumar and Kono, 2020).

1.3.2 Heterochromatin homeostasis

Heterochromatin plays an important role in maintaining cell health, with its disruption often associated with cancer and ageing (Janssen et al., 2018). The processes of ageing is caused by a buildup of genomic damage over time, causing the loss of function of tissues and organs (Lee et al., 2020). The majority of this damage is the result of reactive oxygen species which cause DNA base mutations and single and double stranded DNA breaks, while heterochromatin acts as cellular defence through its compact structure (Ljungman and Hanawalt, 1992; Takata et al., 2013; Strand et al., 2014). Over time, heterochromatin becomes dysregulated and reduced due to changes in distribution and levels of heterochromatic marks such as H3K9me2/3 and changes to HP1 levels (Feinberg et al., 2016; Slee et al., 2012; Vad-Nielsen et al., 2016). This results in aberrant gene expression and altered nuclear architecture (Haithcock et al., 2005; Larson et al., 2012; Apostolou et al., 2013). Distorted nuclear architecture caused by heterochromatin dysregulation is associated with increased metastatic behaviour of cancer cells (Norwood et al., 2006), and is used in pathology for identifying

malignancies (Stephens et al., 2019).

1.3.3 Establishing heterochromatin

The canonical mode of constitutive heterochromatin establishment is through the histone code, where histone mark writers; histone deacetylases and histone methyltransferases, remove euchromatic acetylation marks and place heterochromatic methylation marks. These are recognised by effector proteins which then spread the chromatin compaction (Janssen et al., 2018). HP1α, of which constitutive heterochromatin is strongly enriched, binds to H3K9me2/3 through its CD (Bannister et al., 2001; Daujat et al., 2005; Kumar and Kono, 2020). The CSD of HP1α then binds other proteins and enables HP1α dimerisation and oligomerisation (Figure 1.8). This multivalent interaction of HP1α with the chromatin fibre accelerates the binding of HP1α to chromatin, and prolongs chromatin retention (Kilic et al., 2015).

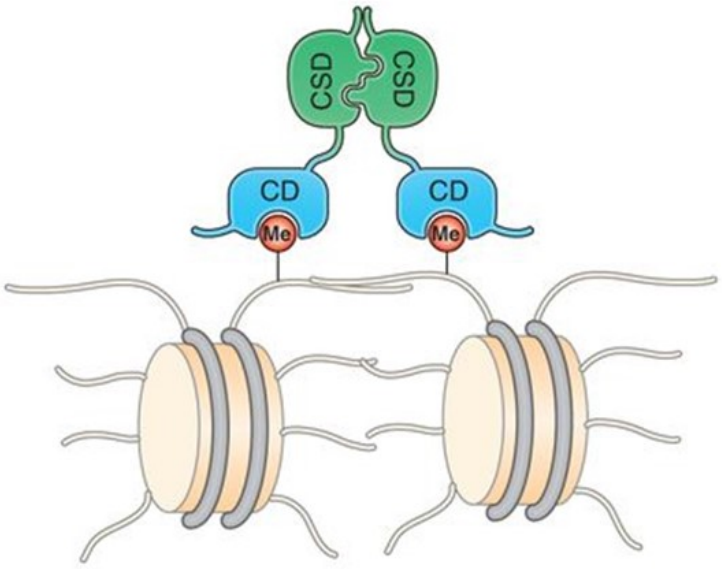

Figure 1.8: Schematic diagram canonical heterochromatin formation. Formation of heterochromatin through HP1α CD (blue) binding to H3K9me2/3 while the CSD (green) dimerises. Adapted from Nishibuchi and Nakayama (2014).

As the basis of heterochromatin formation, H3K9me2/3 can not be the sole determinant as it is present throughout the genome (Muchardt et al., 2002), and

thus it is insufficient in providing specificity in targeting HP1α to heterochromatin (Cowell et al., 2002; Stewart et al., 2005). It has been identified that the formation of constitutive heterochromatin requires the presence of H1 (Bednar et al., 1998), and that H1 is involved in targeting of HP1α to heterochromatin (Meehan et al., 2003). The RNA binding ability of the HP1α hinge region has also been identified as being involved in HP1α targeting (Muchardt et al., 2002). An interaction between H1 and the HP1α hinge region has been shown to be sufficient *in vitro* to bind HP1α to chromatin, in the absence of H3K9me2/3 (Meehan et al., 2003), however this interaction leaves much to be explored.

1.3.4 Targeting of HP1α to heterochromatin by RNA

Early chromosomal studies identified a unique subgroup of protein interacting RNA contained within chromosomes, referred to at the time as chromosomal RNA (Holmes et al., 1972), which associates predominantly with histones (Bonner and Widholm, 1967; Huang and Bonner, 1965). The role of chromosomal RNA has long been queried and its exact purpose is still unknown, however, roles in both inducing heterochromatin formation (Grewal, 2010; Hall and Lawrence, 2016; Johnson et al., 2017) and preventing chromatin compaction in euchromatin have been demonstrated (Hall and Lawrence, 2016). The loss of this RNA often leads to development of euchromatic characteristics (Rodriguez-Campos and Azorín, 2007). RNA within chromatin has been denoted as architectural RNA and is required for the higher organisation of both facultative and constitutive heterochromatin (Nickerson et al., 1989; Soyer-Gobillard and Herzog, 1985; Thakur et al., 2019).

As the RNA binding ability of the HP1α hinge is required for its targeting to constitutive heterochromatin, and non-coding RNA is a component of heterochromatin, RNA may be important in providing the specificity of targeting to genomic loci. *De novo* targeting of HP1α to constitutive pericentric heterochromatin is dependent on the non-coding MSR RNA, which targets Small ubiquitin-like modifier-(SUMO)-ylated HP1α to pericentric heterochromatin (Maison et al., 2011). MSR RNA forms a non-canonical secondary structure containing stem and loop regions (Camacho et al., 2017), which may direct an affinity for HP1α binding.

The HP1α hinge region has been identified to have a strong preference for TERRA, another non-coding RNA, which has a non-canonical G-quadruplex (G4) structure of parallel topology (Roach et al., 2020). TERRA molecules consist of UUAGGG single stranded repeats and can be 100 bp to 9 kb in length (Azzalin et al., 2007; Schoeftner and Blasco, 2008), which form an intra-molecular G4 structure (Martadinata and Phan, 2009; Randall and Griffith, 2009). TERRA facilitates the formation and maintenance of heterochromatin at the telomeres by interacting with telomeric associated proteins such as HP1α (Deng et al., 2009), thus TERRA may target HP1α to telomeres.

1.4 Interaction between H1.4 and HP1α

H1.4 is enriched in heterochromatin (Th'ng et al., 2005), specifically at the telomeric and centromeric regions (Parseghian et al., 2001), and it promotes heterochromatinization (Parseghian, 2015). It is also the only H1 variant which interacts with HP1α (Daujat et al., 2005; Hale et al., 2006). Two different modes of interaction between H1.4 and HP1α have been identified (Figure 1.9). H1.4 has an analogous modification to the H3K9me2/3 mark, of di- and tri-methylated lysine 26 (H1.4K26me2/3), to which the HP1α CD binds (Daujat et al., 2005). At stages during mitosis, POGZ binds to HP1α and activates Aurora B which then phosphorylates H1.4 serine 27 (H1.4S27p) and H3 serine 10 (H3S10p) (Hergeth et al., 2011). This phosphorylation then inhibits the HP1α CD binding H1.4K26me2/3 and H3K9me2/3, and HP1α is evicted from the chromatin fibre (Daujat et al., 2005; Nozawa et al., 2010).

The second interaction is between the H1.4 CTD and HP1α hinge region (Hale et al., 2006). This interaction is regulated by CDK2 which phosphorylates the T/SPKK sites on the H1.4 CTD within the chromatin fibre, and inhibits the interaction of the H1.4 CTD with the hinge region of HP1α (Hale et al., 2006). The interaction between the HP1α hinge region and H1.4 CTD is a potential means of providing specificity in targeting HP1α to heterochromatic regions, which could be mediated by noncoding RNA (Figure 1.9).

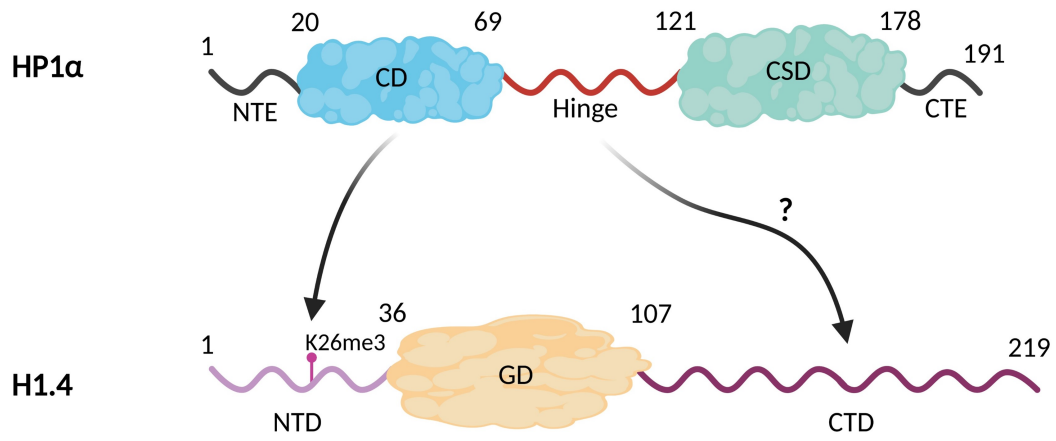

Figure 1.9: Schematic of known and unknown potential interactions of HP1α and H1.4. The CD of HP1α is known to bind H1.4K26me3 while the mechanism of the interaction of the HP1α hinge region and H1.4 CTD is unknown. Both the HP1α hinge and H1.4 CTD contain nucleic acid binding region, providing a possible method of binding. Created with BioRender.

1.4.1 Unpublished data

The previous work showing the interaction between the H1.4 CTD and HP1α hinge was performed as a pulldown assay using bacterially expressed GST-HP1α, where bacterial RNA was potentially mediating the interaction in initial experiments. The interaction was lost when the GST-HP1α was treated with RNase and was restored when total RNA extracted from mammalian cells was added back. However, the type of RNA which could mediate the interaction is yet to be identified.

1.5 Objectives

Given the important roles that histone H1.4 (Duffney et al., 2018; Flex et al., 2019; Tatton-Brown et al., 2017) and HP1α (Feinberg et al., 2016; Norwood et al., 2006; Vad-Nielsen et al., 2016) have been shown to play in heterochromatin, this research seeks to understand how HP1α is targeted to and compacts heterochromatin. Identifying if long noncoding RNA mediates this interaction, and how this interaction affects the behaviour of HP1α in the nucleus, will build on our knowledge and understanding of heterochromatin.

It is hypothesised that the interaction of HP1α with H1.4 is mediated by TERRA and that this establishes heterochromatin.

The aims of this research are to:

1. Determine if long non-coding RNA mediates the interaction of HP1α and H1.4.

   Objectives:

   (a) Develop *in vitro* pulldown assays with His-HP1α and FLAG-H1.4 using total RNA.

   (b) Perform *in vitro* pulldown assays to identify if the long non-coding RNA TERRA mediates the interaction.

2. Investigate if the interaction of H1.4 and HP1α with RNA occurs within a nucleosomal context.

   Objectives:

   (a) Prepare mononucleosomes.

   (b) Use nucleosomal arrays with H1.4 bound in the presence or absence of RNA to test the ability of HP1α to interact with the array and condense it.

Chapter 2

Materials and methods

2.1 Materials

Listed below are the primary antibody (Table 2.1), secondary antibody (Table 2.2) and plasmids (Table 2.3) used in this research.

Table 2.1: Primary antibody used in this research

Antibody	Manufacturer	Raised in	WB dilution
Anti-FLAG	Sigma-Aldrich (F3165)	Mouse	1:1,000

Table 2.2: Secondary antibody used in this research

Antibody	Type	Manufacturer	Raised in	WB dilution
Anti-mouse	HRP	Cytiva (NA931)	Sheep	1:10,000

2.2 Protein expression and purification

2.2.1 Expression and purification of His-HP1α

Competent *Escherichia coli* (*E. coli*) BL21 DE3 cells (Sigma-Aldrich) were transformed with 100 ng of the pET24a plasmid (Sigma-Aldrich) containing hexahistidine-tagged HP1α (His-HP1α) cDNA (Table 2.3) (Roach et al., 2020), using heat shock at 42 °C for 45 seconds. Super Optimal Catabolite (SOC) medium (Sigma-Aldrich) was then added to the cells before a 1 hour incubation at 37 °C with shaking. Cells were then plated on Luria-Bertani (LB) agar containing 50 µg/mL Kanamycin and incubated overnight (16-18 hours) at 37 °C. A single colony was used to inoculate 10 mL of LB broth containing 50 µg/mL Kanamycin and incubated overnight at 37 °C. The overnight culture was centrifuged at 3000 xg for 10 minutes and the pellet, resuspended in fresh LB broth, was then added to 1 L of LB broth containing 50 µg/mL Kanamycin and grown at 30 °C with shaking at 200 rpm until it reached an absorbance of 0.4 at 600 nm. The culture was then chilled for 15 minutes, followed by the addition of isopropyl β-D-1-thiogalactopyranoside (IPTG) to a final concentration of 0.4 mM to induce expression for 18 hours at 22 °C with shaking at 200 rpm. The cells were then centrifuged at 4000 xg for 10 minutes at 4 °C, and the pellet was washed in 10 mM Tris HCl [pH 8] with 100 mM NaCl.

Table 2.3: Plasmids used in this research

Plasmid	Insert	Expression system	Source
pET24a_His-HP1α	Hexahistidine tagged *mus musculus* HP1α cDNA	BL21 DE3 with IPTG	CRG laboratory
pET3d_FLAG-H1.4	FLAG tagged *homo sapien* H1.4 cDNA	BL21 DE3 with IPTG	CRG laboratory
pET3_mH2A	*Mus musculus* H2A type 1 cDNA	BL21 DE3 with IPTG	
pET3_mhH2B	*Mus musculus*/*homo sapien* H2B type 1 cDNA	BL21 DE3 with IPTG	David Tremethick,
pET3_mhH3.1	*Mus musculus*/*homo sapien* H3.1 cDNA	BL21 DE3 with IPTG	The John Curtin
pET3_xH4	Xenopus/*homo sapien* H4 cDNA	BL21 DE3 with IPTG	School of Medical
pUC18_3x200_601	Three repeats of 200 bp containing the 147 bp Widom 601 sequence, with a 33 bp linker upstream and 20 bp linker downstream	PCR amplification	Research, Australian National University
pUC18_1x200_601	200 bp containing the 147 bp Widom 601 sequence with a 33 bp linker upstream and 20 bp linker downstream	PCR amplification	This research
pUC18_TERRA96	T7 RNA promoter upstream of 16 repeats of GGGTTA followed by a BpiI restriction site	*In vitro* T7 RNA polymerase transcription	Carlos Gonzáles, Instituto de química física Rocasolano

The suspended cells were centrifuged at 3000 xg for 10 minutes at 4 °C and then resuspended in 400 mL of lysis buffer (20 mM NaH_2PO_4, 50 mM NaCl, cOmplete™, EDTA-free Protease Inhibitor Cocktail (11873580001, Roche), 1 mM Tris HCl [pH 8], 1 mg/mL lysozyme). After a freeze-thaw, 50 µL of TURBO DNase (Invitrogen) was added, along with imidazole to a final concentration of 20 mM. The lysate was centrifuged at 10,000 rpm for 10 minutes at 4 °C to pellet the cellular debris and the supernatant was filtered through a 0.45 µm filter. The His-HP1α was purified using the ÄKTA Prime Plus (GE Healthcare) chromatography system with a nickel-nitrilotriacetic acid (Ni-NTA) IMAC column. The lysate was loaded onto the column followed by a wash with equilibration buffer (20 mM sodium phosphate, 300 mM NaCl, 20 mM imidazole, [pH 7.5]), and a wash with wash buffer (20 mM sodium phosphate, 300 mM NaCl, 50 mM imidazole, [pH 7.5]). The His-HP1α was then eluted with elution buffer (20 mM sodium phosphate, 300 mM NaCl, 300 mM imidazole, [pH 7.5]), followed by concentrating of selected elution fractions, determined by sodium dodecyl sulfate (SDS) polyacrylamide gel electrophoresis (PAGE) (Section 2.8.1), using the ultrafiltration device Vivaspin 20 (5 kDa MWCO) and then the addition of TCEP to 10 mM.

Size exclusion chromatography (SEC) was performed using the NGC Chromatography System (BioRad) with a Superdex 200 10/300 GL column (GE Healthcare). The purified His-HP1α was eluted (100 mM KCl, 50 mM NaCl, 20 mM NaH_2PO_4, [pH 8]) and the final selected fractions, determined by SDS-PAGE were concentrated. The resultant His-HP1α was quantified using the Pierce™ BCA Protein Assay Kit (Thermo Scientific), determining the purified His-HP1α was 14 mg/mL. The diluted His-HP1α and bovine serum albumin (BSA) standards from the bicinchoninic acid assay were analysed by SDS-PAGE to confirm the bicinchoninic acid assay concentration.

To confirm the presence of secondary structure in the His-HP1α, Circular Dichroism spectra were obtained on the Chirascan (Applied Photophysics Ltd). A 200 µL 50 µM sample of HP1α was measured from 180-350 nm in a 0.1 mm quartz cuvette, with a 1 nm step size. Five spectra were obtained and averaged. Buffer spectra were recorded and subtracted from sample spectra. The spectra was then smoothed 10 points. The Chirascan instrument operation and data analysis were performed using Chirascan v.4.4.1.

2.2.2 Expression and purification of FLAG-H1.4

The pET3d plasmid containing FLAG-tagged H1.4 (FLAG-H1.4) cDNA (Table 2.3) (Hale et al., 2006), 100 ng, was transformed into competent *E. coli* BL21 DE3 cells (Sigma-Aldrich) using heat shock at 42 °C for 45 seconds. SOC medium (Sigma-Aldrich) was then added to the cells, followed by a 1 hour incubation at 37 °C with shaking. Cells were then plated on LB agar containing 100 µg/mL Ampicillin and incubated overnight (16-18 hours) at 37 °C. A single colony was used to inoculate 10 mL of LB broth containing 150 µg/mL Carbenicillin and incubated at 37 °C with shaking for roughly 4 hours until the absorbance reached 0.7 at 600 nm, and then placed at 4 °C overnight. The culture was centrifuged for 5 minutes at 4400 rpm at 4 °C. The pellet was then resuspended in the same volume of fresh LB broth with 150 µg/mL Carbenicillin. To 200 mL of LB broth containing 150 µg/mL Carbenicillin, 5 mL of the resuspended pellet was added. The culture was grown at 37 °C with shaking until the optical density reached an absorbance of 0.7 at 600 nm. To induce the expression of FLAG-H1.4, IPTG was added to a final concentration of 0.4 mM and incubated at 37 °C with shaking at 225 rpm for 2.5 hours. The cultures were then centrifuged at 4000 xg for 5 minutes at 4 °C. The pellet was then resuspended in 100 mL wash buffer (10 mM Tris HCl [pH 8], 100 mM NaCl) and centrifuged at 4000 xg for 5 minutes at 4 °C. The resultant pellet was frozen with liquid nitrogen and stored at -80 °C.

Bacterial pellets were thawed on ice, resuspended in 4 mL Elb lysis buffer (400 mM NaCl, 50 mM HEPES [pH 7.5], 5 mM ethylenediaminetetraacetic acid (EDTA) [pH 8], 0.1 % IGEPAL) with cOmplete™ Protease Inhibitor Cocktail (11697498001, Roche) and placed in 50 mL tube. After a freeze-thaw with liquid nitrogen and a 37 °C water bath, the cells were sonicated at 10 % amplitude for 30 seconds on followed by 30 seconds off for a total of 2 minutes of sonication, followed by an additional freeze-thaw as before. To cells, 364 µL 60 % perchloric acid (PCA) was added, followed by vortexing and incubating on ice for 10 minutes with additional vortexing every 5 minutes. The cells were then centrifuged for 15 minutes at 3700 rpm at 4 °C. The supernatant was aliquoted into 1.7 mL tubes with 1 mL per tube and placed on ice. To each tube, 220 µL 100 % trichloroacetic acid solution (Sigma) was added. The tubes were vortexed and incubated on ice for 30 minutes with additional vortexing every 10 minutes. The extracted proteins were centrifuged 14,000 rpm for 30 minutes at 4 °C followed by washing with 750 µL

acidified acetone (acetone with 0.5 % (v/v) concentrated HCl) and centrifuged for 2 minutes at 14,000 rpm, followed by aspiration of the supernatant. The pellet was then washed with 1 mL acetone (no HCl), centrifuged for 2 minutes at 14,000 rpm and the supernatant aspirated, followed by a second wash in 1 mL acetone. The pellet was then dried by vacuum to remove any remaining acetone. The protein was then resuspended in 250 µL Tris-buffered saline (TBS) (20 mM Tris HCl [pH 7.5, 150 mM NaCl]) with cOmplete™ Protease Inhibitor Cocktail and the 4 tubes were combined. The pH was measured and adjusted to between pH 7 and 8 with 1 M Tris HCl [pH 8].

FLAG-H1.4 was purified from the remaining bacterial protein through a FLAG affinity column containing ANTI-FLAG M2 affinity gel (A2220, Millipore) using gravity flow. The total protein was diluted with the addition of 4 mL TBS with cOmplete™ Protease Inhibitor Cocktail per 1 mL total protein. The purified FLAG-H1.4 was eluted in 0.1 M glycine [pH 3.5] and collected in 500 µL fractions. To the fractions, 12.5 µL 1 M Tris HCl [pH 8] and 20 µL 25x cOmplete™ Protease Inhibitor Cocktail were added.

The resultant FLAG-H1.4 was quantified using the Pierce™ BCA Protein Assay Kit (Thermo Scientific), replacing the provided BSA standards with Calf Thymus Histone, determining the concentration of the FLAG-H1.4 was 0.5 µg/µL. The FLAG-H1.4 and Calf Thymus Histone standards from the bicinchoninic acid assay were analysed by SDS-PAGE (Section 2.8.1) to confirm relative concentrations.

2.2.3 Core histone expression and purification

2.2.3.1 Core histone expression

Competent *E. coli* BL21 DE3 cells (Sigma-Aldrich) were transformed with 100 ng of the pET3 plasmid containing either mH2A, mhH2B, mhH3.1 or xH4 cDNA (Table 2.3), kindly gifted by David Tremethick (The John Curtin School of Medical Research, Australian National University, Canberra, Australia), using heat shock for 45 seconds at 42 °C. SOC medium (Sigma-Aldrich) was then added to the cells before a 1 hour incubation at 37 °C with shaking. Cells were then plated on LB agar containing 100 µg/mL Ampicillin and incubated overnight

(16-18 hours) at 37 °C. A single colony was used to inoculate 10 mL of LB broth containing 150 µg/mL Carbenicillin and incubated with shaking at 200 rpm at 37 °C until just cloudy (4 hours) and then stored at 4 °C overnight. To 100 mL of pre-warmed LB broth containing 150 µg/mL Carbenicillin, 2.5 mL of starter culture was added. The inoculated culture was then grown at 37 °C with shaking until the optical density reached an absorbance of 0.6 at 600 nm. Expression of the histones was induced by the addition of IPTG to a final concentration of 0.4 mM, and incubated for 3-4 hours with shaking at 180 rpm at 37 °C. The cells were then centrifuged at room temperature for 10 minutes at 4000 xg and the pellet was resuspended in 5 mL of wash buffer (50 mM Tris HCl [pH 7.5], 100 mM NaCl, 1 mM β-mercaptoethanol). Cells were then frozen at -80 °C and then stored at -20 °C.

To extract the histones from the cells, inclusion bodies were formed. The cells were thawed in a 37 °C water bath until they were highly viscous followed by the addition of 50 µL of 10 mg/mL lysozyme. The volume was then adjusted to 10 mL with wash buffer and kept on ice. The cells were sonicated at 10 % amplitude for 30 seconds on followed by 30 seconds off for 2 minutes total of sonication, until no longer viscous. The lysate was centrifuged at 4 °C at 18,000 xg for 10 minutes. The inclusion body pellet was resuspended in 5 mL of wash buffer containing 1 % (v/v) Triton X-100 and was dounced in a 15 mL dounce homogeniser with sufficient passes of the pestle to produce a homogeneous solution. The suspension was centrifuged at room temperature at 18,000 xg for 10 minutes and the supernatant discarded. The dounce homogenising with wash buffer with Triton X-100 was repeated and centrifuged as above, followed by two more rounds of douncing with wash buffer without Triton X-100. The pellet was then stored at -20 °C.

To unfold the inclusion bodies, the pellets were resuspended in 2 mL of unfolding buffer by dounce homogenising (6 M guanidinium HCl, 20 mM NaAc [pH 5.2], 1 mM dithiothreitol) and stirred for 2 hours. The inclusion bodies were then centrifuged at room temperature at 18,000 xg for 10 minutes to separate the undissolved proteins from the soluble proteins. The supernatant was then concentrated using Amicon Ultra-0.5 Centrifugal Filter Unit (UFC5010, Millipore).

2.2.3.2 Core histone purification by SEC

SEC was performed using an NGC Chromatography System (BioRad) with a Superdex 200 10/300 GL column (GE Healthcare). The purified histones were eluted in histone SEC buffer (7 M urea, 20 mM NaOAc [pH 5.2], 200 mM NaCl, 5 mM β-mercaptoethanol, 1 mM EDTA). Appropriate fractions, determined by SDS-PAGE (Section 2.8.1) were pooled and dialysed using 6-8 kDa MWCO dialysis tubing by performing three incubations for 6 hours or overnight, at 4 °C in fresh 5 mM β-mercaptoethanol. The dialysed histones were then slowly frozen to -20 °C. The histones were lyophilised and resuspended in water. The concentration of each histone was then determined by measuring the absorbance at 280 nm and calculating the concentration using the molecular weight and extinction coefficient of each histone. The histones were then aliquoted into 45 nmol aliquots, lyophilised and stored at -20 °C.

2.2.3.3 Core histone purification by ion exchange chromatography

Lyophilised histones were resuspended in 4.5 mL urea buffer (7 M urea, 20 mM NaOAc, 2 mM β-mercaptoethanol). The resuspended histones were purified by ion exchange chromatography using a 4 mL bed volume of SP Sepharose FF (Cytiva) in a Glass Econo-Column® Column (Bio-Rad) with gravity flow. The purified histones were eluted with sequential 10 mL additions of increasing NaCl concentrations, listed in Table 2.4. Selected fractions, determined by SDS-PAGE (Section 2.8.1), were pooled and dialysed using 6-8 kDa MWCO dialysis tubing with three 6 hour or overnight incubations at 4 °C in fresh 5 mM β-mercaptoethanol. The dialysed histones were then slowly frozen to -20 °C, lyophilised and resuspended in water. The concentration of each histone was then determined by measuring the absorbance at 280 nm and calculating the concentration using the extinction coefficient and molecular weight of each histone. The histones were then aliquoted into 45 nmol aliquots, lyophilised and stored at -20 °C.

Table 2.4: Ion exchange chromatography buffers

Buffer	Composition
S100	7 M urea, 100 mM NaCl, 20 mM NaOAc, 2 mM β-mercaptoethanol
S150	7 M urea, 150 mM NaCl, 20 mM NaOAc, 2 mM β-mercaptoethanol
S200	7 M urea, 200 mM NaCl, 20 mM NaOAc, 2 mM β-mercaptoethanol
S300	7 M urea, 300 mM NaCl, 20 mM NaOAc, 2 mM β-mercaptoethanol
S500	7 M urea, 500 mM NaCl, 20 mM Tris HCl [pH 8], 2 mM β-mercaptoethanol
S1000	7 M urea, 1000 mM NaCl, 20 mM Tris HCl [pH 8], 2 mM β-mercaptoethanol

2.3 TERRA96 *in vitro* transcription and purification

A Telomeric repeat-containing RNA (TERRA) of 96 nucleotides, TERRA96, was transcribed *in vitro* based on methods previously outlined (McKenna et al., 2007; Garavís et al., 2014) and described below.

2.3.1 TERRA96 *in vitro* transcription

The pUC18_TERRA96 plasmid (Table 2.3, Figure A.2), kindly gifted by Carlos Gonzáles (Instituto de química física Rocasolano, Madrid, Spain) was linearised with BpiI (Thermo Scientific) at 0.2 U/µg with a total of 1 µg of plasmid in a 20 µL volume. The number of units of BpiI per µg of plasmid template was determined first by titrating at 1 U/µg, 0.2 Uµg and 0.02 U/µg. The reactions were incubated at 37 °C for 16-18 hours, followed by inactivation of BpiI at 65 °C for 20 minutes. Completion of linearisation was confirmed through 1 % agarose gel electrophoresis (Section 2.8.2).

To optimise transcription, TERRA96 was transcribed using 30 units of T7 RNA Polymerase (EP0111, Thermo Scientific) with 1 µg of linearised pUC18_TERRA96 plasmid per 50 µL, with reactions titrating $MgCl_2$ concentration at 6 mM, 10 mM, 15 mM, 20 mM, 25 mM and 30 mM. The transcription reactions were incubated at 37 °C for 2 hours, followed by deactivation of the T7 RNA Polymerase at 70 °C for 10 minutes. Transcription was confirmed through denaturing 6.5 M urea 10 %

PAGE (Section 2.8.3). Transcription was then further optimised, with the chosen $MgCl_2$ concentration of 6 mM, through titrating the template amount per 50 µL reaction at 0.5 µg, 1.0 µg and 1.5 µg. The transcription reactions were incubated at 37 °C for 2 hours, followed by deactivation of the T7 RNA Polymerase at 70 °C for 10 minutes. Transcription was confirmed through denaturing 6.5 M urea 10 % PAGE. An equal volume of 30 mM KPi [pH 7] was added to the TERRA96 to give a final concentration of 15 mM KPi. The TERRA96 was then heated at 95 °C for 5 minutes and then cooled slowly to room temperature. The concentration of the TERRA96 was then determined by measuring the absorbance at 260 nm and calculating the concentration using the molecular weight and extinction coefficient.

For large scale TERRA96 production, TERRA96 was transcribed using 80 simultaneous *in vitro* transcription reactions with 30 units T7 RNA Polymerase, 0.5 µg of linearised pUC18_TERRA96 plasmid per 50 µL reaction with 6 mM $MgCl_2$ (as provided in manufacturers buffer), with a total volume of 4 mL. The transcription reactions were incubated at 37 °C for 2 hours, followed by deactivation of the T7 RNA Polymerase at 70 °C for 10 minutes. Transcription was confirmed through denaturing 6.5 M urea 10 % PAGE.

2.3.2 Purification of large scale TERRA96 transcript

Transcribed TERRA96 was purified from the plasmid digestion and transcription enzymes through three successive phenol:chloroform:isoamyl alcohol extractions by the addition of 4 mL UltraPure™ Phenol:Chloroform:Isoamyl Alcohol (25:24:1, v/v) (15593031, Thermofisher), vortexed for 1 minute to combine all phases and centrifuged at 3000 xg for 10 minutes. Residual phenol was then removed through the addition of 4 mL of chloroform, vortexed for 1 minute to combine all phases and centrifuged at 3000 xg for 10 minutes. To desalt and remove any residual chloroform, the aqueous phase was then applied to a Econo-Pac 10DG column (732-2010) following the general protocol using RNA buffer (10 mM mono/di basic phosphate [pH 6.6], 100 mM NaCl). The eluted RNA was then stored at 4 °C overnight. The semi-purified TERRA96 was then concentrated by Amicon Ultra-0.5 Centrifugal Filter Unit to 1 mL. SEC was performed using an NGC Chromatography System (BioRad) with an ENrich™ SEC 70 10 x 300 Column

(7801070, Bio-Rad) to remove any template DNA or aberrant RNA products. The purified TERRA96 was eluted in RNA buffer and selected fractions were pooled and concentrated using Amicon Ultra-0.5 Centrifugal Filter Unit (UFC5010, Millipore). To fold the TERRA96, 1 M KCl was added to a final concentration of 15 mM KCl, then heated to 95 °C for 5 minutes and cooled slowly to room temperature. The concentration of the TERRA96 was then determined by measuring the absorbance at 260 nm and calculating the concentration using the molecular weight and extinction coefficient.

2.4 Total RNA extraction

Total RNA was extracted from either MCF7 or NIH3T3 cells using the QIAGEN RNeasy Kit according to the manufacturers instructions and quantified using a DeNovix spectrophotometer by measuring the absorbance at 260 nm.

2.5 *In vitro* pulldown assay

HisPur™ Ni-NTA Resin was washed three times in cold RNA Binding Buffer (150 mM KCl, 25 mM Tris HCl [pH 8], 0.2 % IGEPAL, 10 mM imidazole [pH 8]) by pelleting beads at 700 xg for 2 minutes at 4 °C. Purified His-HP1α was then bound to the beads (30 µg per 20 µL bed volume per reaction) as a 10 % bead solution, equivalent buffer was added in place of HP1α when HP1α was omitted. Incubation was carried out at room temperature with gentle rotation for 1 hour. The beads were then thoroughly washed with cold Wash Buffer (1x Dulbecco's phosphate-buffered saline (10x 14200166, ThermoFisher), 25 mM imidazole [pH 8]) by pelleting beads at 700 xg for 2 minutes at 4 °C, followed by a wash with cold RNA Binding Buffer and resuspended in RNA Binding Buffer to give a 20 % bead solution. Beads were aliquoted to 100 µL per sample with RNA as indicated, along with additional RNA Binding Buffer to give a total reaction volume of 600 µL. The beads were incubated at 4 °C with gentle mixing for 2 hours, followed by a thorough wash with cold H1.4 Binding Buffer (25 mM Tris HCl [pH 8], 10 % glycerol, 250 mM NaCl, 0.225 % IGEPAL, 10 mM imidazole [pH 8]) by

pelleting the beads at 700 xg for 2 minutes. Purified FLAG-H1.4 (2.6 µg) was added to the beads, along with 700 µL cold H1.4 Binding Buffer, 6 µL acetylated BSA (5 µg/µL) and 5 µL SUPERase•In (20 units/µL). The binding reaction was incubated overnight (16-18 hours) at 4 °C with gentle rotation. The beads were then washed four times with cold H1.4 Binding Buffer by pelleting the beads at 700 xg for 2 minutes at 4 °C. The bound proteins were then eluted with 1.5x SDS-PAGE loading dye (93.75 mM Tris HCl pH [6.8], 2.51 % SDS, 11.25 % glycerol, 0.015 % bromophenol blue, 53.63 mM β-mercaptoethanol) by heating at 95 °C for 5 minutes and resolved by 12 % SDS-PAGE (Section 2.8.1).

Western blot was performed by transferring the proteins from the gel to 0.1 µm nitrocellulose (GEHE10600010, Amersham) in a Trans-Blot® Cell (BioRad) with AMPSO transfer buffer (25 mM AMPSO [pH 9.5], 20 % v/v methanol) at 60 volts for 2 hours at 4 °C. The nitrocellulose membrane was then blocked in western blocking buffer (5 % non-fat milk, 1x TBS, 0.05 % Tween-20) for 1 hour on a rocker at room temperature. Primary antibody (Table 2.1) was diluted in western blocking buffer and incubated on the membrane overnight on a rocker at 4 °C. The blot was rinsed with 1x TBS with 0.05 % Tween-20, followed by two 5 minute washes and two 10 minute washes in 1x TBS with 0.05 % Tween-20 at room temperature on an orbital shaker. Secondary antibody (Table 2.2) was diluted in western blocking buffer and incubated on the blot for 1 hour at room temperature on a rocker. The blot was rinsed with 1x TBS with 0.05 % Tween-20, followed by two 5 minute washes and two 10 minute washes in 1x TBS with 0.05 % Tween-20 at room temperature on an orbital shaker. The blot was then developed using the ECL Prime (Amersham) system and imaged using the chemiluminescence function on an Azure c600 (Azure Biosystems), with the exposure time as indicated.

2.6 *In vitro* nucleosome assembly

2.6.1 Histone octamer reconstitution by salt gradient dialysis

Lyophilised 45 nmol histone aliquots were dissolved in 0.5 mL unfolding buffer (6 M guanidinium HCl, 20 mM NaAc [pH 5.2], 1 mM dithiothreitol) and incubated at room temperature for at least 30 minutes, until all powder was dissolved. One of each histone aliquot were then combined, giving a total volume of 2 mL. To form octamers, the histone mix was dialysed at 4 °C against 1.5 L of refolding buffer (2 M NaCl, 10 mM Tris HCl [pH 7.5], 1 mM EDTA) with 5 mM β-mercaptoethanol for 4 hours using 6-8 kDa MWCO dialysis tubing. The histones/octamers were then dialysed against 2 L of refolding buffer with with 5 mM β-mercaptoethanol overnight at 4 °C, and subsequently dialysed against 1 L of refolding buffer with 5 mM β-mercaptoethanol for 2 hours. The octamers were recovered from the dialysis tubing and centrifuged at room temperature at 14,000 rpm for 5 minutes to remove any precipitate. The supernatant was then concentrated using an Amicon Ultra-0.5 Centrifugal Filter Unit (UFC5010, Millipore).

SEC was performed using an NGC Chromatography System (BioRad) with a Superdex 200 10/300 GL column (GE Healthcare). The purified octamers were eluted in refolding buffer with 1 mM dithiothreitol and selected fractions, determined by SDS-PAGE (Section 2.8.1), were pooled and concentrated using Amicon Ultra-0.5 Centrifugal Filter Unit (UFC5010, Millipore). The octamers were then quantified by measuring the absorbance at 280 nm and calculating the concentration using the molecular weight and extinction coefficient of the octamer. The octamers were then mixed 1:1 with octamer storage buffer (10 mM Tris HCl [pH 7.5], 1 mM EDTA, 1 mM dithiothreitol, 1 M NaCl, 80 % glycerol) and stored at -20 °C.

2.6.2 Amplification and purification of nucleosome positioning sequence

A pUC18 plasmid containing three repeats of 200 bp containing the 147 bp Widom 601 sequence (Lowary and Widom, 1998), with a 33 bp linker upstream and 20 bp linker downstream (pUC18_3x200_601) (Table 2.3, Figure A.3), was kindly gifted by David Tremethick (The John Curtin School of Medical Research, Australian National University, Canberra, Australia).

2.6.2.1 pUC18_1x200_601 plasmid cloning

Inverse PCR primers (Inv_For and Inv_Rev (Figure A.3) (Table A.1)) were designed to remove two of the three 200 bp repeats. PCR with KAPA HiFi PCR Kit (KK2101, KAPABIOSYSTEMS) was performed as per the manufacturers instructions as a gradient PCR at 62 °C, 64 °C, 66 °C and 68 °C to determine the optimal annealing temperature. The resultant PCR products were resolved through electrophoresis in 1.5 % agarose (Section 2.8.2). The PCR was repeated with the annealing temperature at 62 °C. The PCR products were resolved in 1.5 % agarose and the product of the appropriate length for one repeat was extracted with the QIAquick gel extraction kit (28704, Qiagen). The linear plasmid was then phosphorylated with T4 polynucleotide kinase (EK0031, ThermoFisher) as per the manufacturers instructions. The phosphorylated linear fragment was then quantified through 1 % agarose gel electrophoresis with MassRuler (SM0403, ThermoFisher). The linear plasmid was then ligated with T4 DNA ligase (M0202, New England BioLabs), with 100 ng linear plasmid in a 15 µL reaction, at room temperature for 2 hours, followed by heat inactivation at 65 °C for 10 minutes. Competent *E. coli* DH5α cells (ThermoFisher) were transformed with 5 µL of the ligated plasmid in 50 µL of cells, using heat shock at 42 °C for 45 seconds. SOC medium (Sigma-Aldrich) was then added to the cells, followed by a 1 hour incubation at 37 °C with shaking. The cells were then centrifuged for 5 minutes at 5000 rpm, followed by removal of 400 µL of the supernatant. The cells were then resuspended in the remaining 150 µL of supernatant and plated on LB agar containing 100 µg/mL ampicillin and incubated overnight (16-18 hours) at 37 °C. Multiple overnight cultures were set up with a single colony used to inoculate 5

mL of LB broth containing 100 µg/mL ampicillin and incubated overnight at 37 °C. The plasmids were extracted from the cells using QIAprep Spin Miniprep Kit (27104, Qiagen). To identify correct clones, plasmids were linearised with KpnI as per the manufactures instructions (ER0521, Thermo Fisher) and resolved in 1 % agarose. Clones of the correct length were then sequenced to confirm the insert was correct, followed by amplification and extraction of the plasmid through QIAGEN Plasmid Midi Kit (12143, Qiagen), yielding the pUC18 plasmid with one 200 bp repeat containing the Widom 601 sequence (Lowary and Widom, 1998) (pUC18_1x200_601) (Table 2.3, Figure A.4).

2.6.2.2 Amplification of Alexa488_1x237_601 fragment

PCR primers (Alexa488_601_For and DNA_601_Rev (Table A.1 and Figure A.4)) were designed flanking the 200 bp repeat in the pUC18_1x200_601 plasmid, with the forward primer labelled with the Alexa488 fluorophore and reverse primer unlabelled, generating a 237 bp Alexa488 labelled fragment (Alexa488_1x237_601). PCR with MyTaq™ HS DNA Polymerase (BIO-21112, Bioline) was performed as per the manufacturers instructions as a gradient PCR at 55 °C, 57 °C, 59 °C and 61 °C to determine the optimal annealing temperature, with 35 cycles. The resultant PCR products were resolved through electrophoresis in 1.5 % agarose (Section 2.8.2). The PCR was repeated with the annealing temperature at 61 °C, with the amount of DNA template titrated at 10 ng and 20 ng per 50 µL PCR reaction, and titrating the number of cycles at 35 and 45 cycles to determine optimal PCR conditions. The resultant PCR products were resolved in 1.5 % agarose.

To generate the fragment for mononucleosome formation, 32 simultaneous PCR reactions were performed with 10 ng of template per 50 µL reaction at 61 °C, with 45 cycles. The PCR products were concentrated to 400 µL by vacuum and were resolved in 1.5 % agarose in the dark and extracted using the QIAquick gel extraction kit. The Alexa488_1x237_601 fragment was ethanol precipitated with GlycoBlue™ Coprecipitant (AM9515, ThermoFisher) and resuspended in 10 mM Tris HCl [pH 8.0]. To determine the concentration of the fragment, the absorbance at 260 nm was measured and concentration was calculated using the extinction coefficient and molecular weight.

2.6.3 Mononucleosome formation

Mononucleosome formation reactions were prepared with 2 M NaCl, 1x Tris-EDTA (TE) (10 mM Tris HCl [pH] 7.5, 1 mM EDTA [pH] 8), Alexa488_1x237_601 as indicated, and 25 pmol octamer, added after other components were mixed, in a final volume of 29 µL. After thorough mixing, reactions were then incubated on ice for 30 minutes. Reactions were dialysed in 0.2 mL Eppendorf lids with 6-8 kDa MWCO dialysis membrane against reducing NaCl levels outlined in Table 2.5, with dithiothreitol added when indicated, at 4 °C in the dark. Reconstitution levels were analysed by native PAGE (Section 2.8.4). Mononucleosome concentrations were estimated by measuring the absorbance at 260 nm and using the extension coefficient and molecular weigh of Alexa488_1x237_601 and calculating the concentration of the DNA fragment.

Table 2.5: Mononucleosome dialysis steps

Dialysis time	Dialysis buffer
30 minutes	1x TE, 2 M NaCl
3 hours	1x TE, 1 M NaCl
Overnight	1x TE, 0.7 M NaCl
2 hours	1x TE, 5 mM NaCl

2.7 Electrophoretic mobility shift assay

An electrophoretic mobility shift assay (EMSA) was performed by combining FLAG-H1.4 as indicated with 0.38 pmol mononucleosomes in gel binding buffer 1x (10 mM Tris HCl [pH 7.5], 25 mM NaCl, 25 mM KCl, 0.2 mM dithiothreitol, 4 % polysucrose 400) and incubated at room temperature for 30 minutes. Samples were electrophoresed through 5 % native PAGE (Section 2.8.4).

2.8 Gel electrophoresis

2.8.1 SDS-PAGE

First a 12 % resolving gel was made (12 % 29:1 acrylamide/bisacrylamide, 375 mM Tris HCl [pH 8.8], 0.1 % SDS, 0.1 % ammonium persulfate (APS), 0.1 % tetramethylethylenediamine (TEMED)). Atop of this, a stacking gel was made and set (5 % 29:1 acrylamide/bis-acrylamide, 125 mM Tris HCl [pH 6.8], 0.1 % SDS, 0.1 % APS, 0.1 % TEMED). Samples were mixed with 6x SDS-PAGE loading dye to a final concentration of 1x SDS-PAGE loading dye (62.5 mM Tris HCl pH [6.8], 1.67 % SDS, 7.5 % glycerol, 0.01 % bromophenol blue, 37.75 mM β-mercaptoethanol) and heated at 95 °C for 5 minutes before loading. Samples were electrophoresed through a 5 % stacking gel followed by a 12 % resolving gel in 1x TGS buffer (25 mM Tris, 192 mM glycine, 0.1 % SDS), at a constant 150 volts until the bromophenol blue dye front reached the bottom of the stacking gel. Gels were fixed by incubation in 10 % acetic acid and 40 % ethanol for 15 minutes, followed by staining of the proteins with QC Colloidal Coomassie Stain (Bio-Rad) for 18-20 hours. Gels were de-stained in MilliQ water until the contrast was satisfactory, followed by imaging under white light on a GelDoc. Proteins sizes were estimated using Precision Plus Protein Dual Color Standards (1610374, Bio-Rad).

2.8.2 Agarose gel electrophoresis

An agarose gel, percentage as specified, was made in 1x TAE (40 mM Tris, 20 mM Acetic Acid, 1 mM EDTA) with 0.5 µg/mL ethidium bromide (EtBr). Samples were mixed with 10x Blue Juice (10816015, ThermoFisher) to a final concentration of 1x before loading. Samples were electrophoresed through the agarose gel in 1x TAE with 0.5 µg/mL EtBr at a constant 100 volts until the bromophenol blue had traveled sufficient distance through the agarose. Gels were then visualised and imaged through UV-transillumination on a GelDoc. DNA sizes were estimated using either 1 Kb Plus DNA Ladder (1 Kb+) (10787018, ThermoFisher) or MassRuler DNA Ladder Mix (MR) (SM0403, ThermoFisher), as indicated.

2.8.3 Urea-PAGE

A 10 % gel was made (10 % 19:1 acrylamide/ bisacrylamide, 1x TBE (89 mM Tris, 2 mM EDTA, 89 mM boric acid), 6.5 M urea, 0.08 % APS, 0.04 % TEMED) and pre-run at 150 volts for 30 minutes. Samples were mixed with 2x RNA Loading Dye (B0363AVIAL, New England BioLabs) to a final concentration of 1x and heated at 95 °C for 5 minutes before loading. Samples were electrophoresed through the 10 % gel in 1x TBE buffer at a constant 150 volts until the bromophenol blue dye front reached the bottom of the gel. To stain the RNA, gels were incubated in 0.3 % Stains-All (E9379, Sigma-Aldrich) with 50 % formamide for 30 minutes in the dark, followed by de-staining in MilliQ water in the light until the contrast was satisfactory. Gels were imaged in a lightbox on an iPhone XR to produce multicoloured images. RNA species sizes were estimated using Low Range ssRNA Ladder (N0364SVIAL, New England BioLabs).

2.8.4 Native-PAGE

A 5 % gel was made (5 % 49:1 acrylamide/bisacrylamide, 0.5x TBE (44.5 mM Tris, 1 mM EDTA, 44.5 mM boric acid), 0.1 % APS, 0.1 % TEMED). Gels were pre-run at 150 volts for 30 minutes. Samples were mixed with 5x gel binding buffer to a final concentration of 1x (10 mM Tris HCl [pH 7.5], 25 mM NaCl, 25 mM KCl, 0.2 mM dithiothreitol, 4 % polysucrose 400) and incubated on ice for 30 minutes before loading. Samples were electrophoresed through the 5 % gel in 0.2x TBE buffer (17.8 mM Tris, 0.4 mM EDTA, 17.8 mM boric acid) at a constant 150 volts for 45 minutes, tracking the progression of the samples with 1x gel binding buffer with 0.05 % bromophenol blue, loaded alongside samples. Gels were imaged on FLA-5000 laser scanner at 478 nm, imaging Alexa488 labelled DNA. Proteins were then fixed in the gel by incubation in 10 % acetic acid and 40 % ethanol for 15 minutes, followed by staining of the proteins with QC Colloidal Coomassie Stain (Bio-Rad) for 18-20 hours. Gels were de-stained in MilliQ water until the contrast was satisfactory, followed by imaging under white light on a GelDoc.

Chapter 3

Investigating if TERRA mediates the H1.4-HP1α interaction

3.1 Introduction

An interaction with H1.4, which is enriched in compact chromatin, provides a potential means for targeting HP1α to heterochromatin. While the hinge region of HP1α can bind non-specifically to nucleic acid (Bryan et al., 2017; Meehan et al., 2003; Muchardt et al., 2002; Nishibuchi et al., 2014), *in vitro*, it has been shown to bind non-coding RNA such as Major satellite repeat RNA (MSR RNA) and Telomeric repeat-containing RNA (TERRA)(Maison et al., 2011; Roach et al., 2020). To determine if TERRA can mediate this interaction, an *in vitro* pulldown system using purified HP1α and H1.4 was established. Firstly, His-HP1α and FLAG-H1.4 were prepared, the pulldown assay established and then TERRA prepared and tested to determine if it could mediate the H1.4-HP1α interaction.

3.2 Development of HP1α-H1.4 pulldown assay

The pulldown was to be performed with hexahistidine-tagged HP1α (His-HP1α) and FLAG-tagged H1.4 (FLAG-H1.4), which first needed to be produced.

3.2.1 Expression and purification of His-HP1α

To express His-HP1α (see Section 2.2.1), *E. coli* BL21 DE3 cells were transformed with pET24a_His-HP1α (see Section 2.1, Table 2.3), a plasmid that expresses *mus musculus* HP1α with an amino-terminus hexahistidine-tag. To induce the expression of His-HP1α, isopropyl β-D-1-thiogalactopyranoside (IPTG) was added to the cells and the culture was incubated at 22 °C for 18 hours. The culture was sampled before and after induction, and the cell lysates were resolved by 12 % sodium dodecyl sulfate (SDS) polyacrylamide gel electrophoresis (PAGE) (see Section 2.8.1) to determine the level of His-HP1α induction. In Figure 3.1, the presence of the band in the gel at 25 kDa in the after induction lane, which is absent in the before induction lane, confirmed the expression of His-HP1α. To confirm the His-HP1α was soluble in the cell lysate, the cultured cells were washed, lysed and centrifuged to separate the soluble proteins from the cellular debris. The lysed proteins were then separated by 12 % SDS-PAGE. Figure 3.1

shows that the majority of the His-HP1α was in the soluble fraction, however some did remain in the insoluble fraction.

To purify the His-HP1α from the *E. coli* lysate, the soluble lysate was loaded on a nickel-nitrilotriacetic acid (Ni-NTA) column, washed and then bound proteins were eluted. The elution fractions with high absorbance at 280 nm were analysed by 12 % SDS-PAGE. From the gel (Figure 3.1), fractions 31-34 contained higher levels of His-HP1α and were combined and concentrated. To further purify His-HP1α, the protein was size excluded using a Superdex 200 10/300 GL column to remove contaminating *E. coli* proteins. Size exclusion chromatography fractions with high absorbance at 280 nm were then resolved by 12 % SDS-PAGE to determine which fractions contained His-HP1α. Figure 3.2 shows that fractions B07-B14 contained the highest levels of His-HP1α in the gel, and fractions B07-B15 were combined and concentrated.

To quantify the purified His-HP1α, a bicinchoninic acid assay with bovine serum albumin (BSA) standards was performed, then 1.0 µg and 0.5 µg His-HP1α, based on this quantification, was checked by 12 % SDS-PAGE against the BSA standards. Figure 3.3 shows that the amount of His-HP1α loaded in the gel appears less than the equivalent amount of BSA. However, Coomassie blue staining is more susceptible to differences in protein composition as it binds specific residues, while the bicinchoninic acid assay measurement is based around the protein backbone, making Coomassie less sensitive (He, 2011). To check if the His-HP1α was folded, circular dichroism spectra were obtained to determine if secondary structures were present. The obtained spectra (Figure A.1a) were consistent with previously published HP1α circular dichroism spectra (Figure A.1b) (Roach et al., 2020).

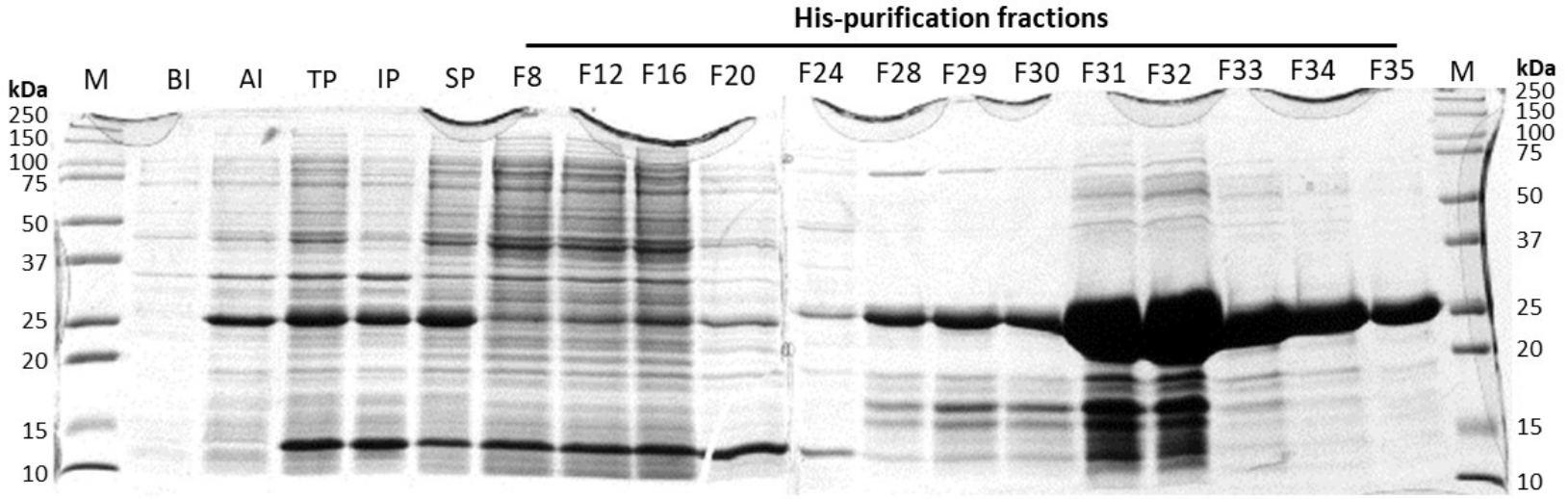

Figure 3.1: Induction of His-HP1α expression and His-purification. Before and after IPTG induction, total protein, soluble and insoluble protein, and Ni-NTA column His-purification elution fractions (20 µL of each fraction) were analysed by 12 % SDS-PAGE, and stained with Coomassie blue. BI - Culture before IPTG induction, 15 µL. AI - Culture after IPTG induction, 15 µL. TP - Total protein of lysed cells, 10 µL. IP - Insoluble protein, 10 µL. SP - Soluble protein, 10 µL. The approximate molecular weight of His-HP1α is 25 kDa. M - Molecular weight marker.

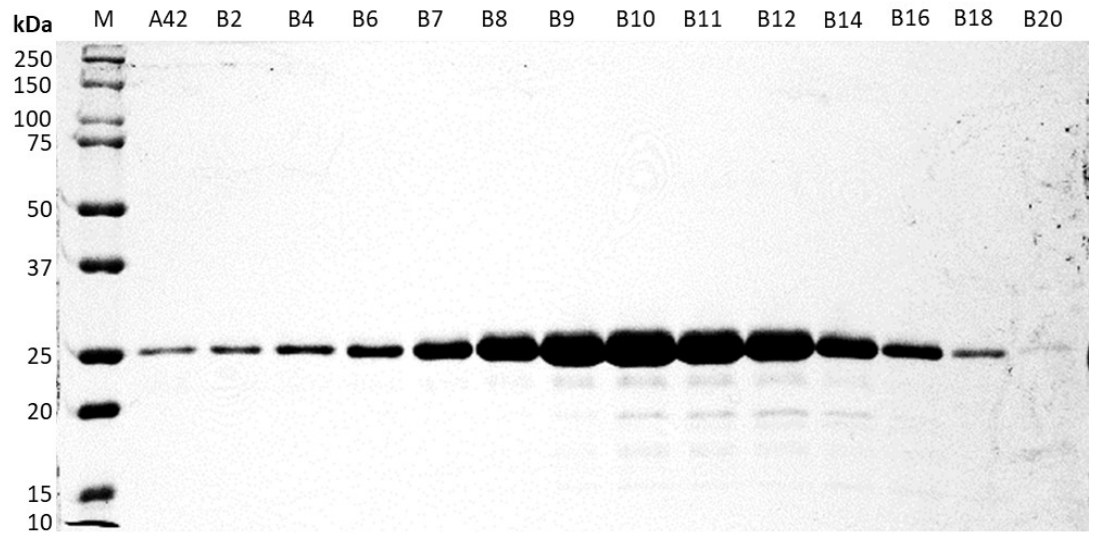

Figure 3.2: His-HP1α size exclusion chromatography purification. His-HP1α size exclusion fractions (2 µL of each fraction) were analysed through 12 % SDS-PAGE, then stained with Coomassie blue. M - Molecular weight marker.

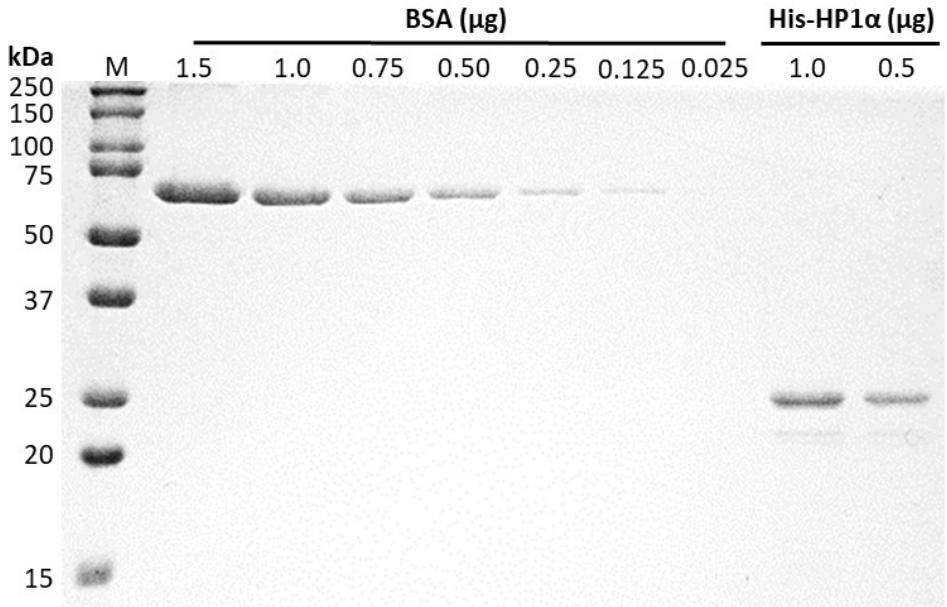

Figure 3.3: His-HP1α quantification. Purified His-HP1α and BSA protein standards were resolved through 12 % SDS-PAGE, and stained with Coomassie blue. M - Molecular weight marker.

3.2.2 Expression and purification of FLAG-H1.4

To express FLAG-H1.4 (see Section 2.2.2), pET3d_FLAG-H1.4 (see Section 2.1, Table 2.3), an amino-terminus FLAG-tagged *homo sapien* H1.4 expression plasmid, was transformed into *E. coli* BL21 DE3 cells. Expression of FLAG-H1.4 was induced by the addition of IPTG to the culture and then incubated for 2.5 hours at 37 °C. Samples of the culture were taken before and after induction and were then separated by 12 % SDS-PAGE (see Section 2.8.1). Shown in Figure 3.4, the absence of a band at 37 kDa in the before induction lane which was then present in the after induction lane confirmed the expression of FLAG-H1.4. FLAG-H1.4 was then extracted from the cellular debris with perchloric acid (PCA), which precipitates the bacterial proteins while the FLAG-H1.4 remains soluble due to its highly basic nature (H1.4 isoelectric point - 11.03 (Osunsade et al., 2018)). FLAG-H1.4 was then precipitated by the addition of trichloroacetic acid, after which the FLAG-H1.4 was resuspended in a neutral buffer. The resuspended FLAG-H1.4 was resolved by 12 % SDS-PAGE. Figure 3.4 confirms the presence of FLAG-H1.4 with a faint band at 37 kDa, and shows that most of the bacterial proteins had been removed.

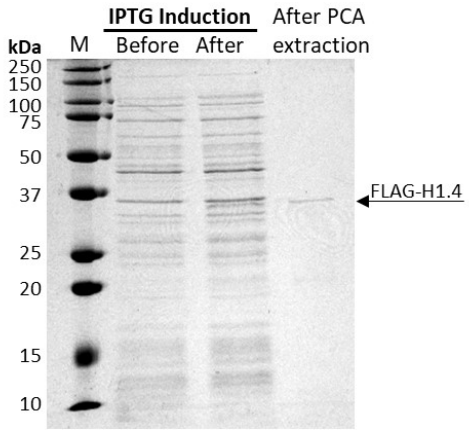

Figure 3.4: Induction of FLAG-H1.4 expression and PCA extraction. Before and after IPTG induction (10 µL of culture) and after PCA extraction (1 µL of 1:20 dilution) samples were analysed through 12 % SDS-PAGE, then stained with Coomassie blue. The approximate molecular weight of FLAG-H1.4 is 23.5 kDa, however, it appears heavier due to the basic nature of the protein. M - Molecular weight marker.

The FLAG-H1.4 was then affinity purified from the remaining *E. coli* proteins using a ANTI-FLAG M2 affinity gel column. The PCA extracted FLAG-H1.4 was applied to the column, washed and then eluted. The sample application flow

through, wash and elution fractions were analysed by 12 % SDS-PAGE. Shown in the gel (Figure 3.5), elution fractions E5-E8 contained the highest levels of FLAG-H1.4 and were combined, with the concentration then determined using a bicinchoninic acid assay. To give a more accurate concentration, as H1 is a highly basic protein, quantitation using the bicinchoninic acid assay was performed with calf thymus histone standards. To check the concentration determined by bicinchoninic acid assay, 0.5 µg and 1.0 µg FLAG-H1.4 and calf thymus histone standards were resolved by 12 % SDS-PAGE. Figure 3.6 confirms the quantification of the FLAG-H1.4.

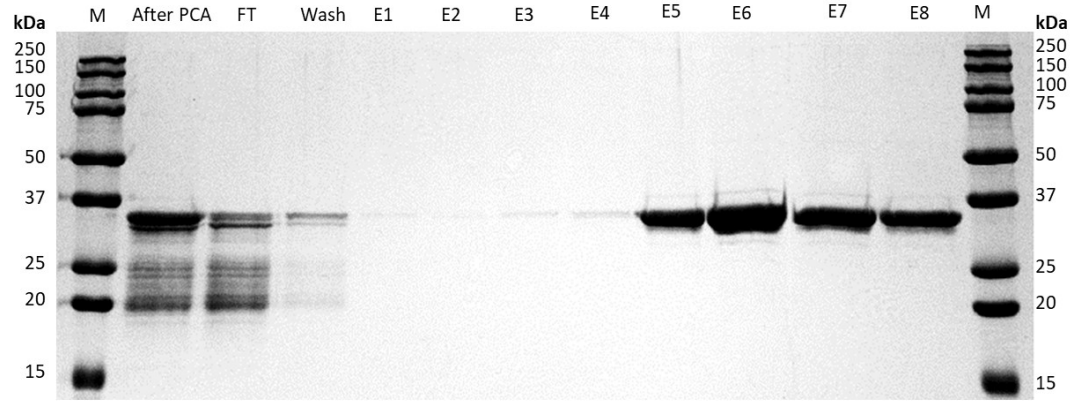

Figure 3.5: FLAG-H1.4 FLAG affinity purification. After PCA extraction (2 µL) and FLAG affinity column sample application flowthrough, wash and elution fractions (10 µL of wash and each fraction) were analysed through 12 % SDS-PAGE, and stained with Coomassie blue. FT - Sample application flowthrough, 10 µL. M - Molecular weight marker.

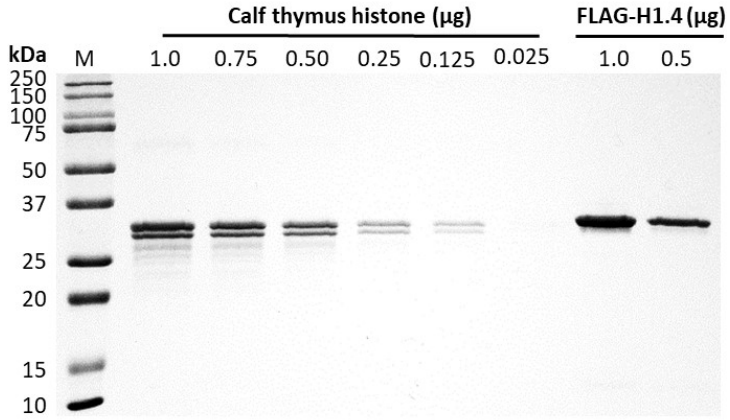

Figure 3.6: FLAG-H1.4 quantification. Purified FLAG-H1.4 and calf thymus histone standards were resolved through 12 % SDS-PAGE, then stained with Coomassie blue. M - Molecular weight marker.

3.2.3 Total RNA mediates the H1.4-HP1α interaction

To establish the His-HP1α pulldown system, initially it was tested if total RNA could mediate the interaction between His-HP1α and FLAG-H1.4. His-HP1α was bound to HisPur™ Ni-NTA beads at 30 µg His-HP1α per 20 µL bed volume for 1 hour at room temperature, and then washed (see Section 2.5 and Figure 3.7). RNA binding reactions were assembled and were incubated at 4 °C for 2 hours, with no RNA, 4 µg or 8 µg of total RNA extracted from MCF7 cells (see Section 2.4). To remove any unbound RNA, the beads were washed. FLAG-H1.4 was then added at 2.6 µg per reaction and then incubated overnight at 4 °C. The beads were then washed to remove any unbound FLAG-H1.4. The resultant complexes from the binding reactions were resolved by 12 % SDS-PAGE (see Section 2.8.1). Immunoblotting was performed with anti-FLAG (see Section 2.1, Table 2.1) to detect if FLAG-H1.4 had been pulled down.

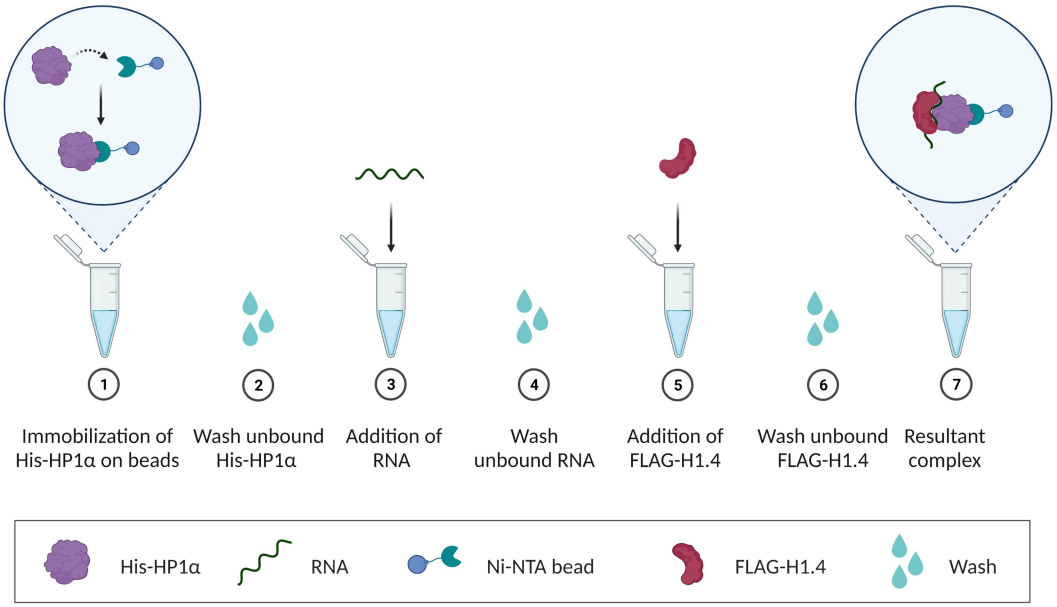

Figure 3.7: Schematic diagram of His-HP1α pulldown. Created with BioRender.

As shown in Figure 3.8, the bands present in the total RNA lanes showed that FLAG-H1.4 had been pulled down by the total RNA at 4 and 8 µg, thus total RNA mediates the interaction between FLAG-H1.4 and His-HP1α. There was no band in the absence of RNA, illustrating that FLAG-H1.4 was not bound. This indicated that not only was RNA required to mediate the interaction, but

additionally the FLAG-H1.4 did not bind directly to the HisPur™ Ni-NTA beads. The FLAG-H1.4 input control was detected, illustrating that the FLAG antibody could detect the FLAG-H1.4.

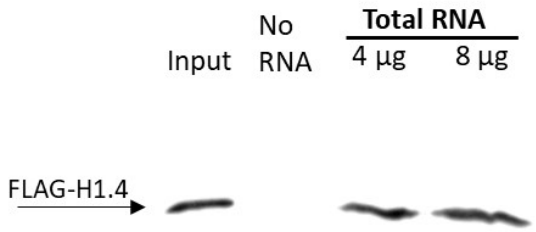

Figure 3.8: Total RNA mediates the H1.4-His-HP1α interaction in an *in vitro* pulldown. *In vitro* His-HP1α pulldown and western blot with the addition of MCF7 total RNA, titrated at 0 µg (no RNA), 4 µg and 8 µg, to His-HP1α bound beads (30 µg His-HP1α per 20 µL bed volume), followed by the addition of 2.6 µg of FLAG-H1.4. Bound FLAG-H1.4 was detected by immunoblotting against FLAG with a FLAG antibody, 5 second chemiluminescence exposure. Input - 23 % FLAG-H1.4.

3.3 *In vitro* transcription and purification of TERRA

Since total RNA was confirmed to mediate the interaction, a 96 nucleotide TERRA molecule, TERRA96, which has previously been shown to interact with HP1α (Roach et al., 2020), was generated by *in vitro* transcription (McKenna et al., 2007; Garavís et al., 2014).

3.3.1 Optimisation of TERRA96 *in vitro* transcription

Before *in vitro* transcription could be performed, the circular plasmid pUC18_TERRA96 (Table 2.3 and Figure A.2), containing a T7 RNA polymerase promoter upstream of a 96 bp telomeric repeat, had to be linearised using the BpiI restriction site downstream of the repeat to ensure transcription stops. To optimise linearisation of pUC18_TERRA96 with BpiI, the restriction digest was performed with 0.2

or 0.02 units of BpiI per 1 µg of pUC18_TERRA96 (Garavís et al., 2014) (see Section 2.3.1). Linearisation of the plasmid was analysed by 1 % agarose gel electrophoresis (see Section 2.8.2). As shown in Figure 3.9, circular supercoiled, undigested pUC18_TERRA96 migrated with an approximate molecular weight of around 1500 bp. Partial digestion of pUC18_TERRA96 occurred with 0.02 units of BpiI, shown by the presence of multiple differently migrating bands, including undigested pUC18_TERRA96 (Figure 3.9). Digestion of pUC18_TERRA96 by 0.2 units of BpiI generated one main digestion product which migrated around 2900 bp, consistent with the expected linear length of 2761 bp (Figure 3.9). This determined that pUC18_TERRA96 could be linearised by 0.2 U of BpiI per 1 µg of pUC18_TERRA96, while 0.02 U of BpiI yielded only partial digestion.

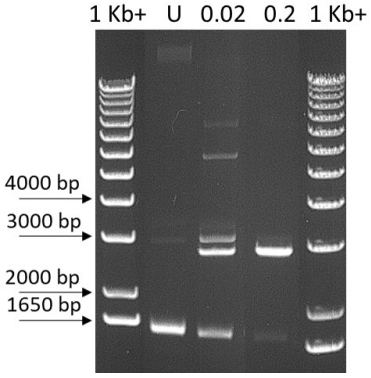

Figure 3.9: Digestion of pUC18_TERRA96 by BpiI reaches completion with 0.2 U of BpiI per 1 µg of pUC18_TERRA96. Restriction digests with 0.02 U of BpiI or 0.2 U BpiI per 1 µg of pUC18_TERRA96 were analysed by EtBr staining in 1 % agarose, with 1 µL aliquots of restriction digests. U - Undigested pUC18_TERRA96, 50 ng. 1 Kb+ - DNA ladder.

The *in vitro* transcription reaction was then optimised. Using 1 µg of linearised pUC18_TERRA96 (Figure 3.10), the first optimisation step was to titrate the amount of $MgCl_2$ present in the transcription reaction. $MgCl_2$ was titrated in 50 µL reactions from 6 mM (no additional $MgCl_2$ to the transcription buffer provided) to 30 mM. Reactions were incubated at 37 °C for 2 hours with 30 units of T7 RNA polymerase. *In vitro* transcription reactions were resolved by 6.5 M urea 10 % PAGE (see Section 2.8.3). Figure 3.11 shows that the most intense band at around 96 bases, was transcribed in 6 mM $MgCl_2$, illustrating that no additional $MgCl_2$ was required in the *in vitro* transcription reaction.

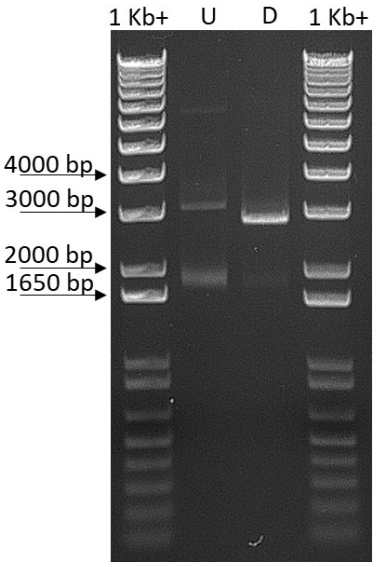

Figure 3.10: pUC18_TERRA96 was digested with BpiI for transcription optimisation. Digestion of pUC18_TERRA96 with 0.2 U of BpiI per 1 µg of pUC18_TERRA96 was analysed by EtBr staining in 1 % agarose. U - Undigested pUC18_TERRA96, 50 ng. D - Restriction digest, 1 µL. 1 Kb+ - DNA ladder.

To further optimise the *in vitro* transcription reaction, the amount of linearised pUC18_TERRA96 added was titrated in an attempt to increase yield. Linearised pUC18_TERRA96 was titrated in 50 µL reactions at 0.5 µg, 1.0 µg and 1.5 µg and reactions were incubated at 37 °C for 2 hours with 30 units of T7 RNA polymerase. The level of *in vitro* transcription in the reactions was analysed by 6.5 M urea 10 % PAGE. Illustrated by Figure 3.12, the most intense band at 96 bases was transcribed in the *in vitro* transcription reaction with 0.5 µg of template. This determined that the optimal *in vitro* transcription conditions were with 0.5 µg of template and no additional $MgCl_2$.

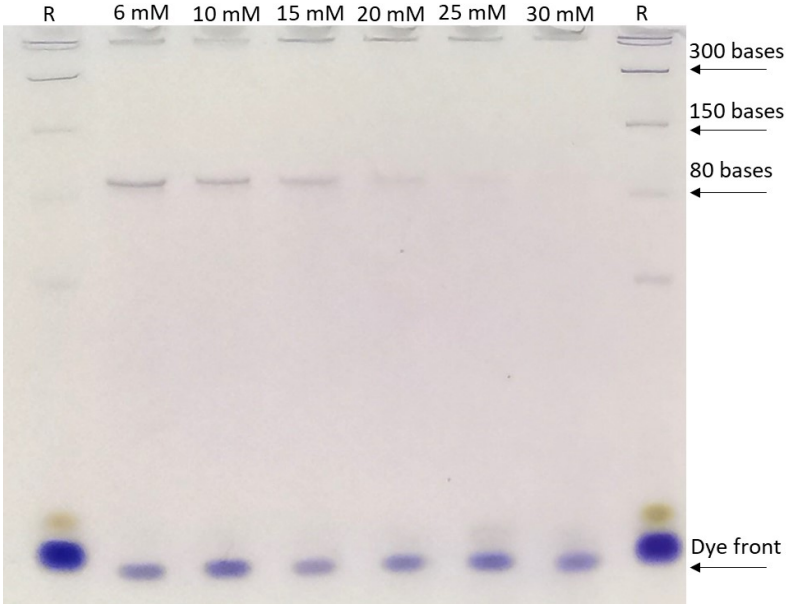

Figure 3.11: No additional $MgCl_2$ is required for TERRA96 transcription. *In vitro* transcription reactions with $MgCl_2$ titrated at 6 mM, 10 mM, 15 mM, 20 mM, 25 mM and 30 mM, with 1 µg of linearised pUC18_TERRA96 in a 50 µL reaction, were analysed through 6.5 M urea 10 % PAGE with 1 µL aliquots. Stained with Stains-All. R - ssRNA ladder.

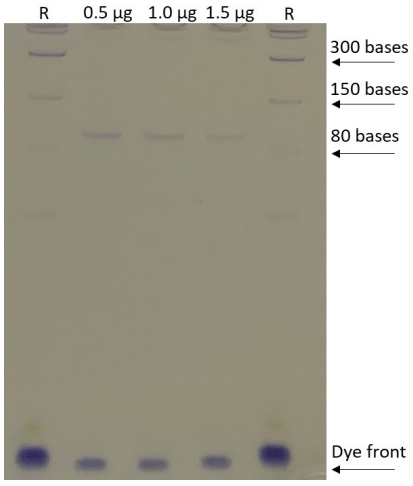

Figure 3.12: TERRA96 transcription is most efficient with 0.5 µg of template. *In vitro* transcription reactions with linearised pUC18_TERRA96 titrated at 0.5 µg, 1.0 µg and 1.5 µg in a 50 µL reaction were analysed through 6.5 M urea 10 % PAGE with 1 µL aliquots. Stained with Stains-All. R - ssRNA ladder.

3.3.2 Testing if TERRA96 mediates the H1.4-HP1α interaction

To determine if the *in vitro* transcribed TERRA96 could mediate the H1.4-HP1α interaction, initially the transcription reaction containing TERRA96 was tested. To ensure the TERRA96 was folded in a G-quadruplex (G4) structure in the *in vitro* transcription reaction, potassium was added to 15 mM to stabilise the G4 (Burge et al., 2006) and was then heated at 95 °C for 5 minutes and cooled slowly to room temperature. In an attempt to estimate the concentration of TERRA96 in the *in vitro* reaction, the absorbance at 260 nm was measured and the concentration was calculated using the molecular weight and extinction coefficient, measuring at 0.5 µg/µL, however, some ribonucleotides may have been present.

HisPur™ Ni-NTA beads were incubated in the presence or absence of His-HP1α for 1 hour at room temperature (see Section 2.5 and Figure 3.7). No RNA, 10 µg or 20 µg of the TERRA96 *in vitro* transcription reaction was then added and incubated at 4 °C for 2 hours. The beads were then washed to remove any unbound RNA. FLAG-H1.4 was then added with 1.3 µg per reaction and incubated overnight at 4 °C. Unbound FLAG-H1.4 was washed from the beads and the resultant complexes were separated by 12 % SDS-PAGE (see Section 2.8.1). Immunoblotting against FLAG was performed to determine if FLAG-H1.4 was bound to the His-HP1α complex.

Illustrated by Figure 3.13, FLAG-H1.4 was detected when 20 µg of the TERRA96 *in vitro* transcription reaction was added. However, no band was observed when 10 µg of the TERRA96 *in vitro* transcription reaction was added, and no input control was detected. While no input control was detected in the input lane, due to a pipetting error, the band detected, when 20 µg of the TERRA96 *in vitro* transcription reaction was added migrated at 37 kDa where FLAG-H1.4 typically migrates (Figure 3.4 - Figure 3.6). The absence of bands in the −HP1α lanes indicated that no FLAG-H1.4 was pulled down when His-HP1α was absent, illustrating that the TERRA96 does not bind to the HisPur™ Ni-NTA beads. The time of exposure and large amount of 'RNA' required was of concern. This is likely due to the *in vitro* transcription reaction interfering with the estimation of the concentration of TERRA96.

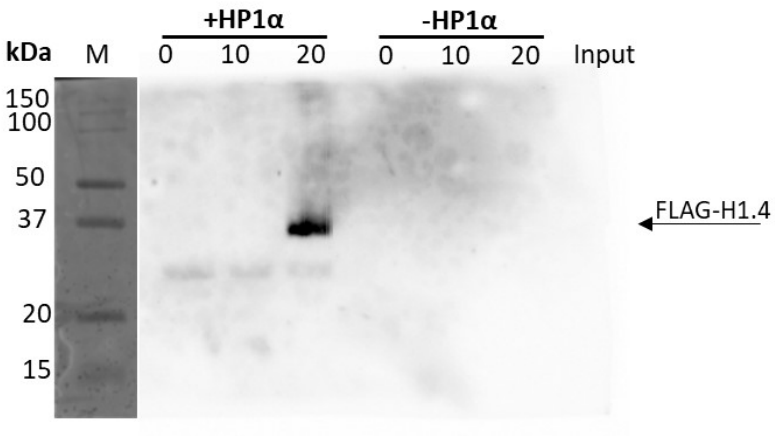

Figure 3.13: Testing if TERRA96 mediates the H1.4-HP1α interaction. *In vitro* His-HP1α pulldown and immunoblot with the presence or absence of His-HP1α and the addition of 0 µg, 10 µg and 20 µg of TERRA96 *in vitro* transcription reaction. Pulled down FLAG-H1.4 was detected by immunoblotting against FLAG with a 10 minute chemiluminescence exposure. Input - 8 % FLAG-H1.4. M - Molecular weight marker.

3.3.3 Large scale transcription and purification of TERRA96

To overcome the overestimation of TERRA96 concentration, TERRA96 needed to be transcribed on a larger scale so it could be purified.

To transcribe TERRA96 *in vitro*, 40 µg pUC18_TERRA96 was digested as before (see Section 2.3.1 and Section 3.3.1). The completion of the digest was confirmed as before by 1 % agarose gel electrophoresis (see Section 2.8.2 and 3.3.1) with the presence of the linear pUC18_TERRA96 at around 2900 bp in both digestion lanes (Figure 3.14). TERRA96 was transcribed with 80 simultaneous *in vitro* transcription reactions with 0.5 µg of linearised template per reaction as before (see Section 2.3.1 and Section 3.3.1), with the total reaction mix divided in four to allow for incubation in 1.7 mL Eppendorfs. *In vitro* transcription of TERRA96 was confirmed as before by 6.5 M urea 10 % PAGE (see Section 2.8.3 and Section 3.3.1), with the presence of the band around 96 bases produced in all four reactions (Figure 3.15).

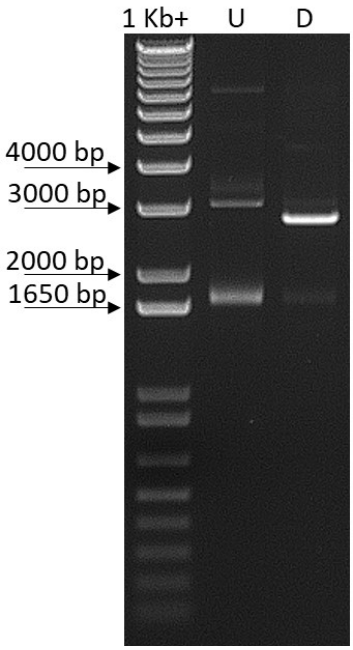

Figure 3.14: pUC18_TERRA96 was digested with BpiI for large scale transcription. Large scale digestion of pUC18_TERRA96 was analysed by EtBr staining in 1 % agarose. U - Undigested pUC18_TERRA96, 50 ng . D - Restriction digest, 1 µL. 1 Kb+ - DNA ladder.

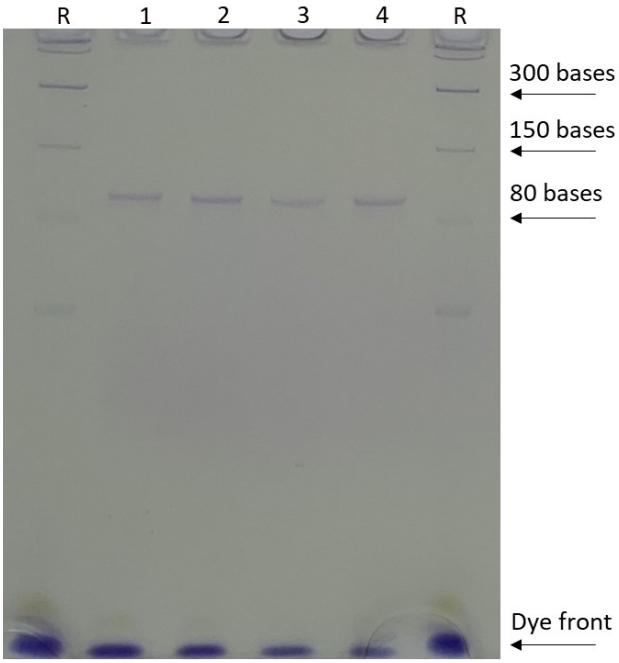

Figure 3.15: TERRA96 was transcribed on a large scale. Large scale *in vitro* transcription of TERRA96 was analysed through 6.5 M urea 10 % PAGE with 1 µL aliquots of the four transcription reactions (1, 2, 3 and 4). Stained with Stains-All. R - ssRNA ladder.

To remove BpiI and T7 RNA polymerase, the TERRA96 *in vitro* transcription reactions were combined and extracted with three sequential phenol/chloroform extractions, followed by a final extraction with chloroform (see Section 2.3.2). The phenol/chloroform extracted *in vitro* transcription reaction was then desalted using a 10DG desalting column and eluted in RNA buffer (10 mM mono/di basic phosphate [pH 6.6], 100 mM NaCl) and then concentrated. Aliquots taken during the extraction and desalting of the TERRA96 were analysed by 6.5 M urea 10 % PAGE. The presence of the band at 96 bases in the gel (Figure 3.16) throughout the processing confirmed TERRA96 had not been lost or degraded .

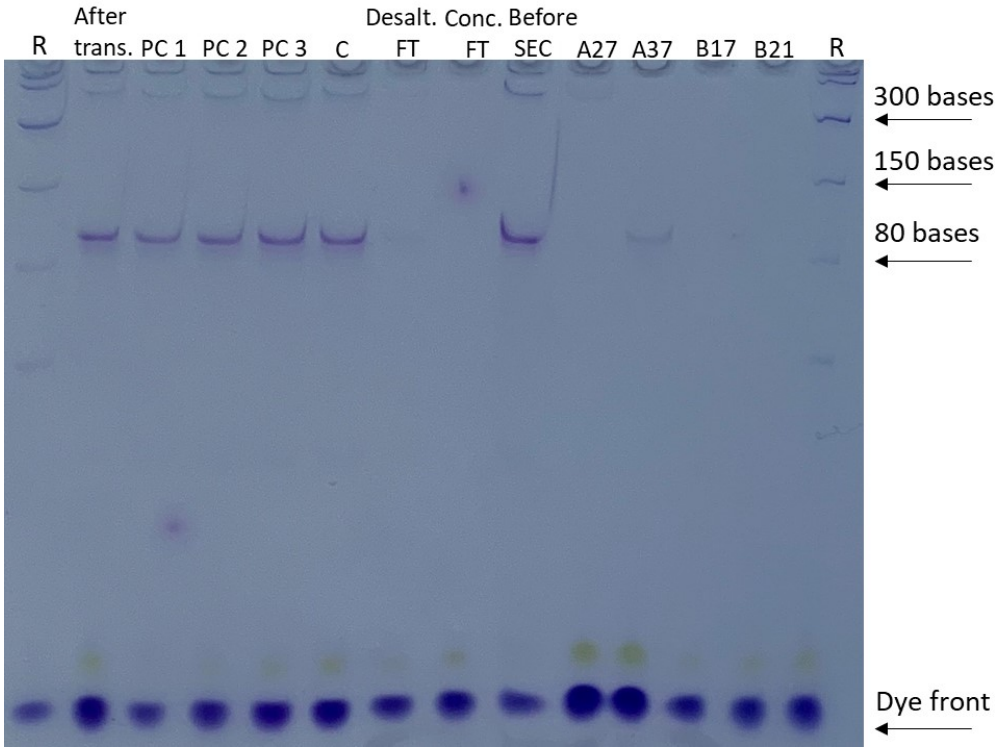

Figure 3.16: Large scale TERRA96 purification. Purification of TERRA96 was tracked by analysis of aliquots though 6.5 M urea 10 % PAGE. After trans. - After *in vitro* transcription, 1 µL. PC 1-3 - Sequential phenol chloroform extractions 1-3, 1 µL. C - Chloroform extraction, 1 µL. Desalt. FT - Desalting column sample application flowthrough, 1 µL. Conc. FT - Concentrator flowthrough, 1 µL. Before SEC - Concentrated TERRA96 before size exclusion chromatography, 1 µL. A27, A37, B17 and B21 - Aliquots of main size exclusion chromatography peaks, 10 µL. Stained with Stains-All. R - ssRNA ladder.

To remove any aberrant transcripts and remaining plasmid, TERRA96 was size excluded using an ENrich™ SEC 70 10 x 300 Column. The chromatogram generated by measuring the absorbance at 260 nm as the fractions were eluted (Figure 3.17) displayed four main absorbance peaks. To determine the elution peak with TERRA96, aliquots of the four main peaks were analysed by 6.5 M urea 10 % PAGE. Shown by Figure 3.16, the presence of the band at 96 bases indicated that TERRA96 eluted in the peak around fraction A37. The two large peaks at B17 and B21 were remaining nucleotides from the transcription reaction, indicating the efficiency of the transcription is low (McKenna et al., 2007), likely due to the G4 structure of the template sequence. To identify all of the fractions containing TERRA96, those surrounding the A37 peak were analysed by 6.5 M urea 10 % PAGE. Seen in Figure 3.18, this identified a secondary transcript of the same length as TERRA96 which eluted slightly earlier around fraction A34. From the gel (Figure 3.18), fractions 36 through 41 contained the most TERRA96 and were combined and concentrated. TERRA96 was then quantified by measuring the absorbance at 260 nm and the concentration calculated using the extinction coefficient and molecular weight, measuring at 32 ng/µL. To confirm that the TERRA96 was not lost during concentrating, aliquots of the MilliQ water used to store the concentrators were analysed by 6.5 M urea 10 % PAGE. Figure 3.19 showed that there was no detectable TERRA96 in the storage MilliQ water or the flowthrough, and that the final TERRA96 was a singular transcript.

For use in a pulldown to determine if TERRA96 could mediate the H1.4-HP1α interaction, the purified TERRA96 was further concentrated, and then folded by the addition of potassium to 15 mM, heated to 95 °C and cooled slowly to room temperature. The TERRA96 was quantified as before, yielding 235 ng/µL.

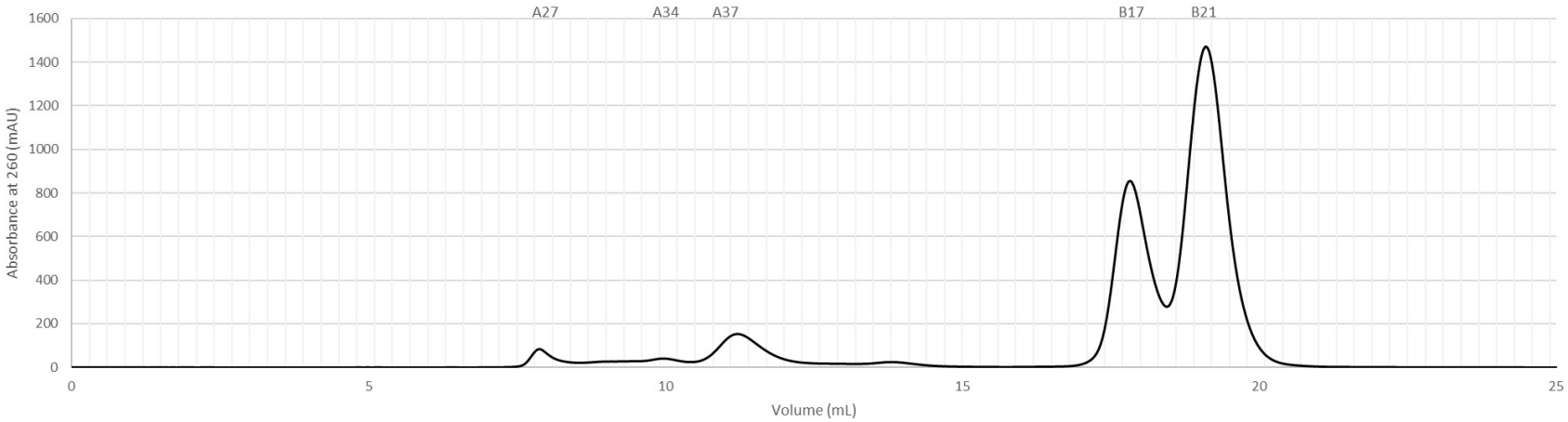

Figure 3.17: TERRA96 size exclusion chromatography chromatogram. Average absorbance at 260 nm of size exclusion chromatography elution fractions, of four TERRA96 sample applications on an ENrich™ SEC 70 10 x 300 Column in RNA buffer. Horizontal gridlines represent each 300 µL fraction.

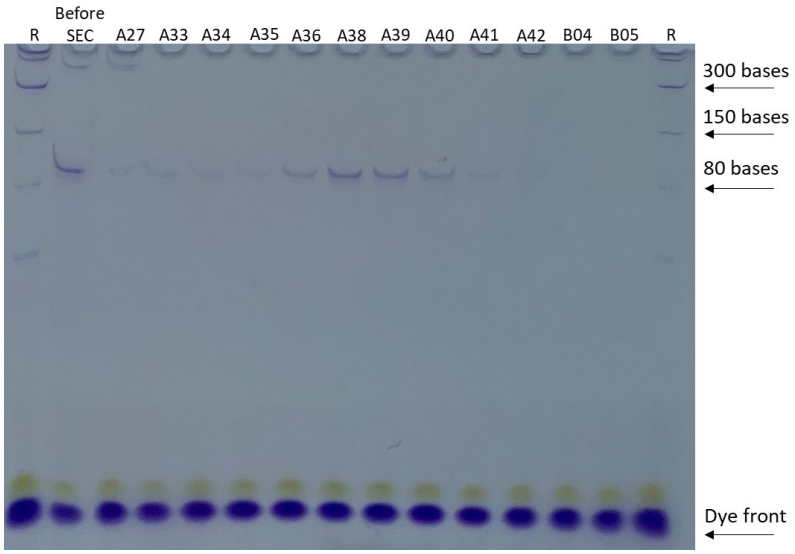

Figure 3.18: TERRA96 size exclusion chromatography fractions. Fractions of TERRA96 size exclusion chromatography were analysed through 6.5 M urea 10 % PAGE with 6 µL aliquots to determine which fractions contained TERRA96. Before SEC - Before size exclusion chromatography, 1 µL. Stained with Stains-All. R - ssRNA ladder.

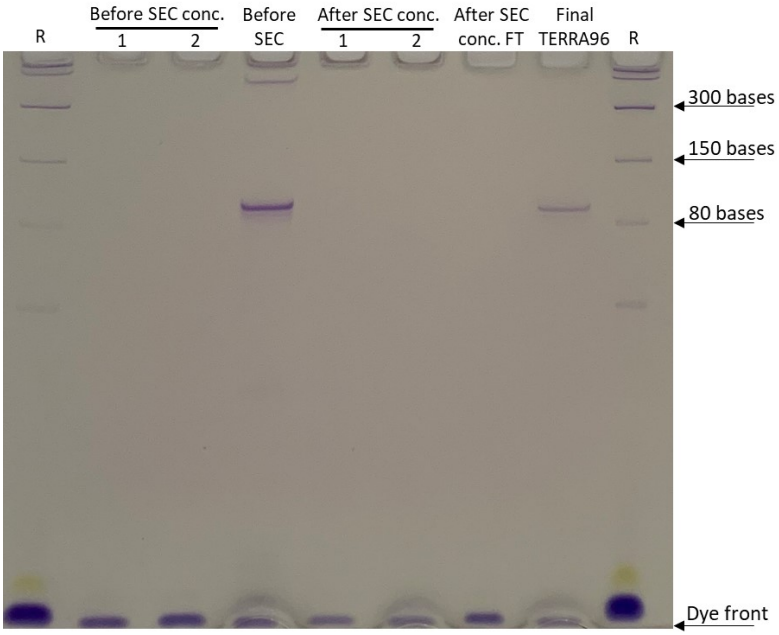

Figure 3.19: Purified TERRA96. Aliquots of the storage MilliQ water from the concentrators were analysed through 6.5 M urea 10 % PAGE. Before SEC conc. 1 and 2 - Storage MilliQ of concentrators (1 and 2) before size exclusion chromatography , 1 µL. After SEC conc. 1 and 2 - Storage MilliQ of concentrators (1 and 2) after size exclusion chromatography , 1 µL. After SEC conc. FT - Combined flowthrough from both concentrators after size exclusion chromatography , 4 µL. Stained with Stains-All. R - ssRNA ladder.

3.3.4 TERRA96 mediates the H1.4-HP1α interaction

To test if TERRA could mediate the H1.4-HP1α interaction, a pulldown was performed using purified TERRA96. Therefore, His-HP1α was bound to HisPur™Ni-NTA beads (see Section 2.5 and Figure 3.7), washed and then incubated with no RNA, 2 µg, 4 µg or 8 µg of TERRA96 or total RNA isolated from NIH3T3 cells (see section 2.4). Any unbound RNA was washed from the beads followed by addition of 2.6 µg of FLAG-H1.4 and then incubated. Unbound FLAG-H1.4 was washed from the beads and the resultant complexes were resolved by 12 % SDS-PAGE (see Section 2.8.1) and Western blot was performed with an antibody against FLAG, detecting if FLAG-H1.4 had been pulled down.

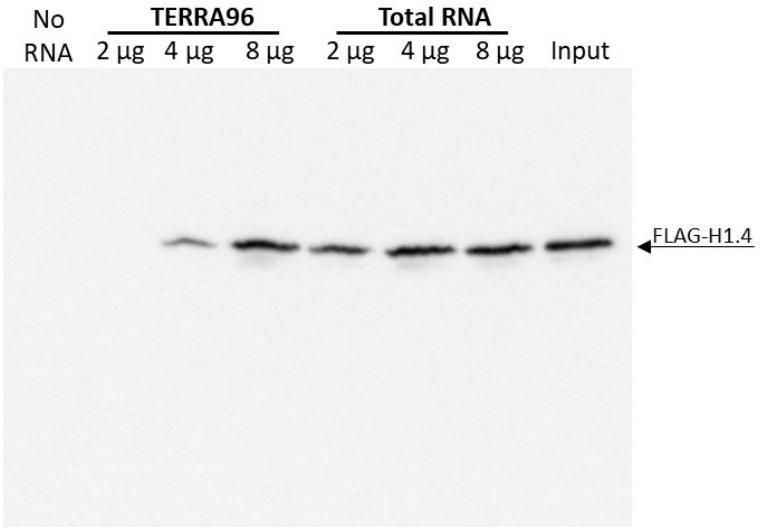

Figure 3.20: TERRA96 mediates the H1.4-HP1α interaction *in vitro*. *In vitro* His-HP1α pulldown with no RNA, 2 µg, 4 µg or 8 µg of TERRA96 or NIH3T3 total RNA, added as indicated. Pulled down FLAG-H1.4 was detected by immunoblotting against FLAG with a 3 second exposure. Input - 23 % FLAG-H1.4.

Figure 3.20 shows that FLAG-H1.4 was pulled down when 4 µg and 8 µg of TERRA96 were added to the system, which indicates that at these levels TERRA96 can mediate the H1.4-HP1α interaction *in vitro*. The total RNA, again was able to mediate the interaction, with FLAG-H1.4 detected when 2 µg, 4 µg and 8 µg were added. There was no band present in the no RNA lane indicating that the FLAG-H1.4 does not bind directly to the beads, while FLAG-H1.4 was detected in the input control, showing that the antibody binds FLAG-H1.4.

Chapter 4

Investigating the H1.4-HP1α interaction in a nucleosomal context

4.1 Introduction

Within the cell, the interaction of histone H1.4 with Heterochromatin protein 1α (HP1α) occurs within chromatin. To replicate this environment, nucleosomes were formed *in vitro*. Mononucleosomes were formed to explore binding and investigate if Telomeric repeat-containing RNA (TERRA) can mediate the interaction between HP1α and H1.4 in a nucleosomal context. Mononucleosomes will then be expanded to trinucleosomes and arrays of 12 nucleosomes to study the role of this interaction on chromatin compaction. As the mononucleosomes were formed on a fluorescently labelled DNA fragment, electrophoretic mobility shift assays (EMSAs) were used to analyse the formation of the mononucleosomes and then the binding of H1.4 to the mononucleosomes.

Nucleosomes can be assembled *in vitro* on DNA fragments containing the 147 bp Widom 601 positioning sequence, to which histones have a high binding affinity (Lowary and Widom, 1998), through decreasing the salt concentration of the solution (Dyer et al., 2003; Flaus, 2011; Germond et al., 1976; Luger et al., 1997b, 1999a,b). This allows a more defined assembly, with the number of 601 repeats determining how many nucleosomes are formed. Histones can either be isolated from tissue or cells, or recombinant histones can be expressed and purified. At 2 M NaCl, there is no association of histones to DNA. Decreasing the salt concentration to 1 M initiates H3-H4 tetramers binding to DNA, at 0.8 M NaCl an H2A-H2B dimer binds to the positioned tetramers, and finally by 0.6 M NaCl the second H2A-H2B dimer binds the hexamer, forming a nucleosome (Carruthers et al., 1999). As the salt concentration is decreased below 0.6 M, arrays of multiple nucleosomes form a more folded structure, however once the NaCl concentration reaches 0.1 M, arrays begin to unfold and reform an extended structure (Carruthers et al., 1999).

4.2 Construction of mononucleosomes

To form mononuclesomes, this requires a fluorophore labelled DNA fragment with the Widom 601 positioning sequence to position octamers (Lowary and Widom, 1998), as well as the four core histones that form the octamer. The mononucleosomes will be formed by salt gradient dialysis in a similar manner as described previously (Luger et al., 1999b; Ryan and Tremethick, 2016). This process is summarised in Figure 4.1.

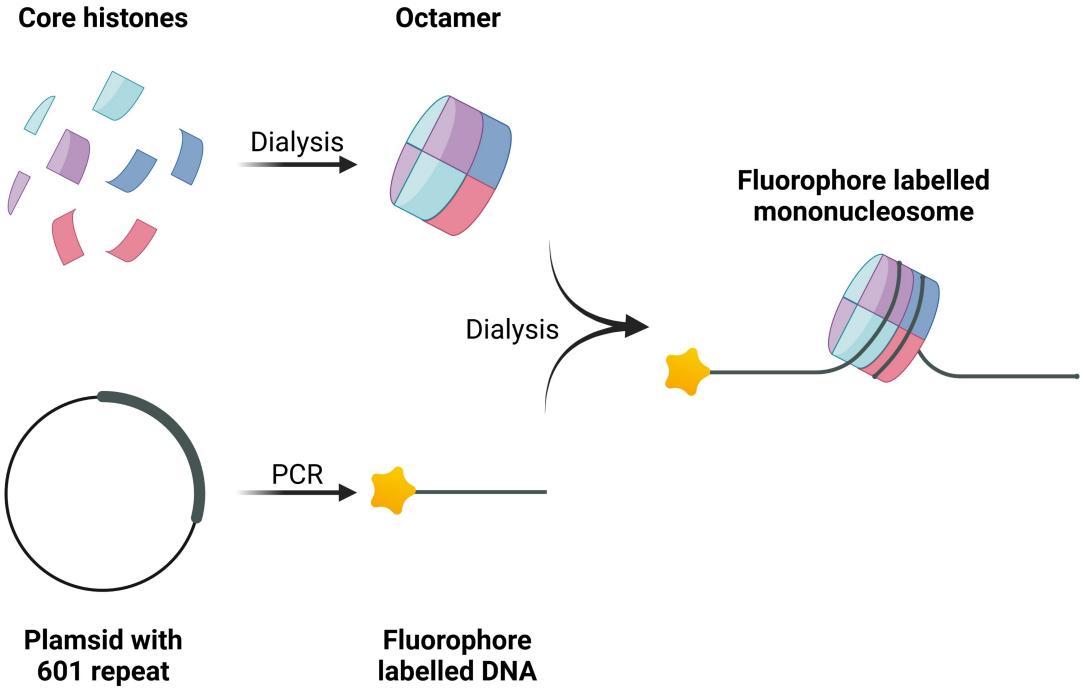

Figure 4.1: Schematic diagram of mononucleosome formation. Core histones were expressed and purified, and then dialysed to form octamers. A plasmid containing one 601 repeat was cloned, followed by PCR amplification to generate a labelled DNA fragment containing one 601 repeat. The octamers and labelled DNA were then combined and dialysed to form labelled mononucleosomes. Created with BioRender.

4.2.1 Expression of core histones and octamer formation

To express the four core histones, *mus musculus* H2A, *mus musculus*/*homo sapien* H2B, *mus musculus*/*homo sapien* H3.1 and *xenopus*/*homo sapien* H4, *E. coli* BL21 DE3 cells were transformed with the respective expression plasmids pET3_mH2A, pET3_mhH2B, pET3_mhH3 and pET3_xH4 (see Section 2.1, Table 2.3). Expression of the four histones was induced by the addition of isopropyl β-D-1-thiogalactopyranoside (IPTG) and the cultures were incubated at 37 °C for 3-4 hours (see Section 2.2.3.1). Samples of each culture before and after induction were analysed by 12 % sodium dodecyl sulfate (SDS) polyacrylamide gel electrophoresis (PAGE) (see Section 2.8.1). Shown in Figure 4.2, the presence of a distinct band in each after induction lane, at around 14.1 kDa for mH2A, 13.9 kDa for mhH2B, 15.4 kDa for mhH3.1 and 11.4 kDa for xH4, that was absent in the before induction lanes confirmed the expression of each of the core histones. The cells were then lysed and sonicated, and the total protein was centrifuged to separate the soluble and insoluble proteins. As the core histones are likely to be in the insoluble fraction of the sonicated lysate (Klinker et al., 2014), to unfold the histones, they were sequentially dounce homogenised with wash buffer containing Triton-X and then wash buffer without Triton-X, and then dounce homogenised with guanidinium hydrochloride, with soluble proteins separated by centrifugation after each step. To track the histones during the extraction process, aliquots of the total sonicated lysate, sonicated lysate supernatant, supernatant of the washes with and without Triton-X, and the supernatant and pellet of the unfolding mixture were separated by 12 % SDS-PAGE. Figure 4.3 shows that both mH2A and mhH2B were partially soluble with the majority of the protein insoluble, determined by the relative intensities of the histone band in the sonicate supernatant and in the total protein, while mhH3.1 and xH4 were completely insoluble as their respective bands were absent in the sonicate supernatant. After washing and unfolding, the histones became soluble as histone bands were absent in the washes and present in the final supernatant. The final pellets also contained histone bands indicating that the histones were not fully unfolded.

To purify the four core histones, the histones were size excluded using a Superdex 200 10/300 GL column (see Section 2.2.3.2). Aliquots of size exclusion chromatography elution fractions which had the highest absorbance at 280 nm

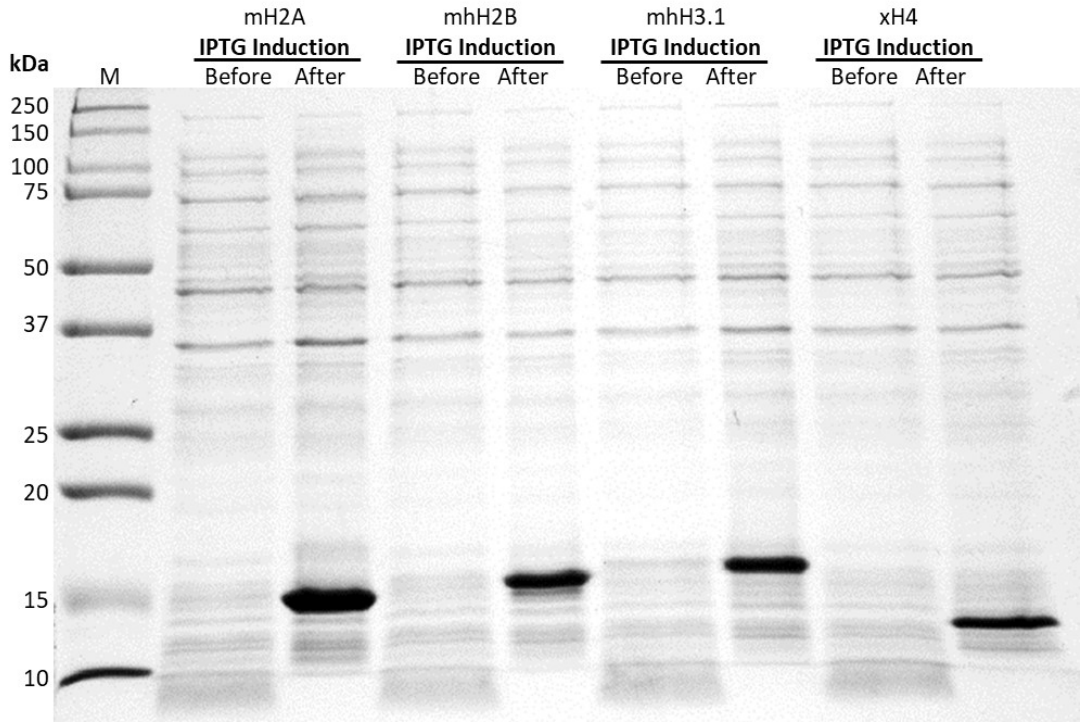

Figure 4.2: Induction of core histone expression. Before (20 µL of 400 mL culture) and after IPTG (1 µL of cells resuspended in 5 mL wash buffer) induction samples of mH2A, mhH2B, mhH3.1 and xH4 were analysed through 12 % SDS-PAGE, and stained with Coomassie blue. The approximate molecular weight of mH2A, mhH2B, mhH3.1 and xH4 are 14.1 kDa, 13.9 kDa, 15.4 kDa and 11.4 kDa respectively. M - Molecular weight marker.

were analysed by 12 % SDS-PAGE to determine which fractions contained the histones. From the gels (Figure 4.4), the fractions containing the highest amount of each histone were identified and combined, mH2A; A35-A37 (Figure 4.4a), mhH2B; A35-A37 (Figure 4.4b), mhH3.1; A35-B1 (Figure 4.4c) and xH4; A37-A39 (Figure 4.4d). The combined histone fractions were then dialysed into water with β-mercaptoethanol and lyophilised. The histones were then resuspended in MilliQ water and the concentrations were determined by measuring the absorbances at 280 nm and calculated by using the molecular weight and extinction coefficient of each histone. To analyse the purity of the histones, 375 µg of each was resolved by 12 % SDS-PAGE. A single discrete band at the correct molecular weight for each of the four core histones in Figure 4.5 demonstrates that only one species is present and that the histones are absent of other proteins. As the staining intensity of each histone is different, this indicates that the concentrations determined may be incorrect (see also Figure 4.15).

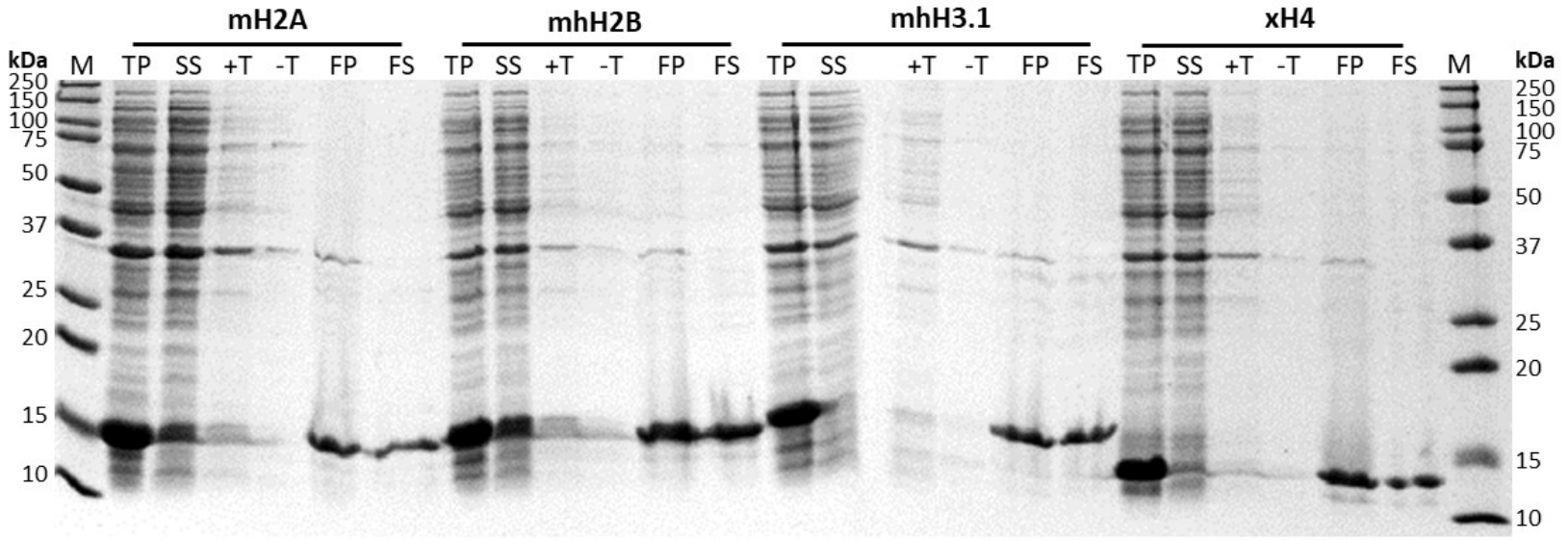

Figure 4.3: Core histone extraction from inclusion bodies. Inclusion body formation and histone extraction aliquots were resolved by 12 % SDS-PAGE, then stained with Coomassie blue. TP - Total protein in sonicated lysate, 5 µL. SS - Sonicate supernatant, 5 µL. +/-T - With or without Triton-X washes supernatant, 5 µL. FP - Final unfolding pellet, 1 µL. FS - Final unfolding supernatant, 1 µL. M - Molecular weight marker.

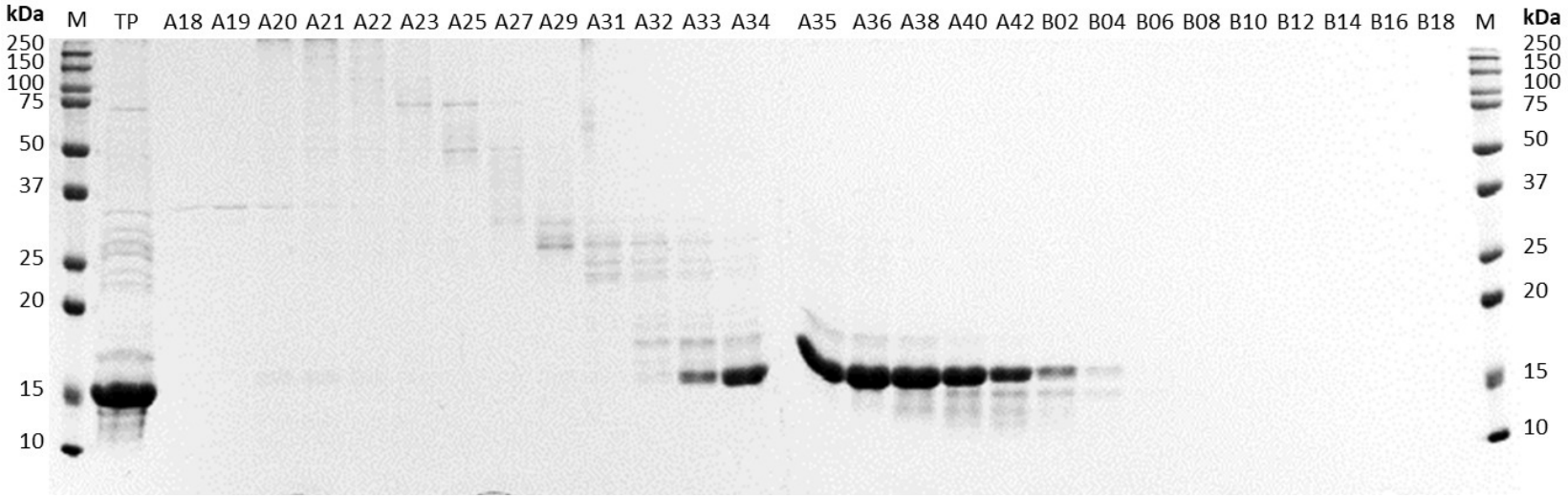

(a) mH2A size exclusion chromatography purification

Figure 4.4: Size exclusion chromatography purification of core histones. Core histone size exclusion chromatography elution fractions (2 µL) were resolved through 12 % SDS-PAGE, and stained with Coomassie blue. TP- Total protein before size exclusion chromatography, 2 µL. M - Molecular weight marker. a) mH2A size exclusion chromatography fractions. b) mhH2B size exclusion chromatography fractions. c) mhH3.1 size exclusion chromatography fractions. d) xH4 size exclusion chromatography fractions.

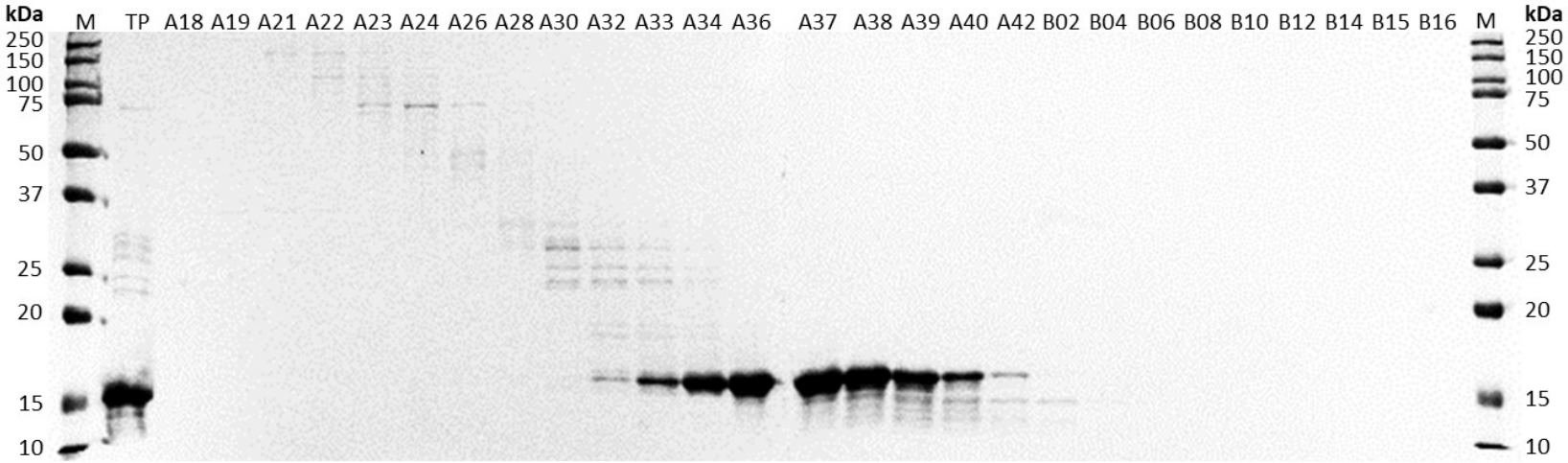

(b) mhH2B size exclusion chromatography purification

Figure 4.4: Size exclusion chromatography purification of core histones. Cont.

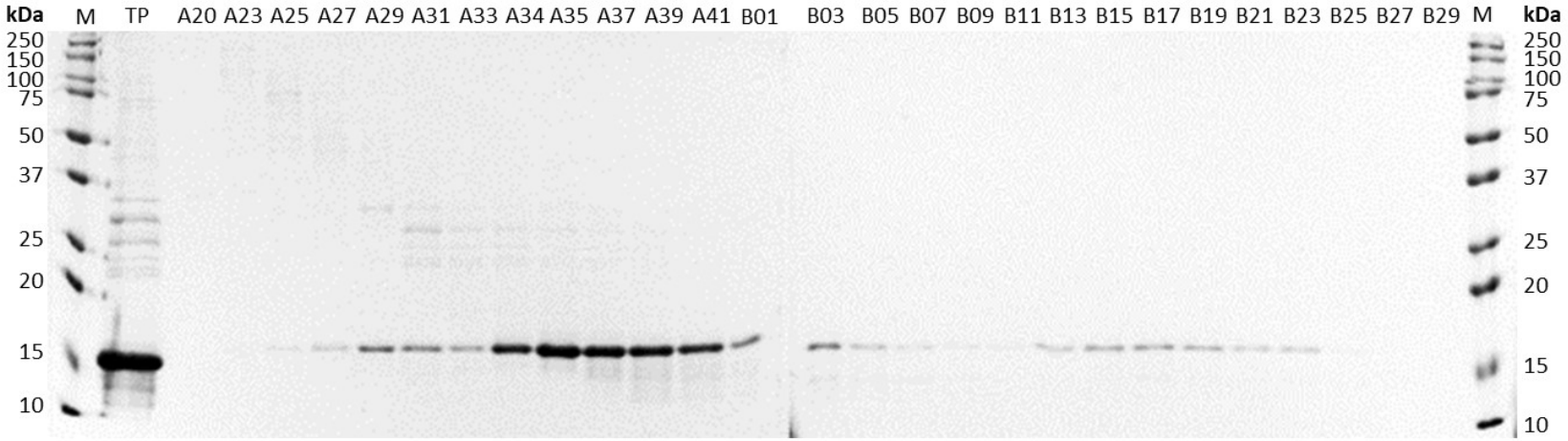

(c) mhH3.1 size exclusion chromatography purification

Figure 4.4: Size exclusion chromatography purification of core histones. Cont.

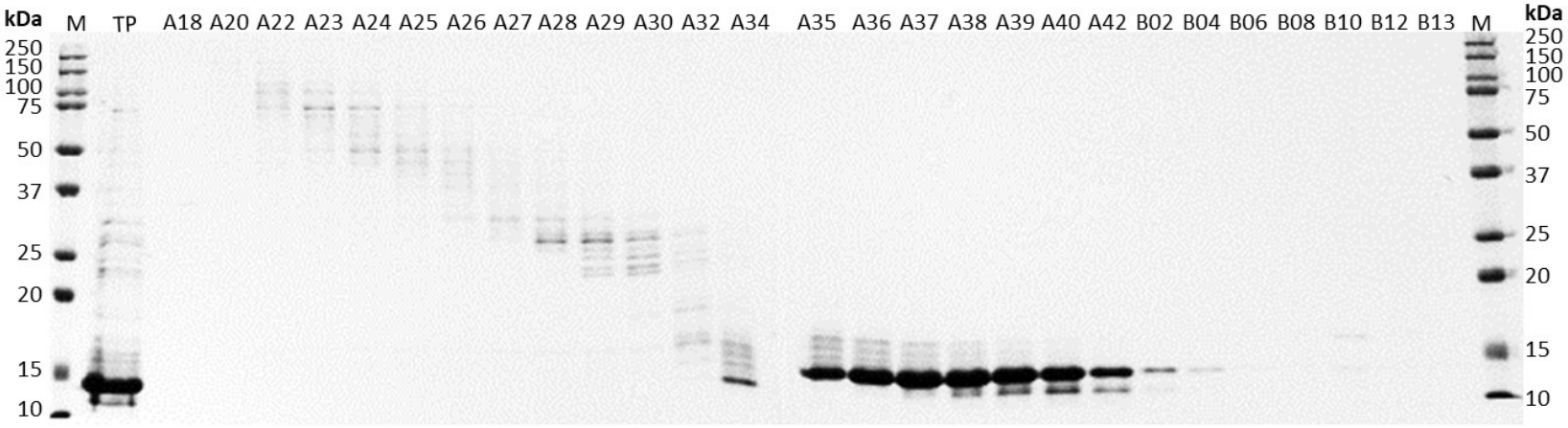

(d) xH4 size exclusion chromatography purification

Figure 4.4: Size exclusion chromatography purification of core histones. Cont.

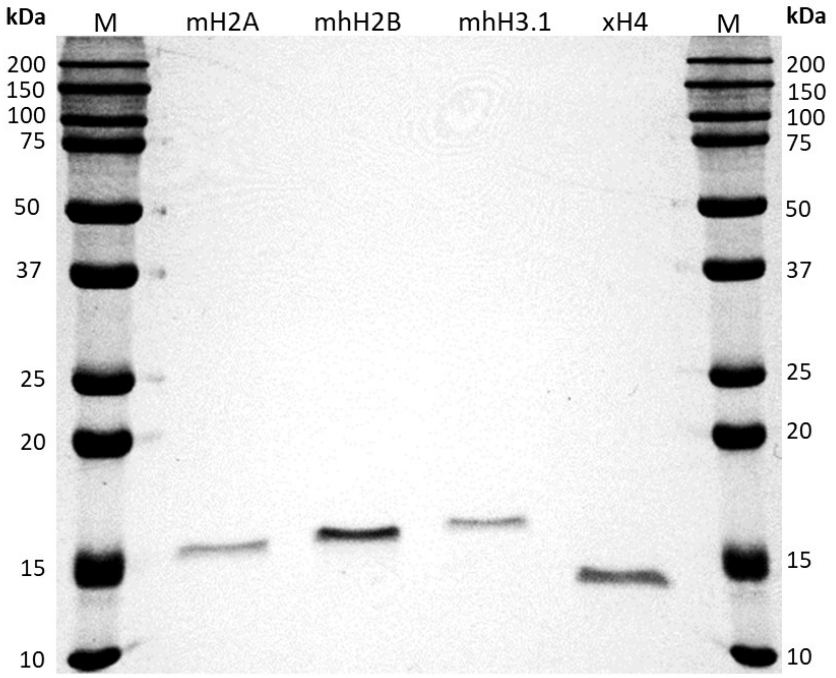

Figure 4.5: Size exclusion chromatography core histones. 375 µg of each mH2A, mhH2B, mhH3.1 and xH4, after size exclusion chromatography, were resolved through 12 % SDS-PAGE, then stained with Coomassie blue. M - Molecular weight marker.

To form histone octamers, the four core histones were mixed at an equimolar ratio in guanidinium hydrochloride (see Section 2.6.1). The histone mix was then dialysed in refolding buffer to allow refolding of the histones and octamer formation through the handshake motif. To purify the octamers from any unbound histones, the octamers were size excluded using a Superdex 200 10/300 GL column. The size exclusion chromatography elution fractions were collected and those with high absorbance at 280 nm were analysed by 12 % SDS-PAGE to determine the fractions that contained the octamers. Figure 4.6 shows that fractions B5-B15 contained similar amounts of each histone, with xH4 seen as the lowest molecular weight band, then mhH3.1 as the highest molecular weight band with mH2A and mhH2B as two non-distinct bands in the middle. It is also shown in Figure 4.6 that either octamers or free histones precipitated during the dialysis. Fractions B4-B15 were combined and concentrated, the histone octamers were then quantified by measuring the absorbance at 280 nm and the concentration calculated using the extinction coefficient and molecular weight of an octamer.

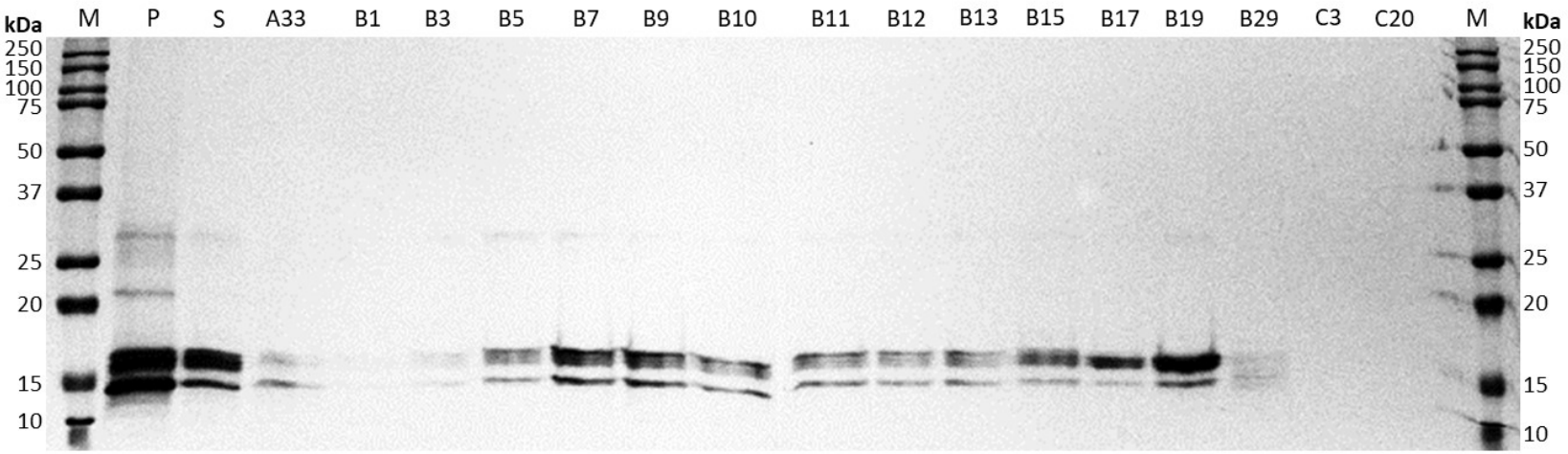

Figure 4.6: Octamer size exclusion chromatography. Size exclusion chromatography fractions (8 µL), along with samples of the precipitate (P - precipitate, 2 µL) and supernatant (S - supernatant, 2 µL) at the end of dialysis, were resolved through 12 % SDS-PAGE, and stained with Coomassie blue. M - Molecular weight marker.

4.2.2 Generation of DNA fragment

A DNA fragment containing the Widom 601 positioning sequence (Lowary and Widom, 1998) was generated for the assembly of mononucleosomes. This required inverse PCR of a plasmid, pUC18_3x200_601 (Table 2.3 and Figure A.3), that contains three 200 bp repeats consisting of the 147 bp Widom 601 sequence, flanked by 33 bp and 20 bp linker DNA. Once the plasmid containing one repeat was obtained, PCR was performed to amplify an Alexa488 labelled fragment with 53 bp and 37 bp of linker DNA flanking the 147 bp Widom 601 sequence. Figure 4.7 shows a schematic outline of these steps.

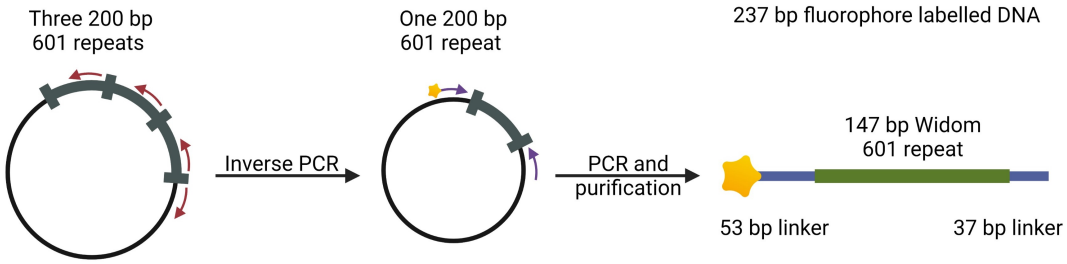

Figure 4.7: Schematic diagram of labelled DNA fragment generation. Inverse PCR was performed on a plasmid containing three copies of a 200 bp repeat consisting of 33 bp linker DNA, the 147 bp Widom 601 positioning sequence followed by 20 bp linker DNA. Two of the three repeats were excised generating a plasmid containing one copy of the 200 bp repeat. PCR amplification was then performed, generating a fluorophore labelled DNA fragment with 53 bp linker DNA, the 147 bp Widom 601 positioning sequence, followed by 37 bp linker DNA. Created with BioRender.

4.2.2.1 Cloning of pUC18_1x200_601 plasmid

To generate a plasmid with one repeat of the 601 positioning sequence, inverse PCR was performed on pUC18_3x200_601 (Table 2.3 and Figure A.3). Primers Inv_For and Inv_Rev were designed to excise two of the three repeats (Table A.1 and Figure A.3). Optimisation of the inverse PCR was performed by titrating the annealing temperature from 62 °C to 68 °C (see Section 2.6.2.1). PCR aliquots were then analysed by 1.5 % agarose gel electrophoresis (see Section 2.8.2). Shown in Figure 4.8, while the linear pUC18_3x200_601 plasmid migrated in the gel at approximately 3,300 bp, the major PCR product of each annealing temperature

migrated at round 2,900 bp, the expected size of the plasmid containing one repeat. The PCR was then repeated with an annealing temperature of 62 °C, as this temperature was the lowest temperature with an intense band. The product was then gel purified through 1.5 % agarose gel electrophoresis. The linear fragment was then phosphorylated and quantified before being circularised by T4 DNA ligase. To isolate the plasmid, *E. coli* DH5α cells were transformed with the ligation reaction and multiple colonies were plasmid extracted. To identify clones of the correct length, the plasmids were linearised with KpnI in a diagnostic digest and analysed by 1 % agarose gel electrophoresis. Figure 4.9 shows that four clones were the expected length and these plasmids were then sequenced to confirm the sequence of the 601 repeat insert, yielding the pUC18_1x200_601 plasmid (Figure A.4).

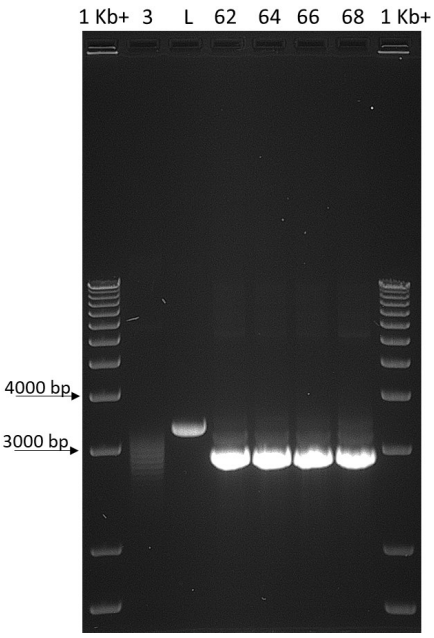

Figure 4.8: Annealing temperature titration for pUC18_3x200_601 inverse PCR. Annealing temperature titration PCR samples, 5 µL, with the annealing temperature titrated at 62 °C, 64 °C, 66 °C and 68 °C, were separated by electrophoresis in 1.5 % agarose, and stained with EtBr. 3 - pUC18_3x200_601, 50 ng. L - Linear pUC18_3x200_601, 50 ng. 1 Kb+ - DNA ladder.

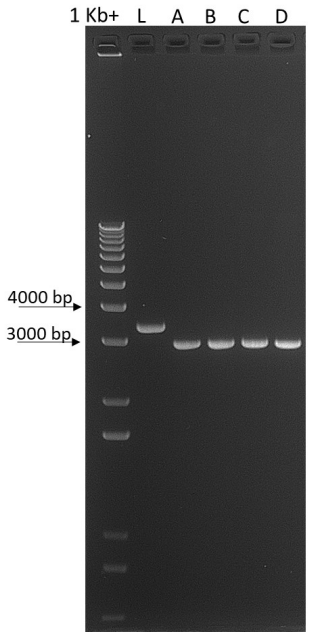

Figure 4.9: Identifying correct pUC18_1x200_601 plasmid clones. Linear pUC18_1x200_601 clones were analysed by electrophoresis in 1 % agarose with EtBr staining. L - Linear pUC18_3x200_601, 50 ng. A-D - Linear clones, 50 ng. 1 Kb+ - DNA ladder.

4.2.2.2 Production of fluorescently labelled 601 DNA fragment

To obtain the 237 bp DNA fragment with the Widom 601 positioning sequence, PCR primers flanking the 200 bp 601 repeat in the pUC18_1x200_601 plasmid were designed, with the forward primer labelled with Alexa488, Alexa488_601_For and DNA_601_Rev (Table A.1 and Figure A.3-A.4). Optimisation was performed by titrating the annealing temperature from 55 °C to 61 °C (see Section 2.6.2.2), with the reactions then resolved by 1.5 % agarose gel electrophoresis (see Section 2.8.2). Shown by Figure 4.10a, there was a product with the expected length of 237 bp in each of the reactions.

For further optimisation and an attempt to increase the yield, the PCR was repeated with an annealing temperature of 61 °C, while the number of annealing cycles and the amount of pUC18_1x200_601 added were titrated. The products from the PCRs were analysed by 1.5 % agarose gel electrophoresis. Figure 4.10b shows that each set of conditions produced the target 237 bp product. The PCR conditions which yielded the 237 bp fragment with the highest intensity in the

gel was 10 ng of pUC18_1x200_601 with 45 annealing cycles.

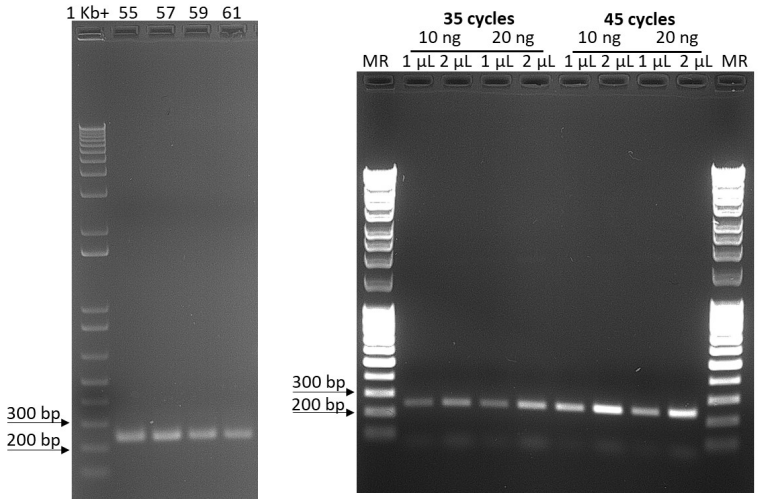

(a) Annealing temperature titration

(b) Annealing cycle and PCR template titrations

Figure 4.10: Alexa488_1x237_601 amplification optimisation. Titration of the annealing temperature, template amount and annealing cycles of the Alexa488_1x237_601 PCR were analysed by electrophoresis in 1.5 % agarose with EtBr staining. a) Annealing temperature titration at 55 °C, 57 °C, 59 °C and 61 °C, 1 µL PCR samples. 1 Kb+ - DNA ladder. b) PCR with template and annealing cycles titrated at 10 ng and 20 ng of pUC18_1x200_601 and 35 and 45 cycles, 1 and 2 µL PCR samples. MR- Mass ruler.

For sufficient fragment to form the mononucleosomes, 32 PCR were performed simultaneously to amplify the Alexa488_1x237_601 fragment, with 10 ng of pUC18_1x200_601 per PCR with 45 cycles and the annealing temperature at 61 °C. To purify the Alexa488_1x237_601 fragment, the PCR reactions were concentrated and resolved by 1.5 % agarose gel electrophoresis. The 237 bp fragment was gel purified, ethanol precipitated, resuspended in Tris HCl [pH 8.5] and quantified.

4.2.3 Mononucleosome formation

To form the mononucleosomes, the histone octamers and Alexa488_1x237_601 fragment were combined in 2 M NaCl (see Section 2.6.3). In an attempt to determine the optimal ratio of octamer to DNA, the amount of octamer was fixed while the amount of Alexa488_1x237_601 was titrated. The reactions were then dialysed by salt gradient with decreasing concentrations of NaCl as outlined in Table 2.5, allowing the association of the histones to the DNA fragment and the DNA to then wrap around the octamer. Mononucleosome formation was then analysed by 5 % native PAGE (see Section 2.8.4). The gel was then scanned for Alexa488 signal, to determine where species containing DNA migrated in the gel, followed by staining with Coomassie blue to determine where protein containing species migrated in the gel. The Alexa488 signal seen in Figure 4.11a shows all three DNA amounts contained high levels of free DNA that has not been bound by octamers and shows the presence of DNA aggregation in the wells, along with four other bands of varying Alexa488_1x237_601 intensity. The Coomassie staining shown in Figure 4.11b illustrates that the aggregation in the wells also contains protein, thus it is either a mixture of aggregated octamer and DNA or aggregated mononucleosomes. The four products seen in the Alexa488 signal were confirmed to be mononucleosomes, as they also appeared in the Coomassie staining in the 1 : 0.85 octamer to DNA reaction. The linker DNA either side of the 601 positioning sequence allows the octamer to bind at multiple sites generating these different mononucleosome species. The 1 : 0.75 octamer to DNA reaction generated no mononucleosome species, while the 1 : 1.15 octamer to DNA reaction generated the slowest migrating mononucleosome species, band 2, and only at a very low level.

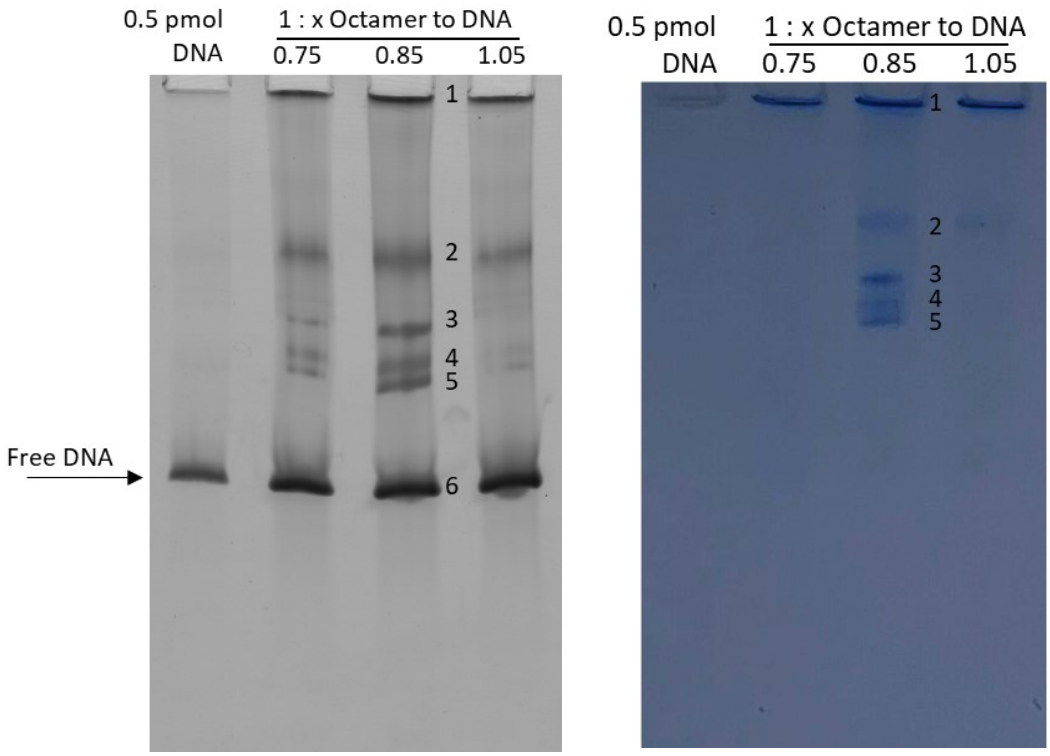

(a) Alexa488 signal **(b)** Coomassie blue staining

Figure 4.11: Mononucleosome formation with Alexa488_1x237_601 titration. Mononucleosome formation reactions with octamer to Alexa488_1x237_601 ratio titration with octamer fixed and DNA titrated at 0.75, 0.85 and 1.05, 5 µL samples, and Alexa488_1x237_601 only (0.5 pmol DNA), were resolved by 5 % native PAGE. 1-6 denote bands with different migration rates. a) FLA-5000 laser scanner at 478 nm. b) Stained with Coomassie blue.

In an attempt to reduce the aggregation (Figure 4.11), the salt gradient dialysis was repeated with the addition of 1 mM dithiothreitol, which prevents the formation of disulfide bridges, in the dialysis buffers (see Section 2.6.3). Additionally, after dialysis, in an attempt to reduce the heterogeneity of the mononucleosome population, heat shifting was used to reposition the octamers on the 601 repeat, with aliquots of the formation reactions heated at 55 °C for 1 hour (Luger et al., 1999b). The mononucleosome assemblies were then analysed by 5 % native PAGE. Figure 4.12 shows that addition of dithiothreitol slightly decreased aggregation of DNA and octamer observed in the wells, while the level of free DNA remained high at each ratio of octamer to DNA. Of note, the Alexa488_1x237_601 DNA only lane contained additional, slower migrating bands that indicates the fragment may be forming secondary structures or that intermolecular interactions are occurring between fragments. Figure 4.12 shows that the ratio of 1 : 0.75 octamer to DNA produced the three mononucleosomal bands, with the heat treatment shifting the mononucleosome species towards that which migrated at band 3.

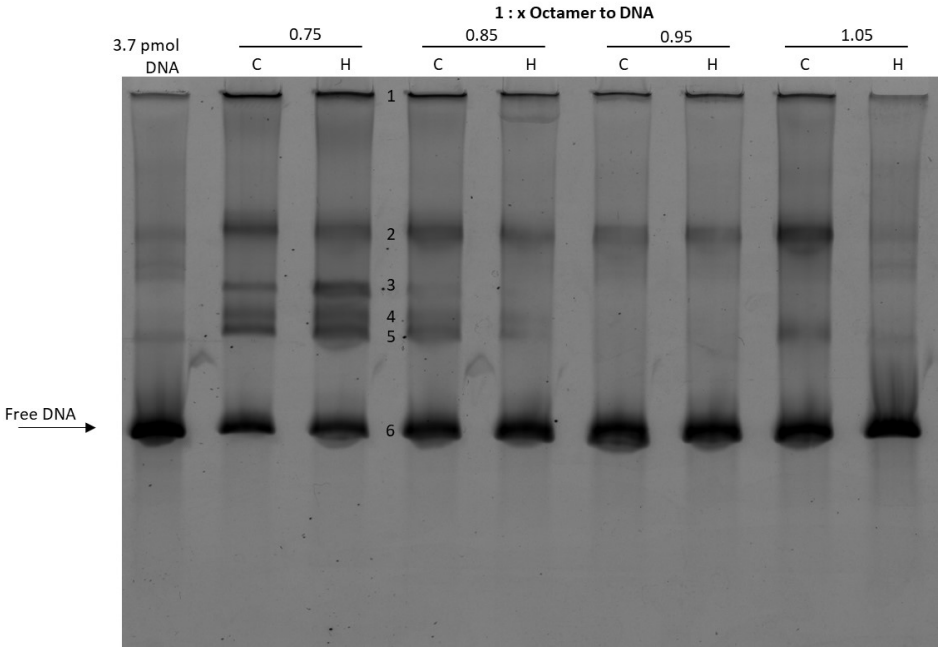

(a) Alexa488 signal

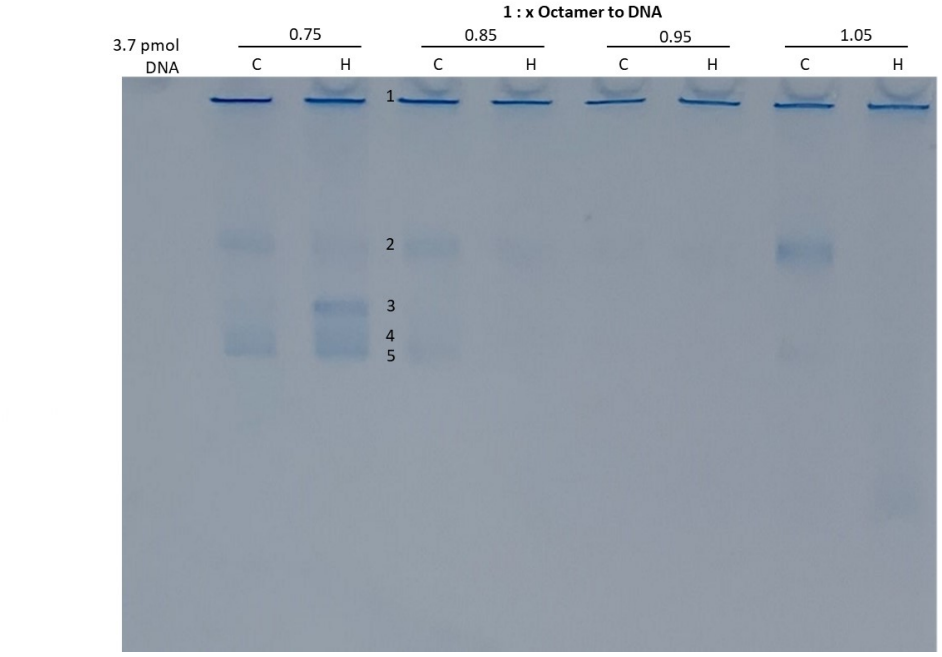

(b) Coomassie blue staining

Figure 4.12: Mononucleosome formation with Alexa488_1x237_601 titration with dithiothreitol. Mononucleosome formation reactions with dithiothreitol with octamer to Alexa488_1x237_601 ratio titrations with octamer fixed and DNA titrated at 0.75, 0.85, 0.95 and 1.05, with untreated (C) and heated (H), 5 µL samples and Alexa488_1x237_601 only (3.7 pmol DNA), were resolved by 5 % native PAGE. 1-6 denote bands with different migration rates. a) FLA-5000 laser scanner at 478 nm. b) Stained with Coomassie blue.

4.3 H1.4 binds to mononucleosomes

Before the H1.4-HP1α interaction can be investigated in a nucleosomal context, the binding of H1.4 needed to be optimised as the appropriate ratio of H1.4 to nucleosome can vary. Since Figure 4.11 showed that not all of the DNA was incorporated into mononucleosomes, to determine the concentration of mononucleosomes the absorbance at 260 nm was measured and the concentration calculated using the extension coefficient and molecular weight of the Alexa488_1x237_601 fragment. The ratio of mononucleosome to total DNA was then calculated to give an estimate of the mononucleosome concentration. Mononucleosomes (see Section 2.6.3 and Section 4.2.3), 0.38 pmol per reaction, were combined with FLAG-H1.4 (see Section 2.2.2 and Section 3.2.2) with the amount of FLAG-H1.4 titrated in a molar ratio at 1 : 0.5, 1 : 1 and 1 : 10 mononucleosome to FLAG-H1.4 (see Section 2.7). Resolution of the reactions by 5 % native PAGE (see Section 2.8.4), showed (Figure 4.13) when FLAG-H1.4 was present in a large molar excess, the mononucleosomes migrated faster in the gel with the generation of two new species with different mobilities. Bands 7 and 8 migrate faster than free mononucleosomes as when FLAG-H1.4 binds the nucleosome the carboxy-terminal tail interacts with the linker DNA of the nucleosome, making the mononucleosome more compact. In the less compact of the two species, the FLAG-H1.4 is likely only interacting with one of the linker DNA, while in the more compact species FLAG-H1.4 is interacting with both linker DNA.

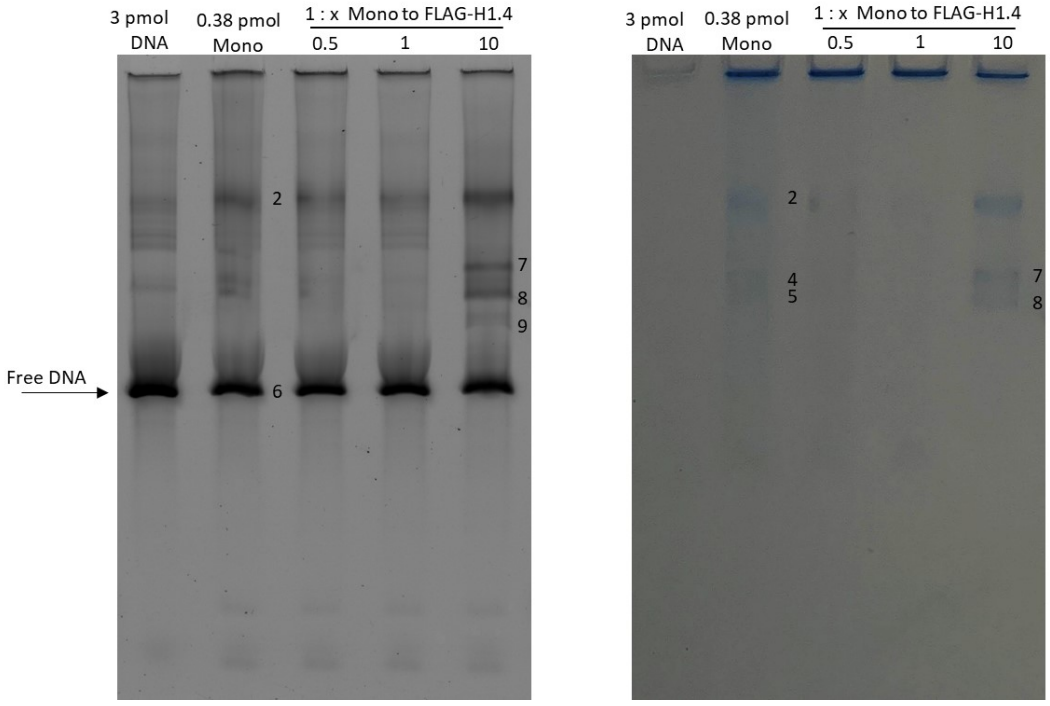

(a) Alexa488 signal **(b)** Coomassie blue staining

Figure 4.13: FLAG-H1.4 binds to Alexa488-mononucleosomes. EMSA of Alexa488-mononucleosome titrated at 1 : 0.5, 1 : 1 and 1 : 10 molar ratio of mononucleosome to FLAG-H1.4, with Alexa488_1x237_601 DNA only (3 pmol DNA) and mononucleosome only (0.38 pmol Mono), resolved by 5 % native PAGE. 1-9 denote bands with different migration rates. a) FLA-5000 laser scanner at 478 nm. b) Stained with Coomassie blue.

4.4 Further mononucleosome optimisation

As the reconstitution reactions did not yield a homogeneous population of mononucleosomes and there was a large proportion of free DNA in the reactions, this needed to be addressed. The first step was to further purify the four core histones, as there were some higher and lower molecular weight bands in the size exclusion chromatography fractions used (Figure 4.4), which may have caused an overestimation of the histone concentrations or interfered in octamer reconstitution. To address this, lyophilised size excluded core histones (see Section 4.2.1) were resuspended in urea buffer and ion exchange chromatography was performed using an SP Sepharose FF column. The histones were eluted with sequential applications of buffer with increasing NaCl concentrations (see Section 2.2.3.3 and Table 2.4). Elution fractions from the column were resolved by 12 % SDS-PAGE (see Section 2.8.1). Shown in Figures 4.14a-d, each of the core histones eluted at 500 mM NaCl in the S500 buffer application, with the histone bands mainly present in S500 and very faint or absent in the other elution lanes.

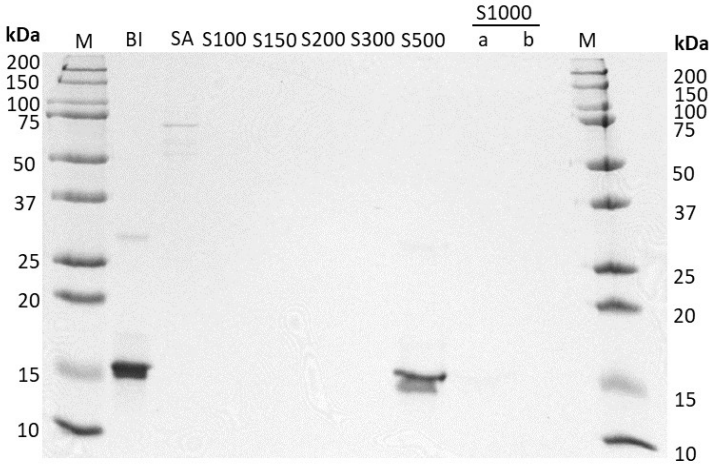

(a) mH2A ion exchange chromatography

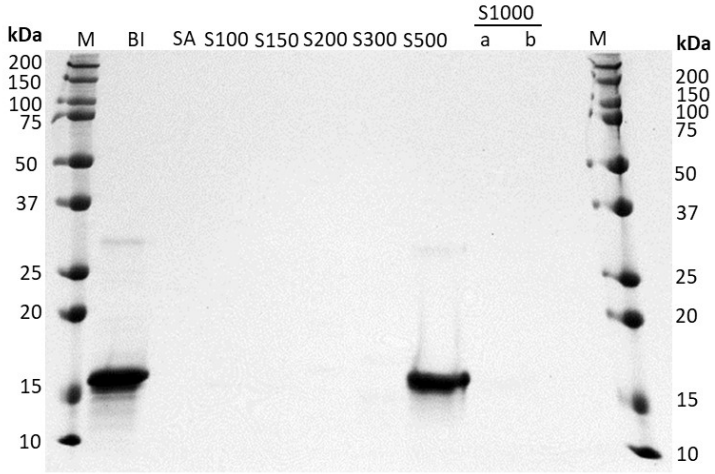

(b) mhH2B ion exchange chromatography

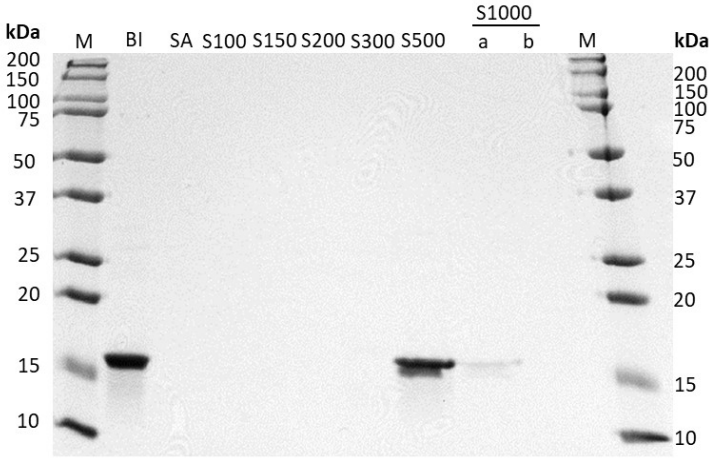

(c) mhH3.1 ion exchange chromatography

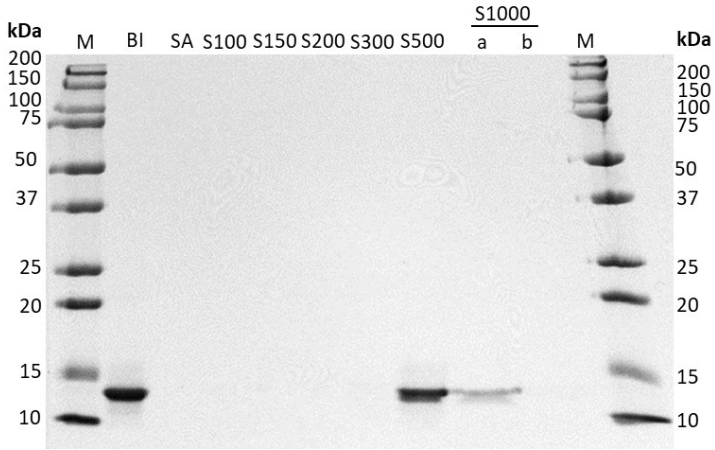

(d) xH4 ion exchange chromatography

Figure 4.14: Core histone ion exchange chromatography. Histones before ion exchange chromatography (BI, 5 µL), sample application flow through (SA, 10 µL) and ion exchange chromatography elution 10 µL samples in S100, S150, S200, S300, S500, S1000a and S1000b, were analysed by 12 % SDS-PAGE, then stained with Coomassie blue. M - Molecular weight marker.

The S500 fraction of each histone was dialysed in 5 mM β-mercaptoethanol, and then lyophilised. The histones were then resuspended in MilliQ water and the concentration of each determined as before (see Section 2.2.3.3 and Section 4.2.1). To check the relative concentration of each of the core histones, 1 µg of each was resolved by 12 % SDS-PAGE. The relative intensity of each histone is different in Figure 4.15, and this also differs from Figure 4.5. It is likely that a contaminant is interfering with the quantification of the histones, most logically explained by residual β-mercaptoethanol from dialysis. The double banded presentation of the histones when electrophoresed, seen in Figure 4.14 and Figure 4.15, is consistent with published core histones (Dacher et al., 2019; Mishima et al., 2013).

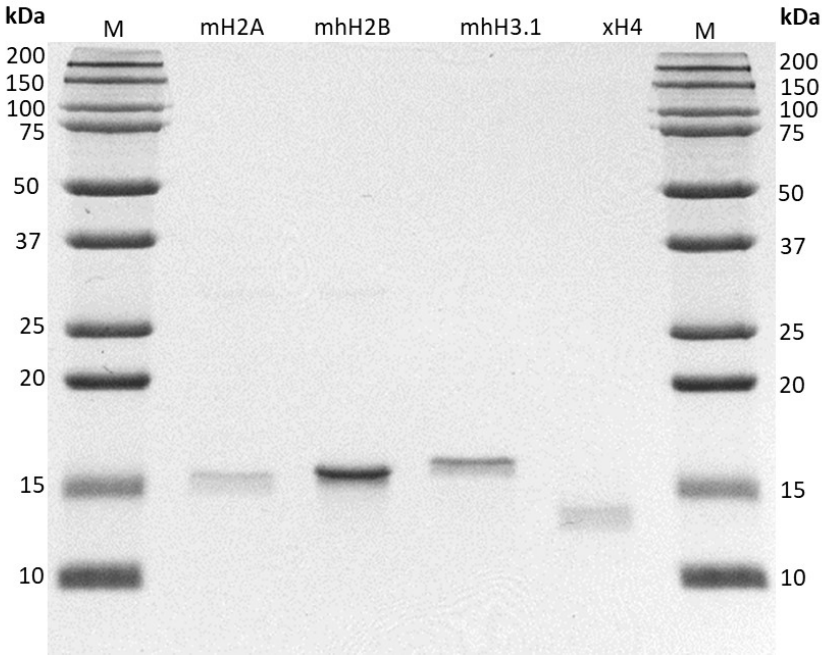

Figure 4.15: Ion exchange chromatography core histones. 1 µg of each core histone after ion exchange chromatography, mH2A, mhH2B, mhH3.1 and xH4 was resolved by 12 % SDS-PAGE, and stained with Coomassie blue. M - Molecular weight marker.

4.5 Summary

Unfortunately, issues in mononucleosome formation were encountered that need to be overcome before the binding of HP1α with RNA to a mononucleosome can be tested. The mononucleosome assembly reactions did not reach saturation nor was a homogeneous population observed (Figure 4.11 and Figure 4.12).

The change in relative intensities when equal amounts of core histone were electrophoresed after size exclusion and then after ion exchange chromatography (Figure 4.5 and Figure 4.15), is of concern and is likely due to contaminating β-mercaptoethanol that remains in the histone samples after dialysis. This then leads to overestimation of their concentration. Quantitation of the core histones will need to be done by performing a reducing agent compatible bicinchoninic acid assay with calf thymus histone standards (see Section 3.2.2).

When bound on the end of a DNA fragment, fluorophores have been implicated in restraining the bending of the DNA (Spiriti et al., 2011), which could inhibit the DNA from wrapping around the histone octamer. While Alexa488 labelled DNA has been used previously in mononucleosome formation (Ryan and Tremethick, 2016, 2018), a new DNA labelling system will be used. Primers with a biotin label will be designed for the amplification of the mononucleosome 601 positioning sequence fragment. Mononucleosomes will then be formed on this biotin labelled fragment and then a streptavidin conjugate with Alexa488 will then be added to allow fluorescent detection of the DNA in EMSAs. This will be done in an attempt to reduce heterogeneity of the mononucleosome population.

Chapter 5

Discussion and future directions

5.1 Discussion

5.1.1 TERRA mediates the interaction between H1.4 and HP1α

This research showed that Telomeric repeat-containing RNA (TERRA) mediates the interaction between Heterochromatin Protein 1α (HP1α) and linker histone H1.4 *in vitro*.

Previously published work showed that the HP1α hinge can interact with the H1.4 carboxy-terminal tail (CTD) (Hale et al., 2006). This work indicated that RNA did not mediate the interaction, with the GST-pulldowns performed with low levels of RNase added to the HP1α binding reactions. However, when GST-HP1α bacterial lysates were treated with RNase and then used in the GST pulldown, the interaction was lost (unpublished data). Using purified components in the His-HP1α pulldown (see Chapter 3) negated the need for RNase treatment of the His-HP1α, and thus removed uncertainty in reliability of results due to the dependency on RNase treatment.

5.1.2 H1.4 in heterochromatin

Truncation of the H1.4 CTD results in dysregulation of heterochromatin and the development of neurological disorders and neurodegenerative diseases (Duffney et al., 2018; Flex et al., 2019; Tatton-Brown et al., 2017), indicating the importance of the H1.4 CTD. The presence of H1.4 in heterochromatin, and its potential to bind structured non-coding RNA may target chromatin associated proteins to these regions.

Within a nucleosomal context, the H1.4 globular domain binds to the nucleosome off dyad, while the CTD interacts simultaneously with both linker DNA (Song et al., 2014; Zhou et al., 2013, 2021). When nucleosome bound H1.4 binds RNA, the question then stands, does the RNA compete the H1.4 CTD off the linker DNA, or can the CTD bind DNA and RNA simultaneously? A competitive behaviour implies that the H1.4 CTD can bind with specificity and with

varied affinities to certain nucleic acids, as it would have to preferentially bind another molecule over the linker DNA. While this has not been tested, it is likely due to the intrinsically disordered nature of the CTD, which displays differential behaviour when interacting with various DNA substrates by acquiring differing conformations (Fang et al., 2012, 2016).

In vitro, the sequestering of the linker DNA by the H1.4 CTD, in the absence of RNA, impedes post translation modification of H3 amino (N)-terminal tail (Stützer et al., 2016). Stützer et al. (2016) showed that the ability of various histone modifying enzymes, including histone methyltransferases, to modify the H3 N-terminal tail in a free nucleosome was markedly reduced when H1.4 was bound.

5.1.3 HP1α in heterochromatin

As heterochromatin formation through the HP1α chromodomain (CD) binding to di- and tri-methylated lysine 9 on histone H3 (H3K9me2/3) is insufficient for providing specificity (Cowell et al., 2002; Stewart et al., 2005), another interaction is required for targeting HP1α. At the centromere, it has been shown that Major satellite repeat RNA (MSR RNA) targets Small ubiquitin-like modifier-(SUMO)-ylated HP1α to pericentromeric heterochromatin (Maison et al., 2011). It has been shown *in vivo* that MSR RNA is essential, as upon RNase treatment, HP1α dissociates from pericentromeric heterochromatin (Maison et al., 2002). Additionally, in the absence of H3K9me2/3, and thus no binding through the HP1α CD, the interaction of SUMOylated HP1α with forward MSR RNA is sufficient to target HP1α to pericentric heterochromatin (Maison et al., 2011).

MSR RNA has also been identified to bind and target Suppressor of variegation 3-9 homolog 1/2 (Suv39h1/2) to pericentric heterochromatin (Camacho et al., 2017). While Suv39h1 binds non-specifically to RNA (Johnson et al., 2017), Suv39h2 binds with high specificity to both MSR RNA and TERRA through a basic arginine rich tail (Camacho et al., 2017). Suv39h2 has also been identified to interact with H1.4 *in vitro* through a GST-pulldown (Healton et al., 2020), however it is yet to be confirmed if this interaction is mediated by RNA. In cellular studies, treatment with RNase A disrupted Suv39h1/2 methylation of H3K9

and HP1α localisation at pericentromeric regions, and conversely, treatment with RNase H, cleaving any RNA-DNA duplexes, did not result in the same disruption (Maison et al., 2002). This indicates that Suv39h1/2 and HP1α are both bound to heterochromatin through RNA, and that this RNA is not interacting with DNA in the chromatin fibre but likely with a protein, such as H1.4. Both Suv39h2 (Camacho et al., 2017) and HP1α (Roach et al., 2020) have been shown to bind with specificity to structured in RNA, however the HP1α hinge has not been tested for binding specificity to MSR RNA.

The spread of heterochromatin can occur through Heterochromatin Protein 1 (HP1) molecules dimerising. While HP1 molecules can heterodimerise, they appear to have preference *in vitro* for homodimerisation (Nielsen et al., 2001). Paralogue specific oligomerisation through self association has been observed (Canzio et al., 2011; Yamada et al., 1999). Additionally, it has been shown that HP1γ can not bridge H3K9me3 dinucleosomes in the absence of H1 while HP1α can (Watanabe et al., 2018).

5.1.4 H1.4-HP1α interaction

In vitro it has been shown that both the hinge region interacting with DNA and CD binding H3K9me3 is required for HP1α to bind mononucleosomes, as in the absence of linker DNA, H3K9me3 or both, HP1α binding is significantly reduced or lost (Mishima et al., 2013). Another study using unmethylated mononucleosomes showed that, again, when no linker DNA is present, the affinity of HP1α for the mononucleosomes was significantly reduced (Ryan and Tremethick, 2018). Additionally, Ryan and Tremethick (2018) illustrated that when H1.4 is present on a mononucleosome, the binding of HP1α is impeded, although not to the extent of no linker DNA. This impedance may be due to H1.4 CTD sequestering the linker DNA, making it less accessible for HP1α to bind.

Building up from one chromatosome, it is then of interest how this interaction affects chromatin compaction, especially as it has been shown *in vitro* that the H1.4 CTD adopts a more compact structure when bound to mononucleosomes (Fang et al., 2012) compared to when bound to arrays of 12 nucleosomes (Fang et al.,

2016). Ryan and Tremethick (2018) demonstrated that in arrays of 12 nucleosomes, as seen with mononucleosomes, the presence of H1.4 impedes the binding of HP1α. Additionally, in these arrays the addition of H3K9me3 was unable to rescue the binding affinity of HP1α (Ryan and Tremethick, 2018). Interestingly, studies by Bryan et al. (2017) showed that in H3K9me3 12 nucleosome arrays, the addition of H1.1 which compacted the array, significantly increased the residency time of HP1α on the array. These studies illustrated that the charge based interaction of HP1 with DNA is instrumental in the initial binding, while the multivalent interactions aid in HP1 array residency (Bryan et al., 2017).

Two mechanisms are proposed for what occurs when RNA is added to a chromatosomes that would then enable HP1α to bind. Firstly, the H1.4 CTD may release the linker DNA in favour of the RNA, allowing the HP1α hinge to bind the now free linker DNA. Secondly, and perhaps more likely as the trimolecular interaction has been demonstrated in the absence of DNA in the pulldown assay, the H1.4 CTD binds the RNA, releasing linker DNA, and the RNA then bridges the interaction between H1.4 and HP1α, allowing HP1α to bind the chromatosome. However, it is not known if H1.4 CTD binds RNA preferentially over DNA. Additionally, any selectivity of the H1.4 CTD in binding structured RNA is unknown, thus it is unclear if H1.4 provides specificity in this interaction.

The order of binding of H1.4 and HP1α to the RNA is yet to be determined, however this could allude functionally to which protein provides specificity. If H1.4 binds RNA non-specifically, any RNA transcribed nearby could bind nucleosome bound H1.4, with the RNA acting as bait for proteins that bind that RNA. If H1.4 was the sole determinant of the specificity, this would bind any RNA interacting proteins nearby to the chromatosome. This is unlikely as HP1α has been shown to have specificity in binding RNA. For effective chromatin compaction, it is most likely that both HP1α and H1.4 bind the RNA with specificity. This would inhibit H1.4 from binding RNA bound by proteins which are not involved in chromatin compaction. Additionally, specificity in HP1α RNA binding would assist with chromatin retention by circumventing eviction from chromatin by non-specific binding to RNA, as seen with Polycomb repressive complex-2 (Davidovich et al., 2013).

5.1.5 TERRA in heterochromatin

Formation of telomeric heterochromatin requires TERRA. *In vivo* studies by Deng et al. (2009) showed through small interfering RNA that depletion of TERRA results in decreased H3K9me3, dysfunctional telomeres and reduced cell viability.

Chromatin immunoprecipitation showed that TERRA associated with both HP1α and H3K9me3 in the cell (Deng et al., 2009). As reviewed by Blasco (2007), both HP1α and H3K9me3 are required for heterochromatin formation at both the telomeres and sub-telomeres.

Transcription of TERRA molecules occurs at the telomeres (Azzalin et al., 2007; Schoeftner and Blasco, 2008). It has been shown through northern blot and RNA dot blot, detecting with strand specific telomeric repeat transcript probes, that cells with longer telomeres transcribe higher levels of TERRA than cells with shorter telomeres, however, the length of telomeres does not dictate the length of TERRA molecules (Schoeftner and Blasco, 2008). Schoeftner and Blasco (2008) also illustrated that the chromatin status can influence TERRA transcription, with more repressed chromatin transcribing less TERRA. Arnoult et al. (2012) reported the opposite, determined using quantitative reverse transcriptase PCR with chromosomal specific primers, that longer telomeres transcribed lower levels of TERRA than shorter telomeres. As longer telomeres were shown to have higher H3K9me3 density, Arnoult et al. (2012) hypothesised that TERRA transcription was repressed by H3K9me3 recruiting HP1α.

TERRA transcription is regulated during the cell cycle, with the highest levels of TERRA measured in early G1-phase and the lowest levels measured in S-phase, determined by immunofluorescence analysis (Flynn et al., 2011) and quantitative reverse transcriptase PCR (Porro et al., 2010). Immunofluorescence studies showed that TERRA occupancy at the telomeres during the cycle fluctuated in line with its transcription, and that HP1α and H3K9me3 displayed similar telomeric occupancy (Arnoult et al., 2012).

In vitro studies have shown that HP1α has a high binding affinity for the parallel g-quadruplex structure of TERRA molecules (Roach et al., 2020). As telomeric heterochromatin is enriched in H1.4 (Parseghian et al., 2001; Th'ng et al., 2005),

and HP1α associates with TERRA in the cell, the interaction of HP1α with H1.4, mediated by TERRA, is proposed as a mechanism for HP1α targeting to telomeres, and for the formation of telomeric heterochromatin.

5.1.6 Model of heterochromatin formation at the telomere

Maintenance of telomeric heterochromatin is essential for genomic stability, however it is not yet fully understood. Here, a model (Figure 5.1) is presented for initiation of heterochromatin formation at the telomeres involving H1.4.

With a more open structure adopted by chromatin during S-phase of the cell cycle, the expression of TERRA after S-phase is proposed to target HP1α to the telomere, mediating an interaction with H1.4 to reestablish telomeric heterochromatin. This interaction provides specific targeting of HP1α, as while all three HP1 paralogues can bind H3K9me3 (Hiragami-Hamada et al., 2011; Nishibuchi et al., 2014), HP1α is the only paralogue which interacts with H1.4 through RNA in the absence of H1.4 lysine 26 methylation (Daujat et al., 2005; Hale et al., 2006), and has been shown *in vitro* to have the highest binding affinity to TERRA (Roach et al., 2020). This model proposes that the binding of H1.4 to nucleosomes acts as a regulator, inhibiting HP1 paralogues β and γ from binding, and that the binding of TERRA to H1.4 in the chromatosome provides a HP1α specific binding site.

As HP1α is more likely to form homodimers opposed to heterodimers, this further enriches the telomeric heterochromatin in HP1α. This dimerisation then increases the affinity of HP1α to H3K9me3, which is low with individual HP1 molecules (Kilic et al., 2015), aiding to propagate the heterochromatin. Thus, HP1α can then bridge nucleosomes with HP1α bound through TERRA and H1.4, and H3K9me3, compacting telomeric heterochromatin.

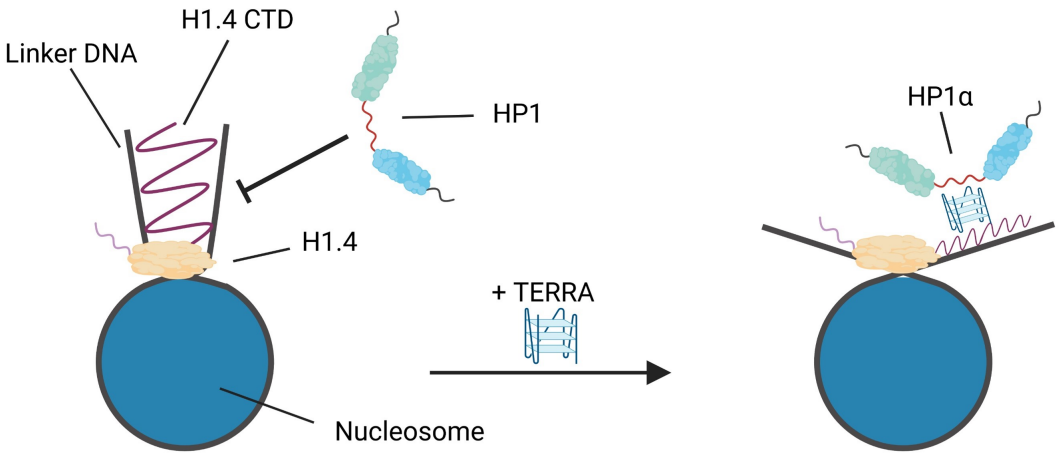

Figure 5.1: H1.4-TERRA-HP1α heterochromatin establishment. Nucleosomes bound by H1.4 act as a HP1α specific binding site, with HP1α targeted to the nucleosomes through TERRA.

5.2 Future directions

5.2.1 Investigate how this interaction affects the behaviour of HP1α in chromatin compaction

As discussed in Section 4.5, to resolve the issues with the mononucleosome formation, histone octamers will be formed with expressed and purified core histones that are quantified using a reducing agent compatible bicinchoninic acid assay. A biotin labelled DNA fragment will be produced, on which mononucleosomes will then be formed.

Once the issues with mononucleosome formation have been addressed, the specificity of the H1.4 CTD for structured RNA will be assessed. Different RNAs, including TERRA, will be tested in competition electrophoretic mobility shift assays (EMSAs). H1.4 will be bound to mononucleosomes and then combined with RNA. Any changes in mobility will indicate if H1.4 binds the RNA and if there is any difference in binding between RNA types. Specificity in the binding of the H1.4 CTD to structured RNA could implicate that the interaction has a regulatory role at specific genomic locations.

To determine if RNA assists in the binding of HP1α when H1.4 is present, EMSAs will be performed with mononucleosomes and trinucleosomes (Ryan and Tremethick, 2018). Mononucleosomes will be tested initially, either as a nucleosome or as a chromatosome with H1.4, followed by the addition of RNA alone and then the addition of HP1α or RNA prebound to HP1α. Prebinding RNA to HP1α or H1.4 will indicate if it is a sequential process. These experiments will be conducted using TERRA96 as it has been shown to mediate the interaction of HP1α to H1.4. The experiments will then be repeated with the determined binding conditions in trinucleosomes. The changes to electrophoretic mobility of the trinucleosomes will indicate if the binding of RNA and HP1α has compacted the nucleosomes.

To investigate the role of the interaction in chromatin compaction, nucleosomal arrays of 12 nucleosomes will be produced, as described previously (Ryan and Tremethick, 2018), where histone H2A was labeled at residue 120 with Alexa488. EMSAs will then be performed, as described for the trinucleosomes, to illustrate the chromatin compaction ability of the H1.4-HP1α interaction.

5.2.2 Confirm that the interaction occurs through the HP1α hinge and H1.4 CTD, and determine the regions involved

The His-HP1α *in vitro* pulldown will be used to confirm that this RNA mediated interaction occurs through the H1.4 CTD and the HP1α hinge region. A previously constructed FLAG-tagged H1.4/1.2 mutant (from CRG Laboratory), where the H1.4 CTD has been exchanged for the H1.2 CTD, will be tested with TERRA96 to determine if the interaction still occurs. The HP1α hinge mutant with the deletion of the nucleic acid binding region, residues 86 to 108 (HP1α HΔ23) (from CRG Laboratory), will be tested to determine if, when TERRA96 is present, the interaction is still mediated. Another HP1α hinge mutant with three positively charged lysines substituted for three uncharged alanines within the nucleic acid binding region, residues 104 to 106 (HP1α 3K-A) (from CRG Laboratory), will also be tested to determine the requirement of this charged patch in mediating the interaction through TERRA96. New mutants may be developed and tested to investigate other specific regions, and will implicate the

importance of these regions in mediating the interaction.

5.2.3 Investigate if H1.4 interacts with MSR RNA to assist HP1α binding to the centromere

To investigate if MSR RNA mediates the interaction of HP1α and H1.4, a MSR RNA *in vitro* transcription plasmid will be constructed so it can be transcribed by the T7 promoter *in vitro*, as previously described (Lehnertz et al., 2003). Forward MSR RNA will then be tested in the *in vitro* pulldown assay with unmodified His-HP1α and FLAG-H1.4 (see Section 2.5). If FLAG-H1.4 is pulled down, this indicates SUMOylation of HP1α is not required for binding to MSR RNA in this *in vitro* interaction.

If no FLAG-H1.4 is pulled down from the reaction mixture, a conclusion cannot be drawn as it could be due to the requirement of the SUMOylation of HP1α (Maison et al., 2011), or MSR RNA does not mediate the interaction of the H1.4 and HP1α, and instead targets HP1α to pericentric heterochromatin through another means. To address this, His-HP1α will be SUMOylated *in vitro*, as previously performed (Maison et al., 2011). The SUMOylated His-HP1α will then be tested with forward MSR RNA in the *in vitro* pulldown. If neither unmodified or SUMOylated His-HP1α pull down FLAG-H1.4 with forward MSR RNA, this indicates that MSR RNA does not mediate HP1α binding to pericentric heterochromatin through H1.4. If FLAG-H1.4 is pulled down with MSR RNA bound SUMO-His-HP1α, this indicates that SUMOylated HP1α is bound to centromeric heterochromatin through H1.4, mediated by forward MSR RNA.

5.3 Summary

The *in vitro* pulldown assay showed that TERRA mediated the interaction between H1.4 and HP1α. This has implications for how HP1α is targeted to heterochromatin within the cell, in that TERRA mediates the interaction of HP1α with heterochromatin, through H1.4. From this, a model for telomeric heterochromatin formation is proposed. The *in vitro* pulldown assay has the potential to

identify regions of importance in both HP1α and H1.4, and if there is a structural element to RNA specificity. Future nucleosomal studies will build on this, in how this interaction occurs in a nucleosome and how this interaction influences chromatin compaction. This research will allude to how HP1α is targeted to and compacts constitutive heterochromatin, thus protecting the genome, defending cells from cancer and aging.

Bibliography

Aagaard, L., Laible, G., Selenko, P., Schmid, M., Dorn, R., Schotta, G., Kuhfittig, S., Wolf, A., Lebersorger, A., Singh, P. B., et al. (1999). Functional mammalian homologues of the drosophila PEV-modifier Su (var) 3-9 encode centromere-associated proteins which complex with the heterochromatin component M31. *The EMBO journal*, 18(7):1923–1938.

Apostolou, E., Ferrari, F., Walsh, R. M., Bar-Nur, O., Stadtfeld, M., Cheloufi, S., Stuart, H. T., Polo, J. M., Ohsumi, T. K., Borowsky, M. L., et al. (2013). Genome-wide chromatin interactions of the Nanog locus in pluripotency, differentiation, and reprogramming. *Cell stem cell*, 12(6):699–712.

Arents, G., Burlingame, R. W., Wang, B.-C., Love, W. E., and Moudrianakis, E. N. (1991). The nucleosomal core histone octamer at 3.1 a resolution: a tripartite protein assembly and a left-handed superhelix. *Proceedings of the National Academy of Sciences*, 88(22):10148–10152.

Arents, G. and Moudrianakis, E. N. (1995). The histone fold: a ubiquitous architectural motif utilized in DNA compaction and protein dimerization. *Proceedings of the National Academy of Sciences*, 92(24):11170–11174.

Arnoult, N., Van Beneden, A., and Decottignies, A. (2012). Telomere length regulates TERRA levels through increased trimethylation of telomeric H3K9 and HP1α. *Nature structural & molecular biology*, 19(9):948–956.

Azzalin, C. M., Reichenbach, P., Khoriauli, L., Giulotto, E., and Lingner, J. (2007). Telomeric repeat–containing RNA and RNA surveillance factors at mammalian chromosome ends. *Science*, 318(5851):798–801.

Bannister, A. J., Zegerman, P., Partridge, J. F., Miska, E. A., Thomas, J. O.,

Allshire, R. C., and Kouzarides, T. (2001). Selective recognition of methylated lysine 9 on histone H3 by the HP1 chromo domain. *Nature*, 410(6824):120–124.

Bascom, G. and Schlick, T. (2017). Linking chromatin fibers to gene folding by hierarchical looping. *Biophysical journal*, 112(3):434–445.

Bednar, J., Garcia-Saez, I., Boopathi, R., Cutter, A. R., Papai, G., Reymer, A., Syed, S. H., Lone, I. N., Tonchev, O., Crucifix, C., Menoni, H., Papin, C., Skoufias, D. A., Kurumizaka, H., Lavery, R., Hamiche, A., Hayes, J. J., Schultz, P., Angelov, D., Petosa, C., and Dimitrov, S. (2017). Structure and dynamics of a 197 bp nucleosome in complex with linker histone H1. *Molecular cell*, 66(3):384–397.e8.

Bednar, J., Horowitz, R. A., Grigoryev, S. A., Carruthers, L. M., Hansen, J. C., Koster, A. J., and Woodcock, C. L. (1998). Nucleosomes, linker DNA, and linker histone form a unique structural motif that directs the higher-order folding and compaction of chromatin. *Proceedings of the National Academy of Sciences*, 95(24):14173–14178.

Blasco, M. A. (2007). The epigenetic regulation of mammalian telomeres. *Nature Reviews Genetics*, 8(4):299–309.

Bonner, J. and Widholm, J. (1967). Molecular complementarity between nuclear DNA and organ-specific chromosomal RNA. *Proceedings of the National Academy of Sciences of the United States of America*, 57(5):1379.

Bryan, L. C., Weilandt, D. R., Bachmann, A. L., Kilic, S., Lechner, C. C., Odermatt, P. D., Fantner, G. E., Georgeon, S., Hantschel, O., Hatzimanikatis, V., and Fierz, B. (2017). Single-molecule kinetic analysis of HP1-chromatin binding reveals a dynamic network of histone modification and DNA interactions. *Nucleic Acids Research*, 45(18):10504–10517.

Burge, S., Parkinson, G. N., Hazel, P., Todd, A. K., and Neidle, S. (2006). Quadruplex DNA: sequence, topology and structure. *Nucleic acids research*, 34(19):5402–5415.

Camacho, O. V., Galan, C., Swist-Rosowska, K., Ching, R., Gamalinda, M., Karabiber, F., De La Rosa-Velazquez, I., Engist, B., Koschorz, B., Shukeir, N., et al. (2017). Major satellite repeat RNA stabilize heterochromatin retention

of Suv39h enzymes by RNA-nucleosome association and RNA: DNA hybrid formation. *Elife*, 6:e25293.

Canzio, D., Chang, E. Y., Shankar, S., Kuchenbecker, K. M., Simon, M. D., Madhani, H. D., Narlikar, G. J., and Al-Sady, B. (2011). Chromodomain-mediated oligomerization of HP1 suggests a nucleosome-bridging mechanism for heterochromatin assembly. *Molecular cell*, 41(1):67–81.

Carruthers, L. M., Tse, C., Walker III, K. P., and Hansen, J. C. (1999). Assembly of defined nucleosomal and chromatin arrays from pure components. *Methods in enzymology*, 304:19–35.

Chan, F. L., Marshall, O. J., Saffery, R., Kim, B. W., Earle, E., Choo, K. A., and Wong, L. H. (2012). Active transcription and essential role of RNA polymerase II at the centromere during mitosis. *Proceedings of the National Academy of Sciences*, 109(6):1979–1984.

Contreras, A., Hale, T. K., Stenoien, D. L., Rosen, J. M., Mancini, M. A., and Herrera, R. E. (2003). The dynamic mobility of histone H1 is regulated by cyclin/CDK phosphorylation. *Molecular and cellular biology*, 23(23):8626–8636.

Cowell, I. G., Aucott, R., Mahadevaiah, S. K., Burgoyne, P. S., Huskisson, N., Bongiorni, S., Prantera, G., Fanti, L., Pimpinelli, S., Wu, R., Gilbert, D. M., Shi, W., Fundele, R., Morrison, H., Jeppesen, P., and Singh, P. B. (2002). Heterochromatin, HP1 and methylation at lysine 9 of histone H3 in animals. *Chromosoma*, 111(1):22–36.

Dacher, M., Tachiwana, H., Horikoshi, N., Kujirai, T., Taguchi, H., Kimura, H., and Kurumizaka, H. (2019). Incorporation and influence of Leishmania histone H3 in chromatin. *Nucleic acids research*, 47(22):11637–11648.

Daujat, S., Zeissler, U., Waldmann, T., Happel, N., and Schneider, R. (2005). HP1 binds specifically to Lys26-methylated Histone H1.4, whereas simultaneous Ser27 phosphorylation blocks HP1 binding. *Journal of Biological Chemistry*, 280(45):38090–38095.

Davidovich, C., Zheng, L., Goodrich, K. J., and Cech, T. R. (2013). Promiscuous RNA binding by Polycomb repressive complex 2. *Nature structural & molecular biology*, 20(11):1250–1257.

De Laat, W. and Duboule, D. (2013). Topology of mammalian developmental enhancers and their regulatory landscapes. *Nature*, 502(7472):499–506.

Deng, Z., Norseen, J., Wiedmer, A., Riethman, H., and Lieberman, P. M. (2009). TERRA RNA binding to TRF2 facilitates heterochromatin formation and ORC recruitment at telomeres. *Molecular cell*, 35(4):403–413.

Dorer, D. R. and Henikoff, S. (1994). Expansions of transgene repeats cause heterochromatin formation and gene silencing in Drosophila. *Cell*, 77(7):993–1002.

Duffney, L. J., Valdez, P., Tremblay, M. W., Cao, X., Montgomery, S., McConkie-Rosell, A., and Jiang, Y.-h. (2018). Epigenetics and autism spectrum disorder: A report of an autism case with mutation in H1 linker histone HIST1H1E and literature review. *American Journal of Medical Genetics Part B: Neuropsychiatric Genetics*, 177(4):426–433.

Dyer, P. N., Edayathumangalam, R. S., White, C. L., Bao, Y., Chakravarthy, S., Muthurajan, U. M., and Luger, K. (2003). Reconstitution of nucleosome core particles from recombinant histones and DNA. *Methods in enzymology*, 375:23–44.

Eickbush, T. H. and Moudrianakis, E. N. (1978). The histone core complex: an octamer assembled by two sets of protein-protein interactions. *Biochemistry*, 17(23):4955–4964.

Eissenberg, J. C. and Elgin, S. C. (2000). The HP1 protein family: getting a grip on chromatin. *Current Opinion in Genetics & Development*, 10(2):204–210.

Eissenberg, J. C., James, T. C., Foster-Hartnett, D. M., Hartnett, T., Ngan, V., and Elgin, S. (1990). Mutation in a heterochromatin-specific chromosomal protein is associated with suppression of position-effect variegation in Drosophila melanogaster. *Proceedings of the National Academy of Sciences*, 87(24):9923–9927.

Fang, H., Clark, D. J., and Hayes, J. J. (2012). DNA and nucleosomes direct distinct folding of a linker histone H1 C-terminal domain. *Nucleic acids research*, 40(4):1475–1484.

Fang, H., Wei, S., Lee, T.-H., and Hayes, J. J. (2016). Chromatin structure-dependent conformations of the H1 CTD. *Nucleic acids research*, 44(19):9131–9141.

Feinberg, A. P., Koldobskiy, M. A., and Göndör, A. (2016). Epigenetic modulators, modifiers and mediators in cancer aetiology and progression. *Nature Reviews Genetics*, 17(5):284–299.

Ferri, F., Bouzinba-Segard, H., Velasco, G., Hube, F., and Francastel, C. (2009). Non-coding murine centromeric transcripts associate with and potentiate Aurora B kinase. *Nucleic acids research*, 37(15):5071–5080.

Festenstein, R., Sharghi-Namini, S., Fox, M., Roderick, K., Tolaini, M., Norton, T., Saveliev, A., Kioussis, D., and Singh, P. (1999). Heterochromatin protein 1 modifies mammalian PEV in a dose-and chromosomal-context-dependent manner. *Nature genetics*, 23(4):457–461.

Flaus, A. (2011). Principles and practice of nucleosome positioning in vitro. *Frontiers in Life Science*, 5(1-2):5–27.

Flex, E., Martinelli, S., Van Dijck, A., Ciolfi, A., Cecchetti, S., Coluzzi, E., Pannone, L., Andreoli, C., Radio, F. C., Pizzi, S., et al. (2019). Aberrant function of the C-terminal tail of HIST1H1E accelerates cellular senescence and causes premature aging. *The American Journal of Human Genetics*, 105(3):493–508.

Flynn, R. L., Centore, R. C., O'Sullivan, R. J., Rai, R., Tse, A., Songyang, Z., Chang, S., Karlseder, J., and Zou, L. (2011). TERRA and hnRNPA1 orchestrate an RPA-to-POT1 switch on telomeric single-stranded DNA. *Nature*, 471(7339):532–536.

Fyodorov, D. V., Zhou, B.-R., Skoultchi, A. I., and Bai, Y. (2018). Emerging roles of linker histones in regulating chromatin structure and function. *Nature reviews Molecular cell biology*, 19(3):192–206.

Garavís, M., López-Méndez, B., Somoza, A., Oyarzabal, J., Dalvit, C., Villasante, A., Campos-Olivas, R., and González, C. (2014). Discovery of selective ligands for telomeric RNA G-quadruplexes (TERRA) through 19F-NMR based fragment screening. *ACS chemical biology*, 9(7):1559–1566.

Germond, J.-E., Bellard, M., Oudet, P., and Chambon, P. (1976). Stability of nucleosomes in native and reconstituted chromatins. *Nucleic acids research*, 3(11):3173–3192.

Gorkin, D. U., Leung, D., and Ren, B. (2014). The 3D genome in transcriptional regulation and pluripotency. *Cell stem cell*, 14(6):762–775.

Grewal, S. I. (2010). RNAi-dependent formation of heterochromatin and its diverse functions. *Current opinion in genetics & development*, 20(2):134–141.

Grewal, S. I. S. and Jia, S. (2007). Heterochromatin revisited. *Nature Reviews Genetics*, 8(1):35–46.

Haithcock, E., Dayani, Y., Neufeld, E., Zahand, A. J., Feinstein, N., Mattout, A., Gruenbaum, Y., and Liu, J. (2005). Age-related changes of nuclear architecture in Caenorhabditis elegans. *Proceedings of the National Academy of Sciences*, 102(46):16690–16695.

Hale, T. K., Contreras, A., Morrison, A. J., and Herrera, R. E. (2006). Phosphorylation of the linker histone H1 by CDK regulates its binding to HP1α. *Molecular Cell*, 22(5):693–699.

Hall, L. L. and Lawrence, J. B. (2016). RNA as a fundamental component of interphase chromosomes: could repeats prove key? *Current opinion in genetics & development*, 37:137–147.

Hansen, J. C., Tse, C., and Wolffe, A. P. (1998). Structure and function of the core histone N-termini: more than meets the eye. *Biochemistry*, 37(51):17637–17641.

Harshman, S. W., Young, N. L., Parthun, M. R., and Freitas, M. A. (2013). H1 histones: current perspectives and challenges. *Nucleic Acids Research*, 41(21):9593–9609.

He, F. (2011). BCA (bicinchoninic acid) protein assay. *Bio-protocol*, 101:e44.

Healton, S. E., Pinto, H. D., Mishra, L. N., Hamilton, G. A., Wheat, J. C., Swist-Rosowska, K., Shukeir, N., Dou, Y., Steidl, U., Jenuwein, T., et al. (2020). H1 linker histones silence repetitive elements by promoting both histone H3K9 methylation and chromatin compaction. *Proceedings of the National Academy of Sciences*, 117(25):14251–14258.

Heitz, E. (1928). *Das heterochromatin der moose*. Bornträger.

Hergeth, S. P., Dundr, M., Tropberger, P., Zee, B. M., Garcia, B. A., Daujat, S., and Schneider, R. (2011). Isoform-specific phosphorylation of human linker histone H1.4 in mitosis by the kinase Aurora B. *Journal of Cell Science*, 124(10):1623–1628.

Hiragami-Hamada, K., Shinmyozu, K., Hamada, D., Tatsu, Y., Uegaki, K., Fujiwara, S., and Nakayama, J.-i. (2011). N-terminal phosphorylation of HP1α promotes its chromatin binding. *Molecular and cellular biology*, 31(6):1186–1200.

Holmes, D. S., Mayfield, J. E., Sander, G., and Bonner, J. (1972). Chromosomal RNA: its properties. *Science*, 177(4043):72–74.

Horn, P. J., Carruthers, L. M., Logie, C., Hill, D. A., Solomon, M. J., Wade, P. A., Imbalzano, A. N., Hansen, J. C., and Peterson, C. L. (2002). Phosphorylation of linker histones regulates ATP-dependent chromatin remodeling enzymes. *Nature structural biology*, 9(4):263–267.

Horn, P. J. and Peterson, C. L. (2002). Chromatin higher order folding–wrapping up transcription. *Science*, 297(5588):1824.

Huang, R.-C. and Bonner, J. (1965). Histone-bound RNA, a component of native nucleohistone. *Proceedings of the National Academy of Sciences of the United States of America*, 54(3):960.

Hutchinson, J. B., Cheema, M. S., Wang, J., Missiaen, K., Finn, R., Gonzalez Romero, R., Th'ng, J. P., Hendzel, M., and Ausió, J. (2015). Interaction of chromatin with a histone H1 containing swapped N- and C-terminal domains. *Bioscience reports*, 35(3):e00209.

Hyun, K., Jeon, J., Park, K., and Kim, J. (2017). Writing, erasing and reading histone lysine methylations. *Experimental & Molecular Medicine*, 49(4):e324–e324.

James, T. C. and Elgin, S. (1986). Identification of a nonhistone chromosomal protein associated with heterochromatin in Drosophila melanogaster and its gene. *Molecular and cellular biology*, 6(11):3862–3872.

Janssen, A., Colmenares, S. U., and Karpen, G. H. (2018). Heterochromatin: Guardian of the genome. *Annual Review of Cell and Developmental Biology*, 34(1):265–288.

Johnson, W. L., Yewdell, W. T., Bell, J. C., McNulty, S. M., Duda, Z., O'Neill, R. J., Sullivan, B. A., and Straight, A. F. (2017). RNA-dependent stabilization of SUV39H1 at constitutive heterochromatin. *Elife*, 6:e25299.

Kilic, S., Bachmann, A. L., Bryan, L. C., and Fierz, B. (2015). Multivalency governs HP1α association dynamics with the silent chromatin state. *Nature communications*, 6(1):1–11.

Klinker, H., Haas, C., Harrer, N., Becker, P. B., and Mueller-Planitz, F. (2014). Rapid purification of recombinant histones. *PloS one*, 9(8):e104029.

Kumar, A. and Kono, H. (2020). Heterochromatin protein 1 (HP1): interactions with itself and chromatin components. *Biophysical Reviews*, 12(2):387–400.

Larson, K., Yan, S.-J., Tsurumi, A., Liu, J., Zhou, J., Gaur, K., Guo, D., Eickbush, T. H., and Li, W. X. (2012). Heterochromatin formation promotes longevity and represses ribosomal RNA synthesis. *PLoS genetics*, 8(1):e1002473.

Lee, J.-H., Kim, E. W., Croteau, D. L., and Bohr, V. A. (2020). Heterochromatin: an epigenetic point of view in aging. *Experimental & Molecular Medicine*, 52(9):1466–1474.

Lehnertz, B., Ueda, Y., Derijck, A. A., Braunschweig, U., Perez-Burgos, L., Kubicek, S., Chen, T., Li, E., Jenuwein, T., and Peters, A. H. (2003). Suv39h-mediated histone H3 lysine 9 methylation directs DNA methylation to major satellite repeats at pericentric heterochromatin. *Current Biology*, 13(14):1192–1200.

Ljungman, M. and Hanawalt, P. C. (1992). Efficient protection against oxidative DNA damage in chromatin. *Molecular carcinogenesis*, 5(4):264–269.

Lomberk, G., Wallrath, L., and Urrutia, R. (2006). The Heterochromatin Protein 1 family. *Genome Biology*, 7(7):228.

Lowary, P. and Widom, J. (1998). New DNA sequence rules for high affinity binding to histone octamer and sequence-directed nucleosome positioning. *Journal of molecular biology*, 276(1):19–42.

Luger, K., Mäder, A. W., Richmond, R. K., Sargent, D. F., and Richmond, T. J. (1997a). Crystal structure of the nucleosome core particle at 2.8 Å resolution. *Nature*, 389(6648):251–260.

Luger, K., Rechsteiner, T. J., Flaus, A. J., Waye, M. M., and Richmond, T. J. (1997b). Characterization of nucleosome core particles containing histone proteins made in bacteria. *Journal of molecular biology*, 272(3):301–311.

Luger, K., Rechsteiner, T. J., and Richmond, T. J. (1999a). Expression and purification of recombinant histones and nucleosome reconstitution. In *Chromatin Protocols*, pages 1–16. Springer.

Luger, K., Rechsteiner, T. J., and Richmond, T. J. (1999b). Preparation of nucleosome core particle from recombinant histones. In *Methods in Enzymology*, volume 304, pages 3–19. Elsevier.

Maison, C., Bailly, D., Peters, A. H., Quivy, J.-P., Roche, D., Taddei, A., Lachner, M., Jenuwein, T., and Almouzni, G. (2002). Higher-order structure in pericentric heterochromatin involves a distinct pattern of histone modification and an RNA component. *Nature Genetics*, 30(3):329–334.

Maison, C., Bailly, D., Roche, D., de Oca, R. M., Probst, A. V., Vassias, I., Dingli, F., Lombard, B., Loew, D., Quivy, J.-P., and Almouzni, G. (2011). SUMOylation promotes de novo targeting of HP1α to pericentric heterochromatin. *Nature Genetics*, 43(3):220–227.

Martadinata, H. and Phan, A. T. (2009). Structure of propeller-type parallel-stranded RNA G-quadruplexes, formed by human telomeric RNA sequences in K+ solution. *Journal of the American Chemical Society*, 131(7):2570–2578.

McKenna, S. A., Kim, I., Puglisi, E. V., Lindhout, D. A., Aitken, C. E., Marshall, R. A., and Puglisi, J. D. (2007). Purification and characterization of transcribed RNAs using gel filtration chromatography. *Nature Protocols*, 2(12):3270–3277.

Meehan, R. R., Kao, C.-F., and Pennings, S. (2003). HP1 binding to native chromatin in vitro is determined by the hinge region and not by the chromodomain. *The EMBO Journal*, 22(12):3164–3174.

Minc, E., Allory, Y., Worman, H. J., Courvalin, J.-C., and Buendia, B. (1999). Localization and phosphorylation of HP1 proteins during the cell cycle in mammalian cells. *Chromosoma*, 108(4):220–234.

Mishima, Y., Watanabe, M., Kawakami, T., Jayasinghe, C. D., Otani, J., Kikugawa, Y., Shirakawa, M., Kimura, H., Nishimura, O., Aimoto, S., Tajima, S., and Suetake, I. (2013). Hinge and chromoshadow of HP1α participate in recognition of K9 methylated histone H3 in nucleosomes. *Journal of Molecular Biology*, 425(1):54–70.

Muchardt, C., Guillemé, M., Seeler, J.-S., Trouche, D., Dejean, A., and Yaniv, M. (2002). Coordinated methyl and RNA binding is required for heterochromatin localization of mammalian HP1α. *EMBO reports*, 3(10):975–981.

Nickerson, J. A., Krochmalnic, G., Wan, K. M., and Penman, S. (1989). Chromatin architecture and nuclear RNA. *Proceedings of the National Academy of Sciences*, 86(1):177–181.

Nielsen, A. L., Oulad-Abdelghani, M., Ortiz, J. A., Remboutsika, E., Chambon, P., and Losson, R. (2001). Heterochromatin formation in mammalian cells: interaction between histones and HP1 proteins. *Molecular cell*, 7(4):729–739.

Nishibuchi, G., Machida, S., Osakabe, A., Murakoshi, H., Hiragami-Hamada, K., Nakagawa, R., Fischle, W., Nishimura, Y., Kurumizaka, H., Tagami, H., et al. (2014). N-terminal phosphorylation of HP1α increases its nucleosome-binding specificity. *Nucleic acids research*, 42(20):12498–12511.

Nishibuchi, G. and Nakayama, J.-i. (2014). Biochemical and structural properties of heterochromatin protein 1: understanding its role in chromatin assembly. *The Journal of Biochemistry*, 156(1):11–20.

Norwood, L. E., Moss, T. J., Margaryan, N. V., Cook, S. L., Wright, L., Seftor, E. A., Hendrix, M. J., Kirschmann, D. A., and Wallrath, L. L. (2006). A requirement for dimerization of HP1Hsα in suppression of breast cancer invasion. *Journal of Biological Chemistry*, 281(27):18668–18676.

Nozawa, R.-S., Nagao, K., Masuda, H.-T., Iwasaki, O., Hirota, T., Nozaki, N., Kimura, H., and Obuse, C. (2010). Human POGZ modulates dissociation of HP1α from mitotic chromosome arms through Aurora B activation. *Nature cell biology*, 12(7):719–727.

Osunsade, A., Prescott, N. A., Hebert, J. M., Ray, D. M., Jmeian, Y., Lorenz, I. C., and David, Y. (2018). A robust method for the purification and characterization of recombinant human histone H1 variants. *Biochemistry*, 58(3):171–176.

Padeken, J., Zeller, P., and Gasser, S. M. (2015). Repeat DNA in genome organization and stability. *Current opinion in genetics & development*, 31:12–19.

Parseghian, M. H. (2015). What is the role of histone H1 heterogeneity? A functional model emerges from a 50 year mystery. *AIMS biophysics*, 2(4):724.

Parseghian, M. H., Newcomb, R. L., and Hamkalo, B. A. (2001). Distribution of somatic H1 subtypes is non-random on active vs. inactive chromatin II: distribution in human adult fibroblasts. *Journal of Cellular Biochemistry*, 83(4):643–659.

Porro, A., Feuerhahn, S., Reichenbach, P., and Lingner, J. (2010). Molecular dissection of telomeric repeat-containing RNA biogenesis unveils the presence of distinct and multiple regulatory pathways. *Molecular and cellular biology*, 30(20):4808–4817.

Randall, A. and Griffith, J. D. (2009). Structure of long telomeric RNA transcripts: the G-rich RNA forms a compact repeating structure containing G-quartets. *Journal of Biological Chemistry*, 284(21):13980–13986.

Rao, S. S., Huntley, M. H., Durand, N. C., Stamenova, E. K., Bochkov, I. D., Robinson, J. T., Sanborn, A. L., Machol, I., Omer, A. D., Lander, E. S., et al. (2014). A 3D map of the human genome at kilobase resolution reveals principles of chromatin looping. *Cell*, 159(7):1665–1680.

Roach, R. J., Garavís, M., González, C., Jameson, G. B., Filichev, V. V., and Hale, T. K. (2020). Heterochromatin protein 1α interacts with parallel RNA and DNA G-quadruplexes. *Nucleic Acids Research*, 48(2):682–693.

Rodriguez-Campos, A. and Azorín, F. (2007). RNA is an integral component of chromatin that contributes to its structural organization. *PloS one*, 2(11):e1182.

Ryan, D. P. and Tremethick, D. J. (2016). A dual affinity-tag strategy for the expression and purification of human linker histone H1.4 in escherichia coli. *Protein expression and purification*, 120:160–168.

Ryan, D. P. and Tremethick, D. J. (2018). The interplay between H2A.Z and H3K9 methylation in regulating HP1α binding to linker histone-containing chromatin. *Nucleic Acids Research*, 46(18):9353–9366.

Saffery, R., Sumer, H., Hassan, S., Wong, L. H., Craig, J. M., Todokoro, K., Anderson, M., Stafford, A., and Choo, K. A. (2003). Transcription within a functional human centromere. *Molecular cell*, 12(2):509–516.

Saha, A. and Dalal, Y. (2021). A glitch in the snitch: the role of linker histone H1 in shaping the epigenome in normal and diseased cells. *Open Biology*, 11(8):210124.

Sanborn, A. L., Rao, S. S., Huang, S.-C., Durand, N. C., Huntley, M. H., Jewett, A. I., Bochkov, I. D., Chinnappan, D., Cutkosky, A., Li, J., et al. (2015). Chromatin extrusion explains key features of loop and domain formation in wild-type and engineered genomes. *Proceedings of the National Academy of Sciences*, 112(47):E6456–E6465.

Saurin, A. J., Shiels, C., Williamson, J., Satijn, D. P., Otte, A. P., Sheer, D., and Freemont, P. S. (1998). The human polycomb group complex associates with pericentromeric heterochromatin to form a novel nuclear domain. *The Journal of cell biology*, 142(4):887–898.

Schleif, R. (1992). DNA looping. *Annual review of biochemistry*, 61(1):199–223.

Schoeftner, S. and Blasco, M. A. (2008). Developmentally regulated transcription of mammalian telomeres by DNA-dependent RNA polymerase II. *Nature cell biology*, 10(2):228–236.

Shen, C.-H. and Allan, J. (2021). MNase digestion protection patterns of the linker DNA in Chromatosomes. *Cells*, 10(9):2239.

Singer, D. S. and Singer, M. F. (1976). Studies on the interaction of H1 histone with superhelical DNA: Characterization of the recognition and binding regions of H1 histone. *Nucleic acids research*, 3(10):2531–2548.

Slee, R., Steiner, C., Herbert, B., Vance, G., Hickey, R., Schwarz, T., Christan, S., Radovich, M., Schneider, B., Schindelhauer, D., et al. (2012). Cancer-associated alteration of pericentromeric heterochromatin may contribute to chromosome instability. *Oncogene*, 31(27):3244–3253.

Song, F., Chen, P., Sun, D., Wang, M., Dong, L., Liang, D., Xu, R.-M., Zhu, P., and Li, G. (2014). Cryo-EM study of the chromatin fiber reveals a double helix twisted by tetranucleosomal units. *Science*, 344(6182):376.

Soyer-Gobillard, M.-O. and Herzog, M. (1985). The native structure of dinoflagellate chromosomes: involvement of structural RNA. *European journal of cell biology*, 36(2):334–342.

Spiriti, J., Binder, J. K., Levitus, M., and Van Der Vaart, A. (2011). Cy3-DNA stacking interactions strongly depend on the identity of the terminal basepair. *Biophysical journal*, 100(4):1049–1057.

Splinter, E., Heath, H., Kooren, J., Palstra, R.-J., Klous, P., Grosveld, F., Galjart, N., and de Laat, W. (2006). CTCF mediates long-range chromatin looping and local histone modification in the β-globin locus. *Genes & development*, 20(17):2349–2354.

Stephens, A. D., Banigan, E. J., and Marko, J. F. (2019). Chromatin's physical properties shape the nucleus and its functions. *Current opinion in cell biology*, 58:76–84.

Sterner, D. E. and Berger, S. L. (2000). Acetylation of histones and transcription-related factors. *Microbiology and molecular biology reviews : MMBR*, 64(2):435–459.

Stewart, M. D., Li, J., and Wong, J. (2005). Relationship between histone H3 lysine 9 methylation, transcription repression, and heterochromatin protein 1 recruitment. *Molecular and cellular biology*, 25(7):2525–2538.

Strand, J. M., Scheffler, K., Bjørås, M., and Eide, L. (2014). The distribution of DNA damage is defined by region-specific susceptibility to DNA damage formation rather than repair differences. *DNA repair*, 18:44–51.

Stützer, A., Liokatis, S., Kiesel, A., Schwarzer, D., Sprangers, R., Söding, J., Selenko, P., and Fischle, W. (2016). Modulations of DNA contacts by linker histones and post-translational modifications determine the mobility and modifiability of nucleosomal H3 tails. *Molecular cell*, 61(2):247–259.

Takata, H., Hanafusa, T., Mori, T., Shimura, M., Iida, Y., Ishikawa, K., Yoshikawa, K., Yoshikawa, Y., and Maeshima, K. (2013). Chromatin compaction protects genomic DNA from radiation damage. *PloS one*, 8(10):e75622.

Tatton-Brown, K., Loveday, C., Yost, S., Clarke, M., Ramsay, E., Zachariou, A., Elliott, A., Wylie, H., Ardissone, A., Rittinger, O., et al. (2017). Mutations in epigenetic regulation genes are a major cause of overgrowth with intellectual disability. *The American Journal of Human Genetics*, 100(5):725–736.

Thakur, J., Fang, H., Llagas, T., Disteche, C. M., and Henikoff, S. (2019). Architectural RNA is required for heterochromatin organization. *bioRxiv*, page 784835.

Th'ng, J. P., Sung, R., Ye, M., and Hendzel, M. J. (2005). H1 family histones in the nucleus. Control of binding and localization by the C-terminal domain. *Journal of Biological Chemistry*, 280(30):27809–27814.

Tiwari, V. K., McGarvey, K. M., Licchesi, J. D., Ohm, J. E., Herman, J. G., Schübeler, D., and Baylin, S. B. (2008). PcG proteins, DNA methylation, and gene repression by chromatin looping. *PLoS biology*, 6(12):e306.

Vad-Nielsen, J., Jakobsen, K. R., Daugaard, T. F., Thomsen, R., Brügmann, A., Sørensen, B. S., and Nielsen, A. L. (2016). Regulatory dissection of the CBX5 and hnRNPA1 bi-directional promoter in human breast cancer cells reveals novel transcript variants differentially associated with HP1α down-regulation in metastatic cells. *BMC cancer*, 16(1):1–21.

Watanabe, S., Mishima, Y., Shimizu, M., Suetake, I., and Takada, S. (2018). Interactions of HP1 bound to H3K9me3 dinucleosome by molecular simulations and biochemical assays. *Biophysical journal*, 114(10):2336–2351.

Wong, L. H., Brettingham-Moore, K. H., Chan, L., Quach, J. M., Anderson, M. A., Northrop, E. L., Hannan, R., Saffery, R., Shaw, M. L., Williams, E., et al. (2007). Centromere RNA is a key component for the assembly of nucleoproteins at the nucleolus and centromere. *Genome research*, 17(8):1146–1160.

Wu, H., Dalal, Y., and Papoian, G. A. (2019). Binding dynamics of disordered linker histone H1 with a nucleosomal particle. *Biophysical Journal*, 116(3):70a.

Wutz, G., Várnai, C., Nagasaka, K., Cisneros, D. A., Stocsits, R. R., Tang, W., Schoenfelder, S., Jessberger, G., Muhar, M., Hossain, M. J., et al. (2017). Topologically associating domains and chromatin loops depend on cohesin and are regulated by CTCF, WAPL, and PDS5 proteins. *The EMBO journal*, 36(24):3573–3599.

Yadav, T., Quivy, J.-P., and Almouzni, G. (2018). Chromatin plasticity: a versatile landscape that underlies cell fate and identity. *Science*, 361(6409):1332–1336.

Yamada, T., Fukuda, R., Himeno, M., and Sugimoto, K. (1999). Funtional domain structure of human Heterochromatin Protein HP1 Hsa: Involvement of internal DNA-building DNA-binding and C-terminal self-association domains in the formation of discrete dots in interphase nuclei. *The Journal of Biochemistry*, 125(4):832–837.

Zhou, B.-R., Feng, H., Ghirlando, R., Li, S., Schwieters, C. D., and Bai, Y. (2016). A small number of residues can determine if linker histones are bound on or off dyad in the chromatosome. *Journal of molecular biology*, 428(20):3948–3959.

Zhou, B.-R., Feng, H., Kale, S., Fox, T., Khant, H., de Val, N., Ghirlando, R., Panchenko, A. R., and Bai, Y. (2021). Distinct structures and dynamics of chromatosomes with different human linker histone isoforms. *Molecular Cell*, 81(1):166–182.

Zhou, B.-R., Feng, H., Kato, H., Dai, L., Yang, Y., Zhou, Y., and Bai, Y. (2013). Structural insights into the histone H1-nucleosome complex. *Proceedings of the National Academy of Sciences*, 110(48):19390–19395.

Zuin, J., Dixon, J. R., van der Reijden, M. I., Ye, Z., Kolovos, P., Brouwer, R. W., van de Corput, M. P., van de Werken, H. J., Knoch, T. A., van IJcken, W. F.,

et al. (2014). Cohesin and CTCF differentially affect chromatin architecture and gene expression in human cells. *Proceedings of the National Academy of Sciences*, 111(3):996–1001.

Appendix A

Appendix

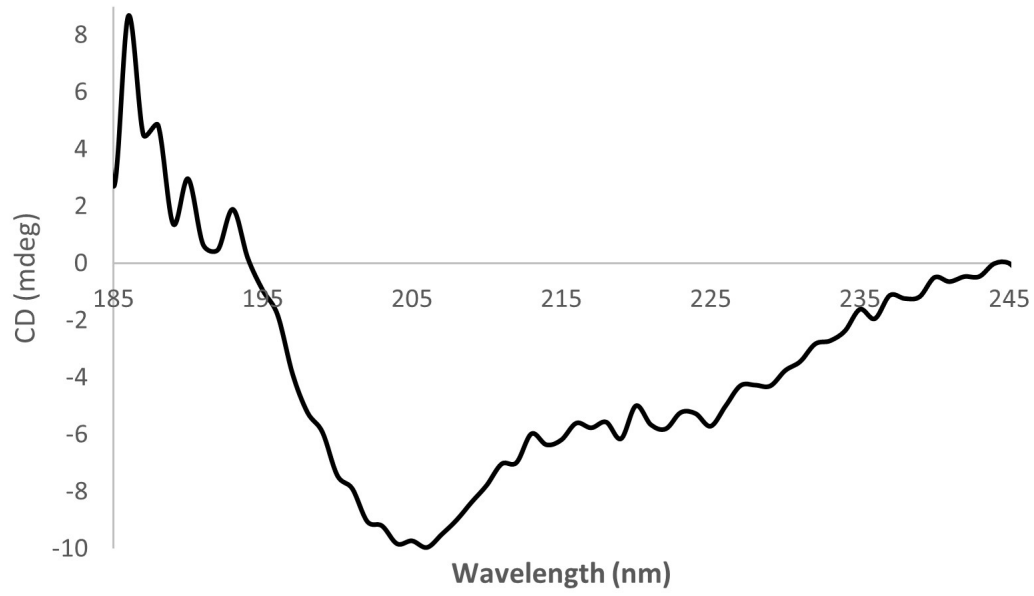

(a) His-HP1α Far UV circular dichroism

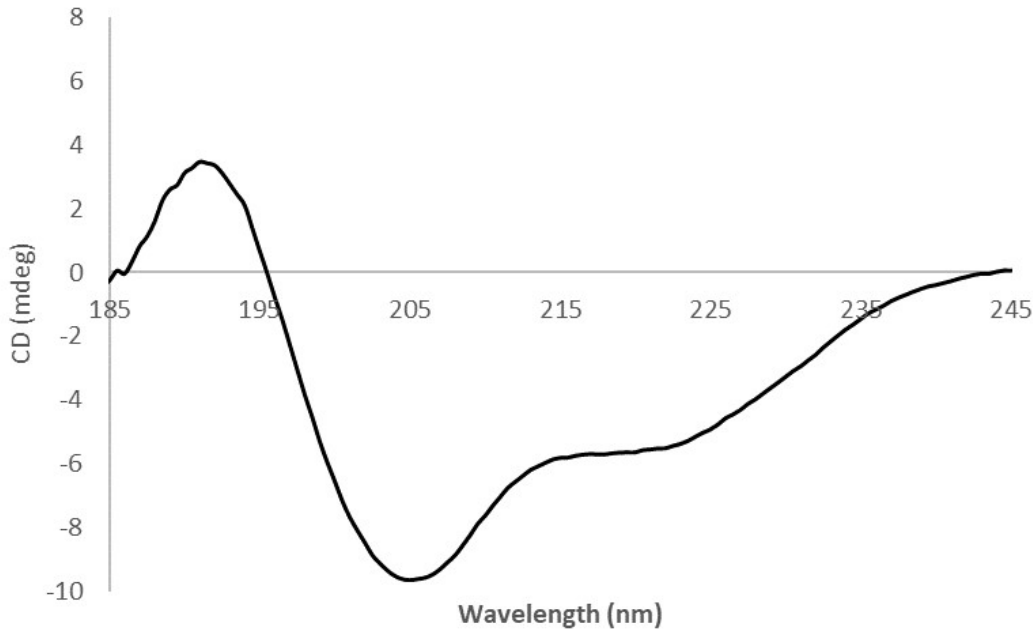

(b) Published His-HP1α Far UV circular dichroism (Roach et al., 2020)

Figure A.1: His-HP1α Far UV circular dichroism. Circular dichroism spectra of purified His-HP1α at 50 µM in HP1α size exclusion elution buffer (100 mM KCl, 50 mM NaCl, 20 mM NaH_2PO_4, pH [8]) were recorded in a 0.1 mm quartz cuvette. a) His-HP1α Far UV circular dichroism. b) Published His-HP1α Far UV circular dichroism from Roach et al. (2020).

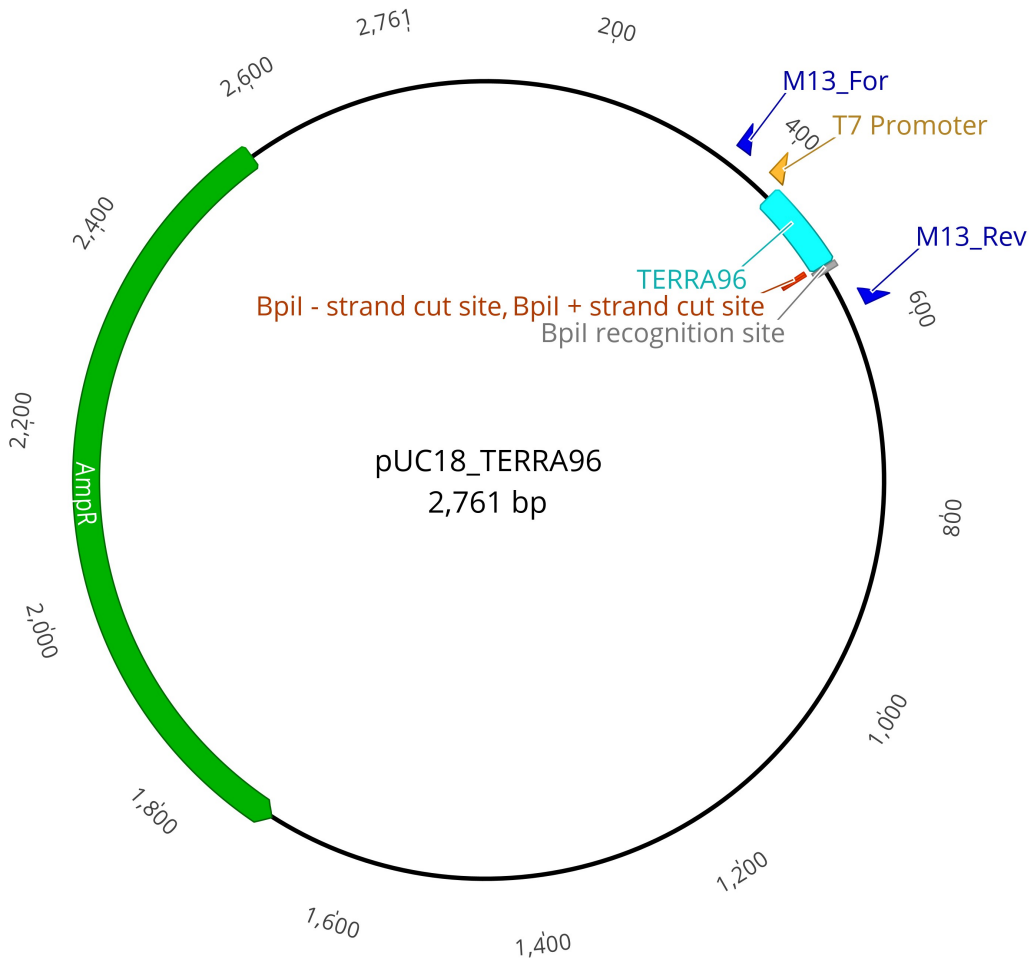

Figure A.2: pUC18_TERRA96 plasmid map. Created using Geneious 9.1.8.

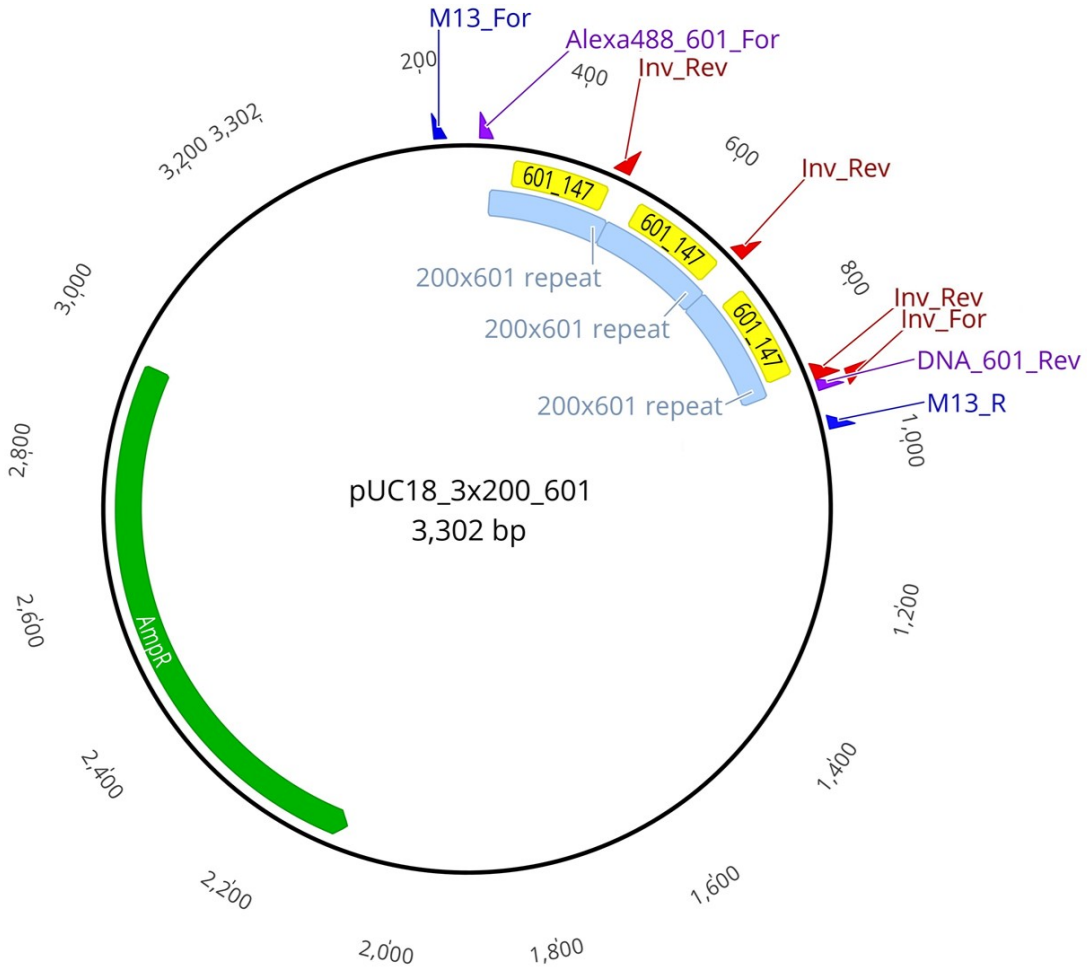

Figure A.3: pUC18_3x200_601 plasmid map. Created using Geneious 9.1.8.

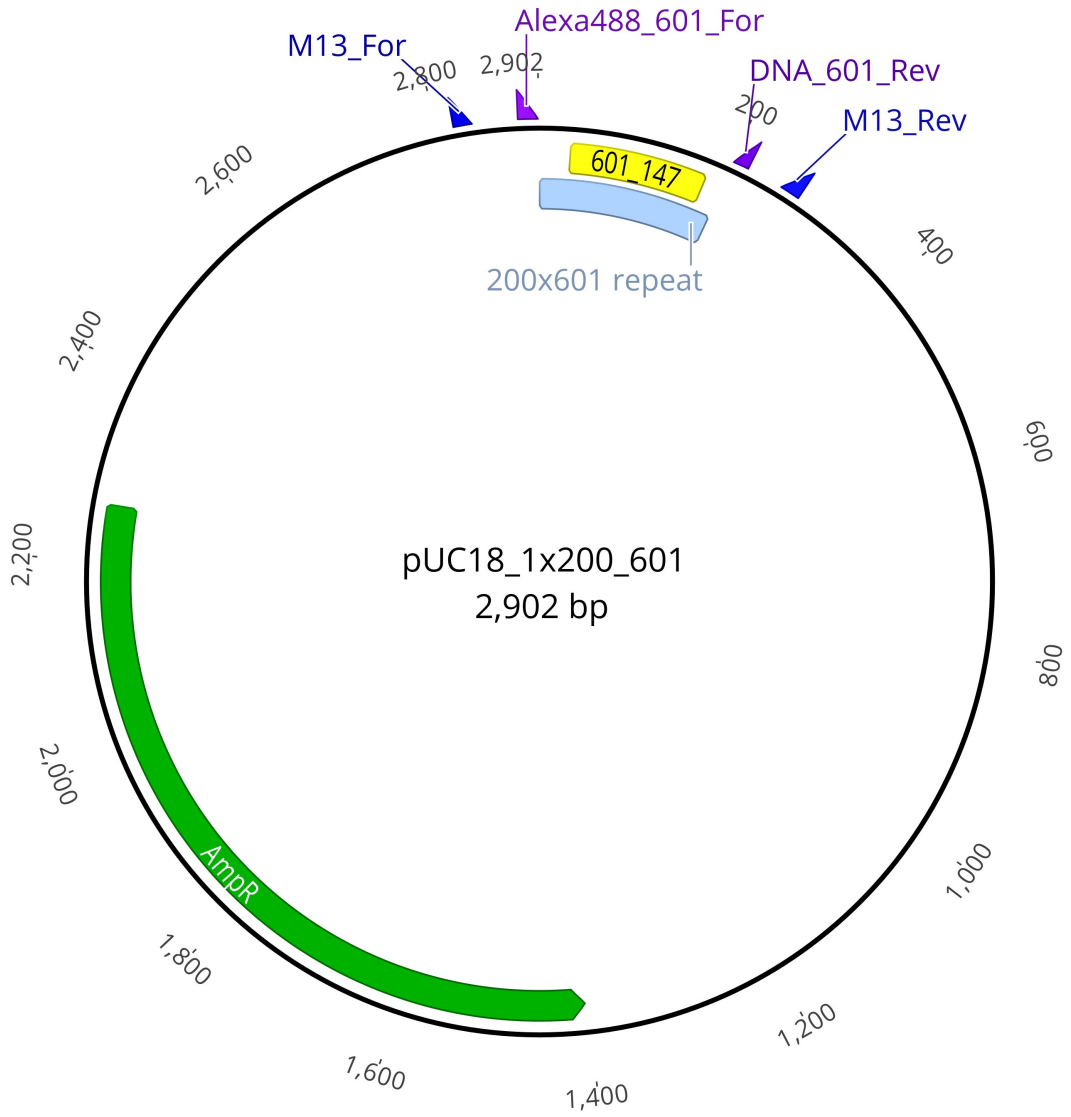

Figure A.4: pUC18_1x200_601 plasmid map. Created using Geneious 9.1.8.

Table A.1: Primer sequences

Primer name	**Primer sequence**
Sequencing	
M13_For	GGTTTTCCCAGTCACGAC
M13_Rev	AGCGGATAACAATTTCACAC
pUC18-_1x200_601 and -3x200_601	
Alexa488_601_For	Alexa488TCTAGAGGATCCCCGATATC
DNA_601_Rev	GGTACCCGATATCCCGA
pUC18_3x200_601	
Inv_For	TCGGGATATCGGGTACCGAGC
Inv_Rev	GTCGCTGTTCAATACATGCACAGG